HIGH-RESOLUTION XRF CHEMOSTRATIGRAPHY OF THE EAGLE FORD GROUP, TEXAS

A Dissertation

by

MATTHEW PAUL WEHNER

Submitted to the Office of Graduate and Professional Studies of
Texas A&M University
in partial fulfillment of the requirements for the degree of

DOCTOR OF PHILOSOPHY

Chair of Committee,	Anne Raymond
Committee Members,	Art D. Donovan
	Michael C. Pope
	Michael M. Tice
	Zoya Heidari
Head of Department,	Michael C. Pope

December 2017

Major Subject: Geology & Geophysics

ABSTRACT

Interest in applications of x-ray fluorescence (XRF) is greatly increasing, but the diversity of applications of XRF data has yet to be fully exploited. This dissertation presents three projects showcasing different applications of XRF. The first one uses molybdenum and uranium ratios (from XRF) and in conjunction with data from sedimentary structures, lack of benthic fauna, and biomarkers suggests that the depositional environment of Eagle Ford Group can be characterized as storm-dominated shallow-water, photic zone, episodically euxinic. Also the paleotopography seems consistent with that of a drowned carbonate platform.

The second project extends the stratigraphy of Eagle Ford Group into Big Bend National Park, at a publicly accessible outcrop, by identifying the sequences boundaries through chemostratigraphy of XRF data and stable isotopes, supported by nannofossil biostratigraphy. This provides a downdip analogue of subsurface Eagle Ford section with intervals not described in outcrops in central and north Texas.

The third project generated a regional stratigraphic correlation of Eagle Ford Group throughout west Texas in the Trans Pecos area. Both a gamma-ray based correlation and carbon isotope chemostratigraphic correlation are provided. These correlations were constrained by nannofossil, biostratigraphy, and unpublished U-Pb ash bed dates. Also euxinia (proxied by covariation molybdenum and uranium ratios) is interpreted to have been diachronous. It was present earlier in the western part of Trans-Pecos during the early-mid Cenomanian, but later was absent during the late Cenomanian. However, it was persistent and was the dominant redox state in the eastern part of the Trans-Pecos as seen in the data

from Antonio Creek and Lozier Canyon. Also the use of iron-sulfur-organic carbon (TOC) data from Antonio Creek revealed that in the Lower Eagle Ford that while the Fe/S ratio parallels the pyrite Fe/S ratio, it has more sulfur than stoichiometry predicts if all sulfur was in pyrite. That the low Fe/S is associated with high TOC seems to support the idea that low Fe/S is because that the TOC is sulfurized, suggesting that in certain mudrock and source rock units, the Fe/S ratio can reveal the presence of sulfurized TOC.

DEDICATION

It is my wish to dedicate this volume of research to my dear and lovely mother who I suspect had always known that I would become a scientist, even when I myself had not realized it. I just wish she could have seen how things turned out.

Melissa Ann Wehner

(1958-2005)

ACKNOWLEDGMENTS

For me writing the acknowledgement page is a little daunting because the journey for obtaining the Ph.D. has not been a straightforward one and has been a long one with many twists and turns. It is my intention to acknowledge as many people as I can remember, but please do not be offended if I inadvertently miss someone since in some cases so much time has passed since the help was received. So I will attempt to inventory the help I have received from family, friends, mentors, and colleagues.

I will start with family since they have always been with me and ultimately knew before me that I was destined to to pursue a Ph.D. I particularly wish to acknowledge my grandmother, Nana, for her unfailing support throughout my entire undergraduate and graduate education. She was always available when I was feeling down or needed personal advice no matter what the day or time was. I want to thank my father for his support, particularly when I was an undergraduate.

I want to thank Dr. Harry Rowe from the Texas Bureau of Economic Geology for providing access to his collection of XRF standards, which are the same ones used to calibrate the Bruker Tracer XRF analyzers. I am most grateful to have been able to calibrate the XRF device.

I want to thank my former academic advisor, Robert Weiss. His ideas about education and insistence on quantitative applications in sedimentology and stratigraphy was influential in developing my ideas about quantitative applications in stratigraphy. Because of him I continued developing my background in mathematics and programming which served

me well when I worked on the Eagle Ford project after Dr. Weiss moved to Virginia Tech University. Also thanks to him, I am writing my dissertation (this document) in LaTeX.

Many of my friends were supportive and helped provide the balance of work and fun that is needed to prevent Ph.D. students from going crazy. No particular preference is implied in the ordering of names. Harsh Patel was instrumental in creating a visualization tool for my data. Harsh Patel was also important for providing company as I struggle to finish my Ph.D. along with Roneet Das. My friend, Dharanidhar Dang aka DD, always had a smile and knew how to cheer me up, especially with his culinary skills. Also Eric Peavey is a fellow traveler, enduring similar circumstances as I have, as well as working Eagle Ford as I do and sharing similar research interests. Eric also was helpful with creating figures. Also I want to include the following in my acknowledgements: Mahmood Ettehad, Trey Lyons, Rand Gardner, and Aris Pramudito.

I want to thank Dr. Barry Katz who in the role of the editor for the Gulf Coast Association of Geological Societies (GCAGS) Journal allowed me to use the article I published in the 6th volume of GCAGS Journal as my second chapter of my dissertation.

CONTRIBUTORS AND FUNDING SOURCES

Contributors

This work was supported by a dissertation committee consisting of Dr. Anne Raymond (advisor), Dr. Art D. Donovan, Dr. Michael C. Pope (also Department Head of the Department of Geology & Geophysics), and Dr. Zoya Heidari (formerly professor in Department of Petroleum Engineering at Texa A&M University, but now at the Department of Petroleum and Geosystems Engineering at The University of Texas at Austin).

BP America provided logistics and access to Lozier Canyon and Antonio Creek in Terrell County, Texas. This was largely mediated by Dr. Art Donovan. I was able to benefit from the support provided to my colleague, Rand Gardner, for his fieldwork. I was able to collect in tandem with him and thus we have a mutual arrangement to share data between us (measured sections, lithology data, field observation, photography, and handheld spectrometry data). BP America also granted access to a handheld XRF device for collecting the XRF data in my research.

For the first manuscript, geochemical data was kindly provided by Ivan Maulana. Some field photos and some data was shared by Trey Lyons. All other work conducted for the dissertation was completed by the student independently.

Funding Sources

For the academic years of 2009/2010 and 2010/2011, the student was supported by the ConocoPhillips Fellowship ($25,000/year) for two years that was awarded by the Berg-Hughes Center for Petroleum and Sedimentary Systems. Between the fall of 2011 and

through the fall of 2014, the student was supported by a series of teaching assistantships from the Department of Geology & Geophysics. The student was independently self-funded while employed as a part-time geologist at W. D. Von Gonten Laboratories from January 2015 through April 2016 when it was still in College Station at the Research Park on West Campus. For the summer of 2016, the student was awarded a Summer 2016 Fellowship from Berg-Hughes Center for Petroleum and Sedimentary Systems, which resulted in a work about quantitative applications of XRF and well log data in sequence stratigraphy. Also the student was independently funded in 2017 as a part-time GED instructor for Region VI Education Service Center and Brazos County. No further financial support was received.

NOMENCLATURE

AIR	Aryl Isoprenoid Ratio
API	unit of radioactivity
BBNP	Big Bend National Park
BP/SLB	BP/Schlumberger
BI	Bioturbation Index
ED-XRF	Energy-Dispersive X-ray Fluorescence
GC-MS	Gas Chromatography-Mass Spectrometry
GOM	Gulf of Mexico
GR	Gamma Ray
GSSP	Global Boundary Stratotype Section and Point
HC	Hydrocarbon
HCS	Hummocky Cross-Bedding
ICP	Inductively Coupled Plasma
ICP-MS	Inductively Coupled Plasma Mass Spectrometry
LEF	Lower Eagle Ford Formation
Mya	million years ago
OAE2	Ocean Anoxic Event 2
Ph	Phytane
Pr	Pristane
ppm	Parts Per Million (also mg/kg)

ps/gs	Packstone/grainstone
SCS	Swaley Cross-Bedding
SGR	Spectral Gamma Ray log
SMA	San Marcos Arch
TGR	Total Gamma Ray (in units of API)
TOC	Total Organic Carbon
UEF	Upper Eagle Ford Formation
WIS	Western Interior Seaway
wt. %	weight percent
XRF	X-ray Fluorescence

TABLE OF CONTENTS

Page

LIST OF FIGURES

FIGURE Page

LIST OF TABLES

TABLE Page

1. INTRODUCTION

1.1 Unifying theme and background

I sought to address several seemingly unrelated questions, but there are some common threads throughout my research that I wish to specify. The following are the main questions I wished to address in my Ph.D. research:

1. Is the depositional environment of Eagle Ford Shale better characterized as deep-water or shallow-water (frequently influenced by storms or rarely).
2. Extend the Eagle Ford sequence stratigraphy and chronostratigraphy into the Trans-Pecos region in west Texas.
3. Report on the findings of the persistence of euxinia during Eagle Ford deposition in west Texas using enrichment factor ratio of molybdenum and uranium (Mo/U). Also explore the possibility of using Fe/S to detect zones of sulfurized organic carbon (TOC).

In this dissertation, I am including three manuscripts that are formatted for submittal to various geoscience journals, meaning that the dissertation has a journal article style format.

These projects had their origin due to the efforts of Dr. Art Donovan. He convinced me to take on a research project in the Eagle Ford after cajoling me by inviting me to inspect the fabulous outcrops of Eagle Ford at Lozier Canyon. Once I agreed, he asked me to look into applications of x-ray fluorescence (XRF) for stratigraphy in the Eagle Ford Shale. Since it turns out that many kinds of applications are possible for XRF data, the projects in my dissertation reflect these two things: Eagle Ford and applications of XRF.

Chapter 2 is the first manuscript that is addressed at answering the first question about depositional environments by integrating the results from XRF and a wide range of other data. Chapter 3 focuses on expending the sequence stratigraphy and isotope stratigraphy into Hot Springs location in Big Bend National Park and provides a publicly accessible outcrop for Eagle Ford Group sediments. Permission to use this chapter was granted by Dr. Barry Katz, editor of the GCAGS Journal. Chapter 4 explores the use of enrichment factor ratios of molybdenum and uranium (Mo/Al and U/Al) to investigate persistence of euxinia. Also we report on the possibility of the use of Fe/S ratio to detect zones of sulfurized high TOC zones.

1.2 Review of XRF data and usage

1.2.1 Review of unconventional reservoirs

The classic model of petroleum system stated a complete petroleum system was needed for petroleum production, which consisted of the following: source, reservoir, and seal. This classical petroleum system model, known as a conventional system, reflects the generality that mudrocks are essentially impermeable on the production scale yet are needed as the source of the hydrocarbons. Because their permeability is on the micro- and nano-meter scale, they were not were seriously considered as a self-sourced reservoir (Loucks et al., 2012). Even as recently as 18 years ago, influential texts, such as Selley (1998), noted that shale gas production was not economical for most petroleum companies. However, according to Selley (2012), the following changes in technology have made unconventional petroleum system economical:

- Ability to drill multiple wells from one pad (same location)
- Directional drilling – needed to steer wells into horizontal positions

- Hydraulic fracturing – needed to induce fracture permeability in otherwise "impermeable" mudrocks or tight rocks.

The advent of unconventional petroleum resources (popularly known as the shale gas revolution) has shifted paradigms, both in the political and scientific realms. From the scientific standpoint, this has resulted in an increase interest in mudrock systems, which historically have been understudied for a host of reasons. Ehlers and Blatt (1982) summarized the problem by noting the following impediments to the study of mudrocks:

- Extreme small grain size (silt and clay size)
- Extreme variation in mineralogy and composition
- Heterogeneity of physical parameters like porosity and permeability
- High susceptibility to diagenesis

These problems can make field differentiation of different mudrocks difficult and sometimes unreliable due to of the lack of macroscopic features and complexity of micro-size features. Just as technology initiated the shale gas technology, new and improved technology has made it possible to study mudrocks in ways not available to geoscientists in previous decades.

Currently mudrocks around the world are actively sought and studied as potential unconventional reservoirs. In 1997, the first major commercial success with unconventional reservoir was in the Barnett Shale in north Texas by Mitchell Energy. This was primarily is a natural gas play and became the first volley of what was later termed shale gas revolution. In 2008 this revolution came to south Texas, when Petrohawk began producing from the Eagle Ford in La Salle County (Cusack et al., 2010). Unlike, the Barnett Shale, the Eagle Ford Shale Play is a mixed oil-gas play depending on the location. The majority of

production in Eagle Ford is in the Maverick Basin, but wells exist all the way up to central Texas. Now the Eagle Ford Play has been extended to the edge of East Texas Basin (Bowman, 2014; Hentz et al., 2015; Hentz and Ruppel, 2010). In this play, the hydrocarbons (HC) produced in south Texas are from the lower half of the mudrock unit, but in north Texas, the Maness Shale is a better reservoir than the Pepper Shale according to A. Hudson (priv. comm.). However, the exact stratigraphic relation of Maness Shale, Pepper Shale, and Eagle Ford Shale is in dispute. An interesting summary of the stratigraphic complications is discussed by Adams and Carr (2010). It is reported that the Maness Shale has fossils consistent with the upper Washita Group even though it is post-Buda and perhaps correlates to the unconformity between Buda and Eagle Ford in west Texas.

An integrated regional basin analysis focused on the Eagle Ford Group, linking novel data types, like ED-XRF and handheld spectrometer (analogous to gamma ray logs) data, with conventional data like stable isotopes and well logs, can help address, extend and refine the sequence stratigraphic model as well as contribute to a better understanding of depositional environment and petroleum systems.

2. SHALLOW-WATER ANOXIC DEPOSITIONAL ENVIRONMENTS IN THE LATE CRETACEOUS EAGLE FORD GROUP (BOQUILLAS FORMATION), WEST TEXAS WITHIN THE WESTERN INTERIOR SEAWAY

2.1 Introduction

The Cenomanian-Turonian Eagle Ford Group (or Boquillas Formation) in west Texas was deposited at the southern end of the Western Interior Seaway (WIS), and contains one of the largest unconventional oil plays in the United States. Its strata share many features characteristic of organic-rich rocks around the world. The mudstone and limestone beds in the Eagle Ford Group contain sedimentological, geochemical, and depositional features that seem contradictory and led to controversy regarding its depositional environment. While all workers agree that the depositional environment was frequently anoxic, interpretations are split on whether it was shallow water and storm dominated (e.g. Donovan et al. 2012) or deep water and turbidite dominated (e.g. Lock and Peschier 2006).

The interbedded carbonate and siliciclastic mudstone strata of the Eagle Ford Group is well exposed in several locations (Fig. 2.1) in Terrell County and partially in Val Verde County (Donovan and Staerker, 2010; Donovan et al., 2016) providing a natural laboratory to study these rocks. The sedimentary structures, bedforms, and trace element and organic geochemistry of the Eagle Ford Group in west Texas indicate that these strata were deposited in a shallow water setting within storm wave base that commonly episodically was anoxic.

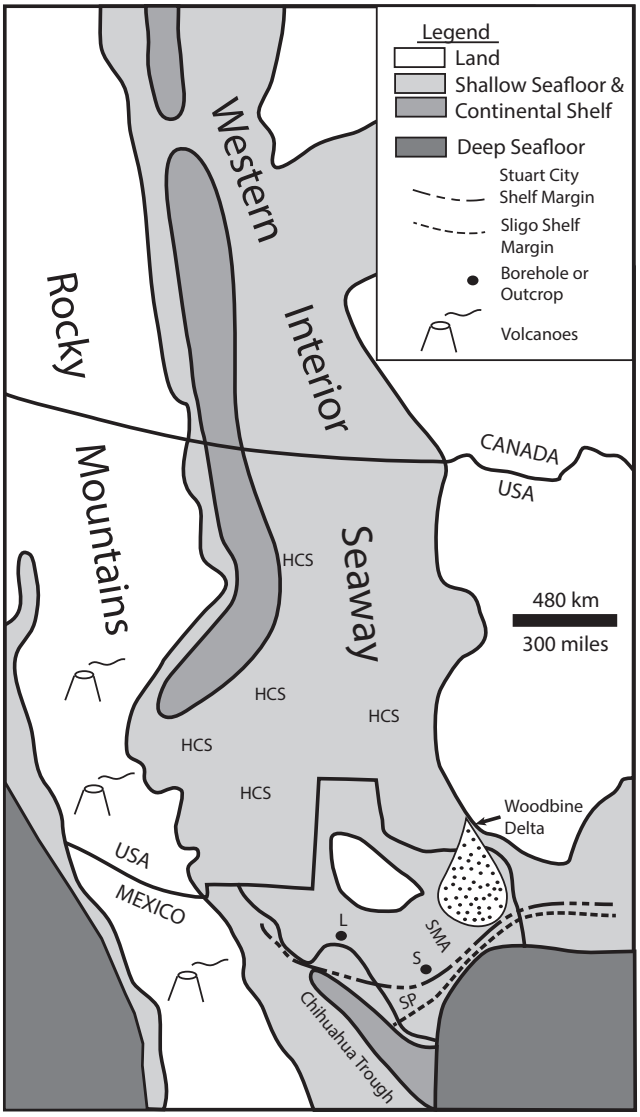

Figure 2.1: Map of central North America during the Cenomanian (modified from Blakey, 2015). Eagle Ford Group sediments at Lozier Canyon (L) outcrop and in the subsurface core, Swenson #1 (S) were utilized for this study. The approximate locations of the Sligo (Hauterivian-Barremian) and Stuart City (Albian) reef margins are marked by dashed lines. The submarine plateau (SP) between the two reef trends marks substantial topographic relief ($\sim$ 400 ft, 160 m). The San Marcos Arch (SMA) marks a syndepositional arch that separated carbonate-rich Eagle Ford sediments west of the arch from siliciclastic-rich Eagle Ford sediments east of the arch. Volcanoes to the west produced the numerous bentonites in the Eagle Ford Group. Tempestites (HCS) similar to those described in this paper occur throughout the southern Western Interior Seaway (locations from Sageman, 1996)

2.2 Geologic setting

After the breakup of Pangaea, the proto-Gulf of Mexico transitioned from a Jurassic rift zone to a Cretaceous passive margin. During the early Cretaceous, rudist-rimmed carbonate reefs lined the proto Gulf of Mexico (GOM), forming at least two major reef margins (the Sligo Margin and Stuart City Trend; Fig. 2.1). Toward the end of the Early Cretaceous, extensive paleobathymetric relief resulted from the exposure of the Comanche Platform and reef margins during a drop in relative sea-level (Dawson, 1997). During the Cenomanian-Turonian, changes in sea-level and regional tectonics in the central US led to continental flooding, forming the Western Interior Seaway (Elder and Kirkland, 1994). The Eagle Ford Group was deposited from at least the Middle Cenomanian through the end of the Turonian (Donovan et al., 2012), making it coeval or partially coeval with many stratigraphic units of WIS (i.e. Graneros Shale, Lincoln Limestone, Hartland Shale, Bridge Creek Limestone, Carlisle Shale, Dakota Sandstone). The Eagle Ford Group does contain the Ocean Anoxic Event 2 (OAE2) in some sections (Eldrett et al., 2014; Lowery et al., 2014). In the study area an informal five-fold facies association sub-division (labeled A-E in Figure 2.2 and hereafter termed units) is utilized for the Eagle Ford Group (Gardner et al., 2013).

2.3 Methods

Data for this study were collected from multiple outcrops and one subsurface core in Texas (Fig. 2.1). Spectral gamma ray (SGR) profiles of the outcrops were acquired at 30 cm intervals using a Terraplus RS-230 scintillometer. We describe bioturbation using a scale of 0-5 for a bioturbation index (BI; Droser and Bottjer 1986). X-ray fluorescence (XRF) data were acquired for outcrop samples and core samples were analyzed by ICP-MS. Biomarker abundances in subsurface core were measured by gas chromatography mass

spectrometry (GC-MS).

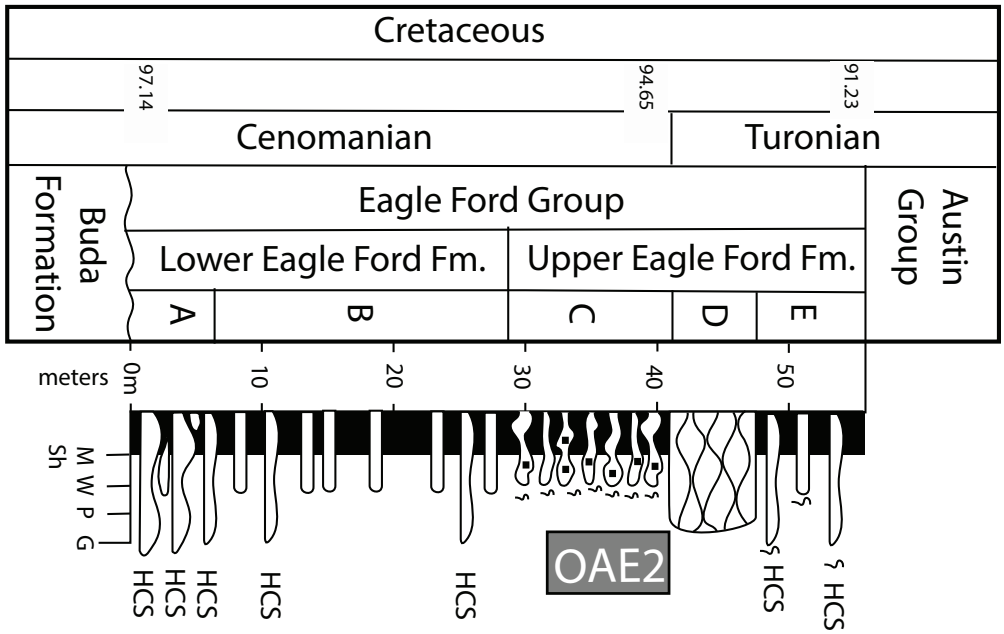

Figure 2.2: Generalized stratigraphic column of the Eagle Ford Group sediments with stratigraphic division (A-E) after Donovan et al. (2012). Absolute ages from Deluca (2016). The column is based on the outcrops at LC/AC. Rock types are M/Sh = carbonate mudstone/organic-matter rich mudstone; W = wackestone; P = packstone; G = grainstone. OAE2 interval inferred from carbon isotope data of Donovan et al. (2012) and Lowery et al. (2014).

2.4 Results

2.4.1 Sedimentary structures

In units A, B, and E, limestone beds are composed of foraminiferal packstone/grainstone (ps/gs) beds and have a wide range of sedimentary structures. Many ps/gs beds have an erosional base, commonly overlain by a lag of inoceramid valves, grading upward into low-angle ripple laminae, many of which are concavo/convex, thickening toward the thicker part of ripple and thinning toward the ripple trough (Fig. 2.3). These bedforms commonly are connected to adjacent ripples, but they also can form isolated ripples. Slabbed examples show that these bedforms are hummocky (three-dimensional) and externally symmetric (see Appendix A) which distinguishes them from other sedimentary structures. Overall these bedforms preserve their depositional geometries, but due to scouring at the base, some beds erode into underlying beds, occasionally forming amalgamated foraminiferal ps/gs beds.

This bedform occurs in association with symmetric wave ripples (Fig. 2.3 and additional examples in Appendix A) and low-angle cross-lamination. This association of sedimentary structures implies deposition between fairweather and storm wave base (10's of meters water depth; Aigner 1982; Aigner 1985). In units A, B, and E, concavo-convex, 3-D, symmetric ripples become scarce as the ps/gs become infrequent and thin, and calcareous mudstone becomes more abundant. Units C and D are more bioturbated (BI 3-5) and their primary depositional structures commonly are obscured. In the Upper Eagle Ford Formation, extensive bioturbation destroyed most of the depositional fabric, but what remains are small symmetric ripples and low-angle cross-laminations in unit E.

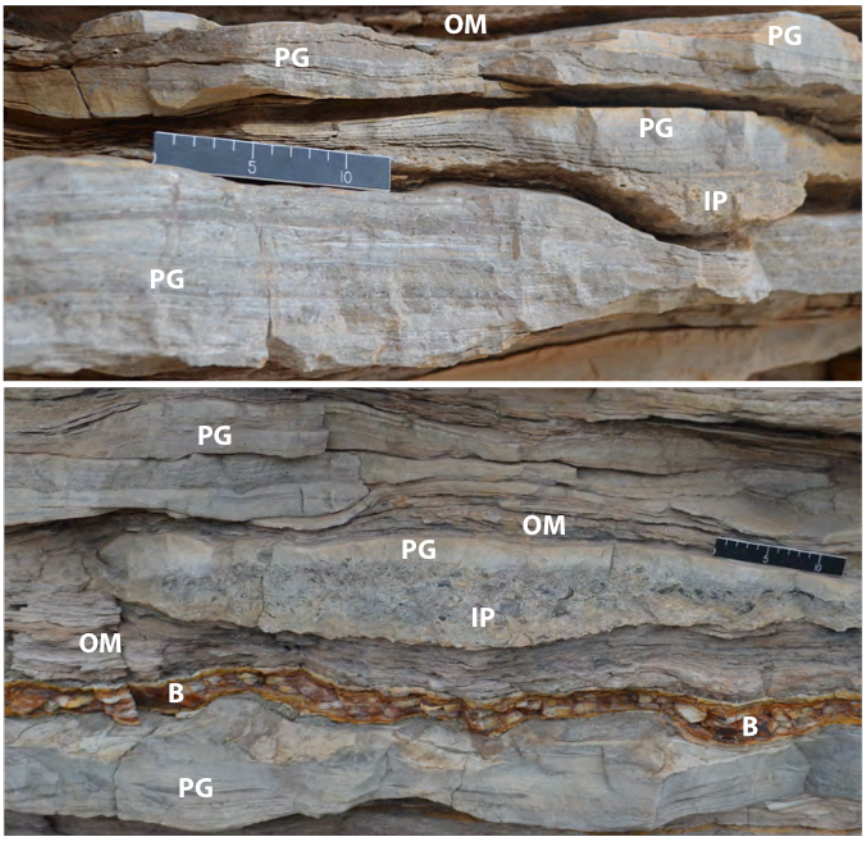

Figure 2.3: Photographs of wavy and hummocky cross-stratified foraminiferal packstone/grainstone (PG), occasionally overlying inoceramid packstone (IP) interbedded with carbonate-rich organic-rich mudstone (OM). Bentonite layer (B) occurs in lower photograph.

2.4.2 Bioturbation and biota

In the Lower Eagle Ford Formation benthic foraminfera and bioturbation are rare. *Planolites* and *Chrondrites* formed on the tops of a few current- and wave-structured foraminiferal ps/gs beds. These bioturbated zones are rare and very thin (mm scale). In the lower part of unit A echinoid fragments occur within the dolomitic beds in the basal 4-5 feet. At the top of unit A in Lozier Canyon are several oyster beds (aff. *Ostrea beloiti*) interbedded with phosphatic lags. Various types of inoceramids are scattered throughout the Lower Eagle Ford Formation, usually as bioclastic fragments.

Unit C is quite bioturbated (BI 3-4); its ichnofauna includes: *Thalassinoides*, *Teichnichnus*, *Taenidium*, *Planolites*, and *Chondrites*. Some of the larger identifiable ichnofossils are up 15 cm in length. Unit D is characterized by numerous echinoids, *Hemiaster jacksonii*, in nodular bedding resulting from extreme bioturbation (BI is 4-5). Identifiable ichnofossils in Unit E include *Taenidium* and *Chondrites* and its BI is about 3.

2.4.3 Geochemistry

The Lower Eagle Ford Formation has a mean uranium content of 13 ± 6 ppm ($\pm$one standard deviation, 47 samples) versus 3.8 ± 3.6 ppm (41 samples) for the Upper Eagle Ford Formation (significantly less with p $= 2 \times 10^{-13}$ for a two-tailed t-test). As in other core collected throughout the Eagle Ford Group in west and south Texas, rocks of the Lower Eagle Ford Group contain abundant Mo (25 ± 14 ppm). Mo abundances generally increased with Al abundance throughout both units A and B of the lower Eagle Ford Group (Fig. 2.4), with Mo/Al $= (2-45) \times 10^{-4}$ with an average of $(21 \pm 11) \times 10^{-4}$, or a 140-fold enrichment above average shale (McLennan, 2001). In contrast, rocks of the Upper Eagle Ford Group contain significantly less Mo relative to Al (p $= 2 \times 10^{-15}$ for a two-tailed

t-test), with Mo/Al $= (0.3 - 6) \times 10^{-4}$ with an average of $(1.6 \pm 1.1) \times 10^{-4}$.

Pristane and phytane are identified in the saturated fraction of organic matter extracts, and C_{13-22} aryl isoprenoids are identified in the aromatic fraction (details included in Appendix A). In addition to aryl isoprenoids, a homologous series of C_{19-23} 2,3,5',6-tetramethyl-2'-alkylbiphenyls (diaryl isoprenoids; IV) is identified based on mass spectra (Koopmans et al., 1996). The C_{40} precursor of aryl isoprenoids, isorenieratane (V), is not observed, probably due to the low proportion of isorenieratene (VI) that is preserved as free isorenieratane (<1%; Koopmans et al. 1996).

2.5 Discussion

2.5.1 Depositional environment

Foraminiferal limestone beds of Units A, B, and E of the Eagle Ford Group contain concavo-convex symmetric ripples interpreted to be hummocky (HCS) and swaley cross-stratification (SCS) where SCS forms in shallower water conditions than HCS (e.g. Dumas et al. 2005). The HCS- and SCS-dominated foraminiferal limestone beds in the Eagle Ford Group are similar to skeletal limestone beds from Cenomanian-Turonian strata in the Western Interior Basin interpreted by Sageman (1996) as tempestites. The following sedimentologic features, observed from units A, B, and E, indicate tempestites: the thickening and thinning of laminae, sharp erosional base, oftentimes with scoured surfaces, with or without a shell lag layer, then mostly planar lamination followed by wave ripples or convoluted lamination or ripples (Einsele and Seilacher, 1991). Shallowing or deepening trends are identified by comparison of the tempestites to two end-member cases. Proximal (shallower) tempestites (as seen at Lozier Canyon) typically have thicker beds or bedsets of foraminiferal pg/gs consisting of multiple amalgamated beds or laminasets. In contrast,

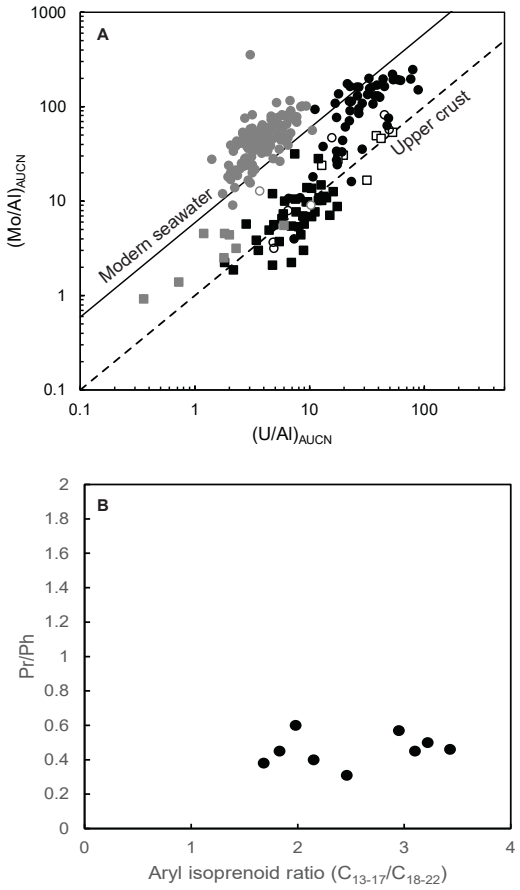

Figure 2.4: Inorganic and organic geochemical proxies for euxinia in Eagle Ford Formation rocks. A) Mo and U enrichment in Eagle Ford Formation rocks from Lozier Canyon/Antonio Canyon (LC/AC), west Texas (black symbols) and Swenson #1 (SW), south Texas (gray symbols). Mo/U ratios in the Upper Eagle Ford Formation, Buda Formation, and Austin Formation are similar to that of average upper crust (McLennan, 2001) and have low overall U enrichment, indicating deposition under a water column that was sulfide-free. In contrast, rocks of the Lower Eagle Ford Formation have Mo/U ratios that approach that of modern seawater with increasing U enrichment, indicating deposition under a euxinic water column. B) Pristane/phytane (Pr/Ph) ratios < 1 and aryl isoprenoid ratios (AIR) > 2 together indicate episodic photic zone euxinia, probably on seasonal timescales. Organic extracts from the Lower Eagle Ford of Swenson #1. The data is in Appendix B.

distal (deeper) tempestites are usually calcisiltites or calcareous mudstone of fine-grained pellets and fine-size bioclastic debris. Based on these criteria, we suggest the majority of Eagle Ford Group carbonate sediments in Units A, B, and E in west Texas accumulated in shallow waters (10's of m water depth), episodically influenced by storm processes. The high bioturbation indices of units C and D indicate they formed in shallow, but better oxygenated waters.

2.5.2 Anoxia

Mo/U ratios in the Upper Eagle Ford, Buda, and Austin formations all are similar to that of average upper crust (McLennan, 2001) and have low overall U enrichment, indicating deposition as reducing sediments under a water column that was sulfide-free. In contrast, Mo/U ratios in the Lower Eagle Ford Formation approach or exceed that of modern seawater with increasing U enrichment, reflecting a sedimentary sink for Mo that approached the efficiency of that for U. At the greatest observed U enrichments, Mo/U ratios decrease slightly, most likely reflecting extreme euxinia and partial depletion of Mo in the basin relative to open seawater (Tribovillard et al., 2012). Elevated Mo/U ratios thus appear to indicate varying amounts of free sulfide in the water column during deposition of the Lower Eagle Ford Formation. Although observed aryl isoprenoids can be diagenetic products of β-carotane, a ubiquitous carotenoid, the presence of diaryl isoprenoids in all samples suggests that both are derived from isorenieratene, an accessory pigment of the green sulfur bacterium *Chlorobiaceae* (Koopmans et al., 1996; Summons and Powell, 1986). Because these bacteria require both free sulfide and light for growth, these compounds imply shallow water (photic zone) euxinia during deposition. Pristane/phytane ratios and aryl isoprenoid ratios together indicate episodic photic zone euxinia, probably on seasonal timescales (Koopmans et al., 1996). Shallow water euxinia would have generally excluded

all but shallow planktonic foraminifera, consistent with high pelagic/benthic foraminiferal ratios observed by other investigators (e.g. Lowery et al. 2014). The lack of bioturbation in most of the Lower Eagle Ford Formation and only sporadic horizons with very shallow (at most a few mm's) burrowing suggests that the oxic/anoxic redox front was rarely below the seafloor.

Unit C carbonate mudstone in proximal settings (Lozier, Antonio, and Osman canyons) was intensely bioturbated, even though it was deposited during OAE2. This contrasts with the globally recognized high-TOC and laminated character of many OAE2 sections. Similar non-typical OAE2 sediments, like those preserved in the USGS Portland #1 core of Colorado, were attributed to increased availability of reactive iron that suppressed hydrogen sulfide accumulation in the sediments, allowing for deepening bioturbation and increased metabolic demand (Meyers et al., 2012). Ubiquitous authigenic cubic pyrite in unit C at Lozier Canyon is consistent with this mechanism. Unit D is the most diversely bioturbated unit, indicating that oxygen levels rose to nearly normal levels following OAE2. Lastly, Unit E, with increased interbedding of laminated foraminiferal ps/gs and calcareous mudstone with locally good preservation of HCS and SCS may indicate a return to more stratified seaway but the abundance of bioturbation suggests significantly oxygenated waters or more frequent mixing of the water column by storms. It was proposed that asynchronous development of global euxinia during OAE2 relative to development of local euxinia and burial of organic matter-rich sediments in the southern WIS represents a paradoxical decoupling of the carbon cycle from the redox evolution of the world's oceans (Eldrett et al., 2014). This discrepancy is only a paradox if Eagle Ford rocks formed in an environment coupled to the global system. Our evidence instead indicates that localized hydrographic conditions, including persistent shallow-water conditions and episodic euxinia, contributed to accumulation of thick organic matter-rich sequences

similar to other locations globally (e.g. Wignall and Newton 2001).

2.6 Conclusion

We suggest the paradox of shallow water sedimentary structures (HCS, SCS, gutter casts and bioclastic clasts) recorded in carbonate beds with only pelagic biota in the Lower Eagle Ford Group can be explained by shallow water (depth much less than 100 m) deposition punctuated by episodic large offshore storms. This suggests that some laminated organic matter-rich fine grained rocks without benthic fauna in this and similar units worldwide result from shallow-water anoxia due to hydrographic factors. The abundance of U, Mo, TOC, and aryl isoprenoids with lack of bioturbation and low Pr/Ph ratios in the calcareous mudstone indicates that the Lower Eagle Ford Formation was deposited under anoxic (periodic euxinic) stratified waters. We propose that the pelagic-rich foraminiferal ps/gs beds were produced by storm reworking of foraminifera deposited under a stratified shallow water mass whose anoxic base prevented benthic foraminifera from living on the seafloor. Episodic storms frequently swept across the carbonate ramp forming tempestites and providing enough oxygenation to temporarily allow shallow burrowing immediately following the storm events, but not during prolonged periods of calcareous organic matter-rich mudstone deposition. Furthermore, increased ichnofauna diversity in Units C, D, and E, and the appearance of benthic foraminifera at the base of Unit C (Lowery et al., 2014), coupled with decreased abundances of U and Mo indicate the Upper Eagle Ford Formation was accumulated in more oxygenated shallow water settings as the Comanche Platform became better connected with the southern WIS. Shallow water anoxia likely produced similar lithofacies associations in offshore settings throughout Earth history.

3. THE EAGLE FORD GROUP RETURNS TO BIG BEND NATIONAL PARK, BREWSTER COUNTY, TEXAS[1]

3.1 Introduction

Geographically, Big Bend National Park (BBNP) is in West Texas along the Rio Grande, the natural boundary between the United States and Mexico (Fig. 3.1). In the Upper Cretaceous, however, the BBNP region was positioned between the Gulf of Mexico (GOM) and the Western Interior Seaway (WIS) (Fig. 3.2). Tectonically, this region was positioned along the collision front of Gondwana and Laurasia in the Late Paleozoic marked by the Ouachita Thust Front (Fig. 3.3), underwent foreland deformation in the Mesozoic and Paleogene (Fig. 3.3), and then Neogene extension with the Rio Grande Rift.

From a stratigraphic standpoint, the Late Jurassic and Cretaceous succession of the region is part the 1st-order Zuni Megasequence of Sloss (1963). The maximum flooding event of this cycle, which is marked by the maximum incursion of the Western Interior Seaway, occurs in the latest Cennomanian and early Turronian. In general, this maximum flooding event coincides with a geochemical event referred to as the Ocean Anoxic Event 2 (OAE2), which is marked by a major positive δ^{13}C isotope excursion (Fig. 3.4). This is a half to one million-year duration anoxic period that led to the extinction of approximately 27% of marine invertebrates, and in particular up to 70% of the ammonite species (Elder, 1989). Works by Donovan et al. (2015b) and Donovan (2016) has documented that in the subsurface of South Texas and outcrops of West Texas the OAE2 event occurs within the Eagle Ford Group, specifically at the base of the Upper Eagle Ford Formation (Figs. 3.5 and 3.6).

[1]Reprinted with permission from "The Eagle Ford Group Returns to Big Bend National Park, Brewster County, Texas" by M. P. Wehner, R. D. Gardner, M. C. Pope, and A. D. Donovan, 2017. *GCAGS Journal*, Volume 6, Pages 161-176, Copyright 2017 by Gulf Coast Association of Geological Societies.

Figure 3.7 is a chronostratigrahic summary of the Cenomanian through Coniancan stratigraphy of Texas. In general, the succession from the base up consists of the Del Rio/Grayson, Buda, Woodbine, Eagle Ford and Austin. The Woodbine Group is early Cenomanian and is identified in the East Texas Basin and not generally defined in South or West Texas. The Eagle Ford Group is middle Cenomanian to late Turonian. Classically, the base of the Coniacian was placed at the base of the Austin. However, a recently published geologic time scale (Ogg et al., 2012) has moved the Turonian/Coniacian boundary up three ammonite zones higher, which now places this boundary well within the Austin Group.

3.2 Previous work in Big Bend

3.2.1 Lithostratigraphy

Udden (1907) published the first geologic descriptions of Big Bend National Park and Brewster County. He divided the Upper Cretaceous (post-Buda) succession into three units: Boquillas Flags, Terlingua Beds, and Tornillo Clays (Fig. 3.8). For his Boquillas Flags, he measured a 585 ft (178 m) thickness, and for the overlying Teringua Beds, an estimated 1250 ft (380 m) thickness. It should be noted that Udden (1907) identified a three-foot thick siliceous bed containing ammonites about half way up his Boquillas Flags. This ammonite-rich bed is now commonly referred to as the *Allocriocreas hazzardi* beds (Cooper and Cooper, 2014).Udden (1907) suggested that the Boquillas Flags correlated with Eagle Ford Group and Terlingua Beds with Austin Group.

Adkins (1932) used what is now referred to as *Allocrioceras hazzardi* beds as the base of the Austin Group in the Big Bend Region and interpreted the 289 ft (88 m) section between it and the top of the underlying Buda as his Boquillas Flags Facies of the Eagle

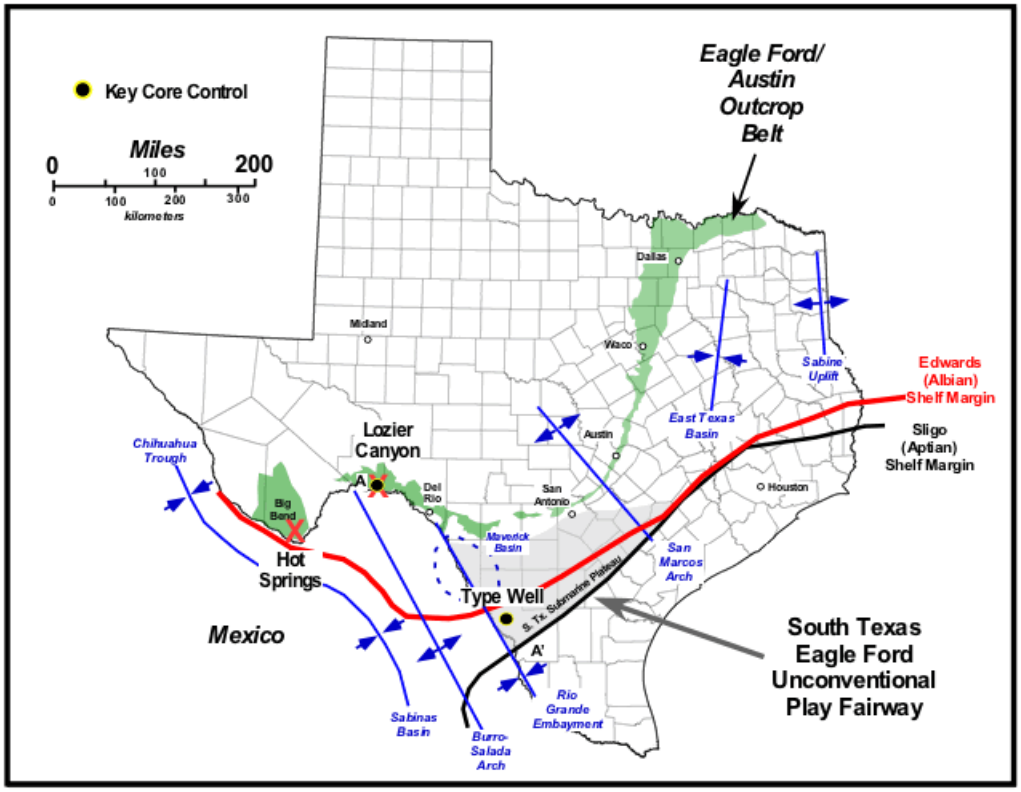

Figure 3.1: Texas map showing the location of Hot Springs in Big Bend National Park (BBNP) along with the locations of the wells used for comparison: BP/SLB Lozier Canyon #1 in Terrell County and a well in Webb County (near the Eagle Ford production trend). The green areas represent the outcrop belt of Eagle Ford and Austin groups in Texas. The blue lines mark the axes of prominent archs/uplifts and basins/troughs during the late Cretaceous. The red line marks the edge of the Edwards (Albian age) shelf margin and the black one is the older Aptian Sligo reef margin. This map is based on maps in Donovan (2015), Donovan et al. (2015b), and Donovan (2016).

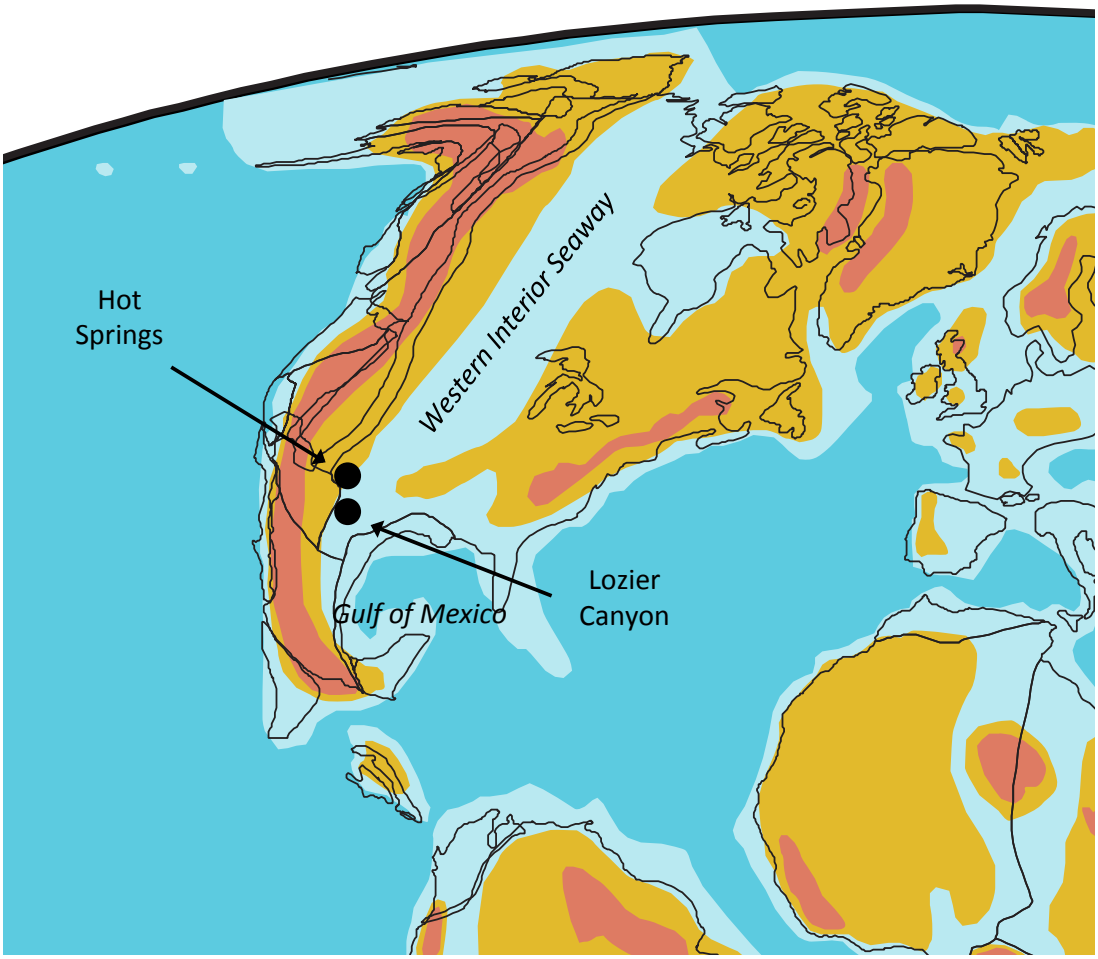

Figure 3.2: A paleogeographic reconstruction of North America circa 90 Mya based on Scotese (1999) where the horizontal is the paleoequator. The red represent highlands while the orange is for lowlands. For the oceans, the light blue is shallow and the darker blue is deep water.

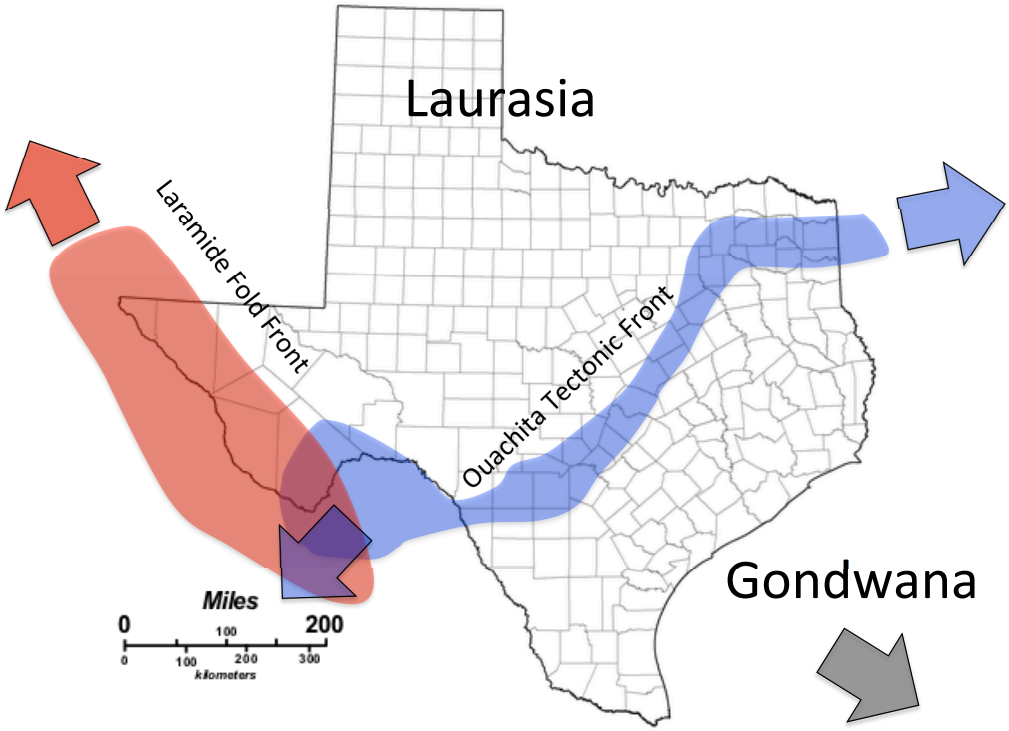

Figure 3.3: A map showing the positioning of the Ouchita Tectonic Front formed during the Pennsylvanian and Permian when Pangaea formed. This had an influence on the Mesozoic paleotography. And the other major tectonically active area was in the Trans-Pecos was at the end of the Cretaceous and early Paleogene when the Laramide orogeny occurred and the edge of the tectonic province is within the Trans-Pecos area. This orogeny did deform the Eagle Ford Group sediments in this region (Ferrill et al., 2016).

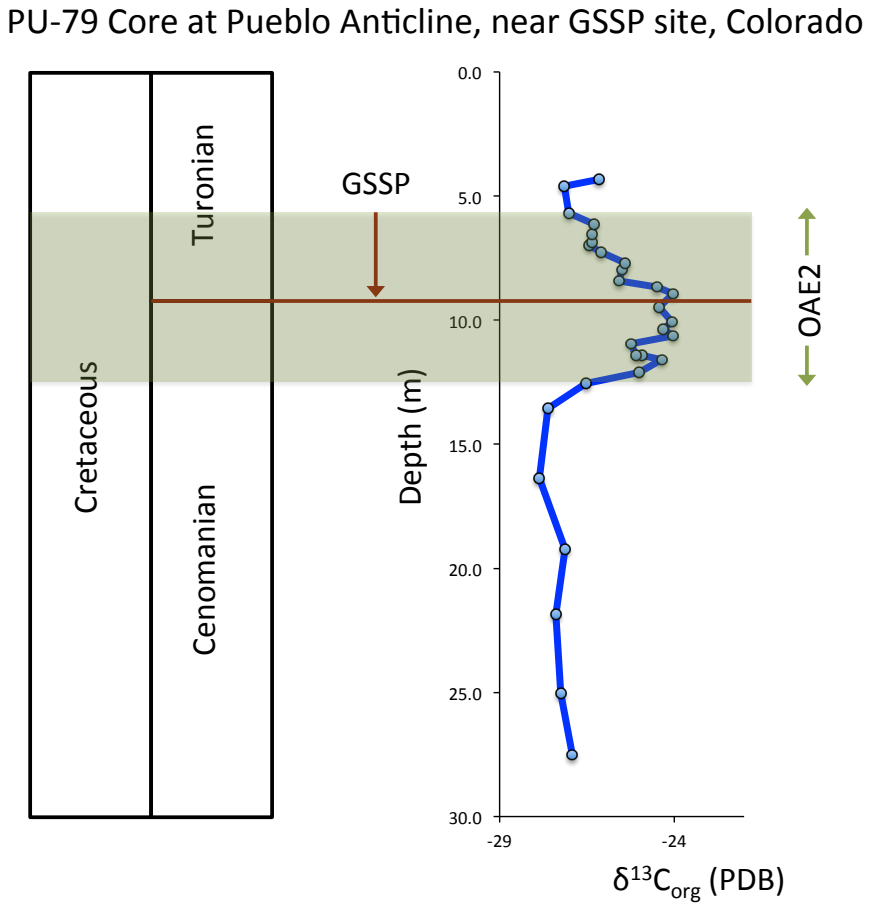

Figure 3.4: An example of the carbon isotope (δ^{13}C) profile of the Ocean Anoxic Event 2 (OAE2) as shown by the isotope profile from the Bridge Creek Member of Greenhorn Formation at the GSSP section near Pueblo, Colorado. The GSSP outcrop is described in detail by Kennedy et al. (2005). The organic δ^{13}C data is from Pratt and Threlkeld (1984) and various versions from this data exist, like Ogg et al. (2012). The shaded area covers the duration of OAE2 as interpreted by Kennedy et al. (2005).

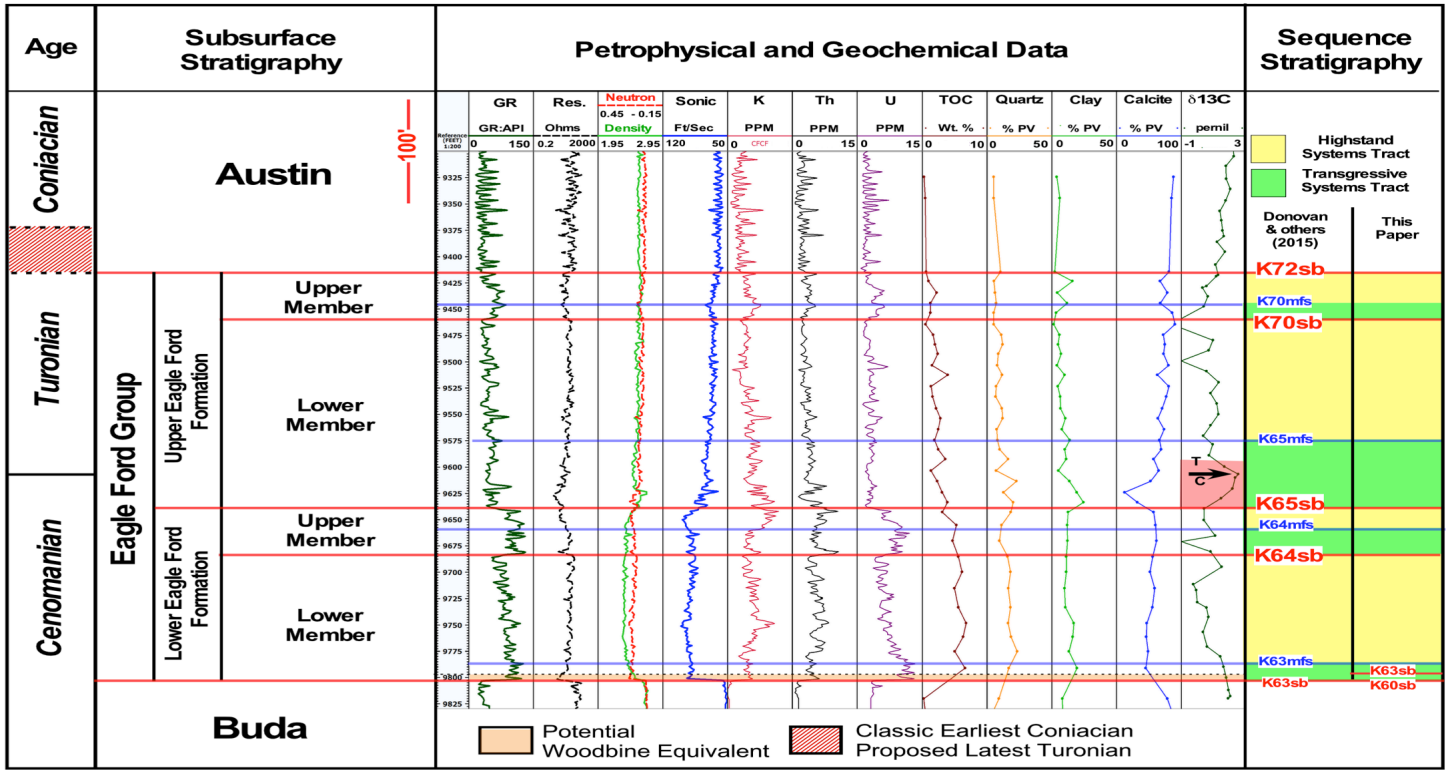

Figure 3.5: A South Texas well (Webb County) is shown with its well logs and petrophysical lab data. The area shaded in a red-pink color, just above the K64sb represents the Ocean Anoxic Event 2 (OAE2), identified based on a positive δ^{13}C curve and matching micro- and nannofossil biostratigraphy (Corbett and Watkins, 2013; Corbett et al., 2014; Lowery et al., 2014). The red-hatched area in geologic age column between Turonian and Coniacian is the time interval that used to be Coniacian (pre-2004 definition) but is considered Turonian under the current iteration of the geologic time scale, like (Ogg et al., 2012). This figure is based on versions presented in Donovan et al. (2015a,b), and Donovan (2016).

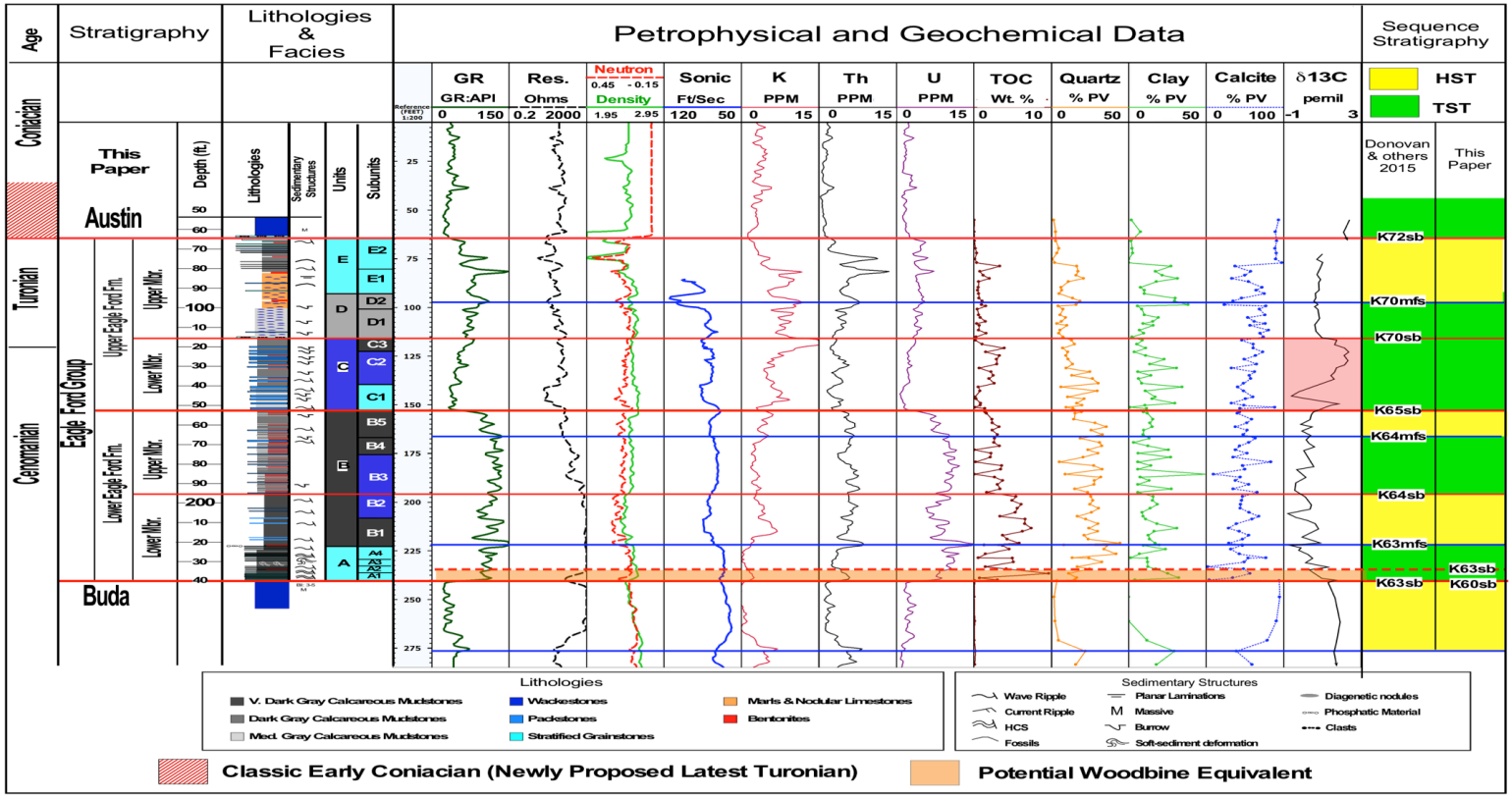

Figure 3.6: For the Lozier Canyon area in Terrell County, West Texas, well log and laboratory petrophysical data is shown from the research borehole, BP/SLB Lozier Canyon #1. The area shaded in a red-pink color between K65sb and K70sb represents the OAE2 mostly based on the δ^{13}C curve. And the orange rectangle above the Buda is the interpreted Woodbine Group equivalent. Like in Figure 5, red-hatched area in the geologic time column is Coniacian under pre-2004 definitions of the Coniacian. This figure is based on versions presented in Donovan et al. (2015a,b), and Donovan (2016).

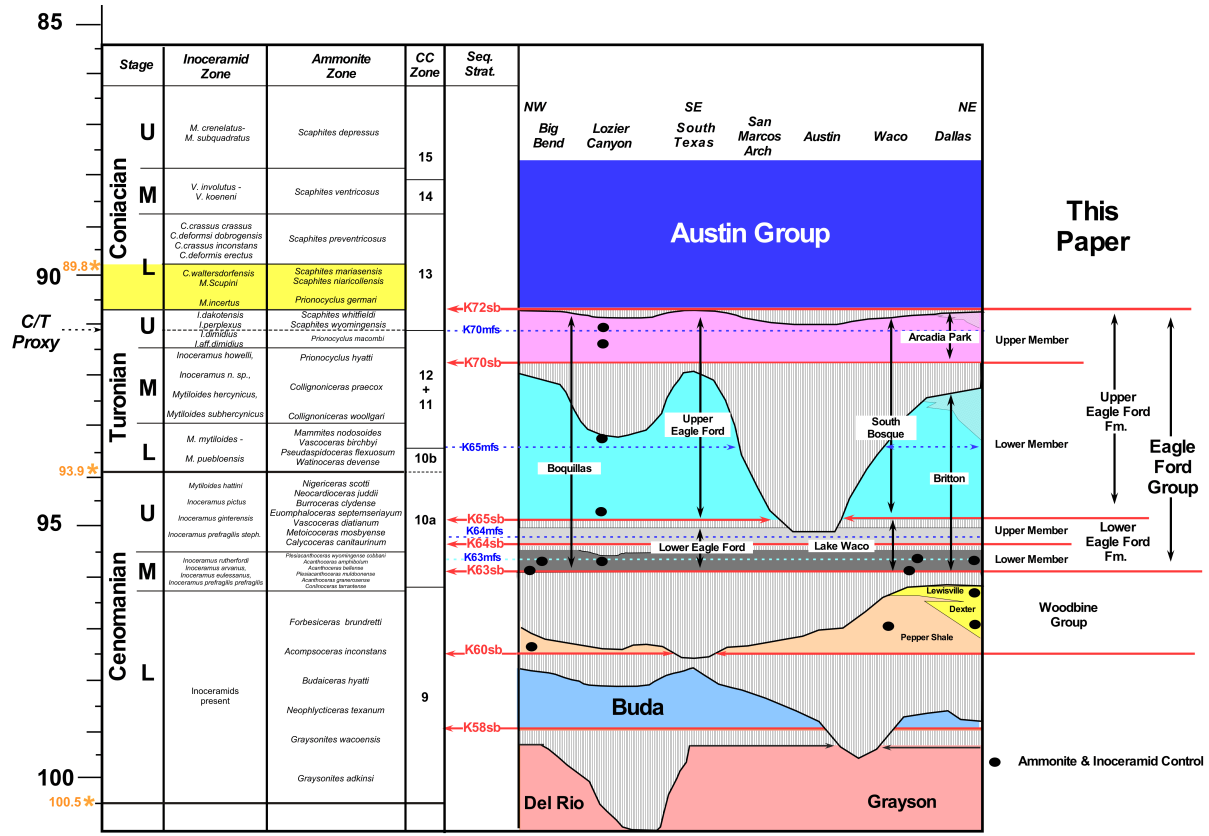

Figure 3.7: A chronostratigraphy for the Cenomanian through Coniacian for Texas going from Big Bend National Park to Dallas, mostly following the outcrop belt as shown in Figure 1 of this paper. This plot record common regional lithostratigraphic terms and graphically records hiatuses with vertical lines as constrained by published ammonite/inoceramid biostratigraphy (Cobban et al., 2008; Kennedy and Cobban, 1990). This figure is based on Donovan et al. (2015a,b).

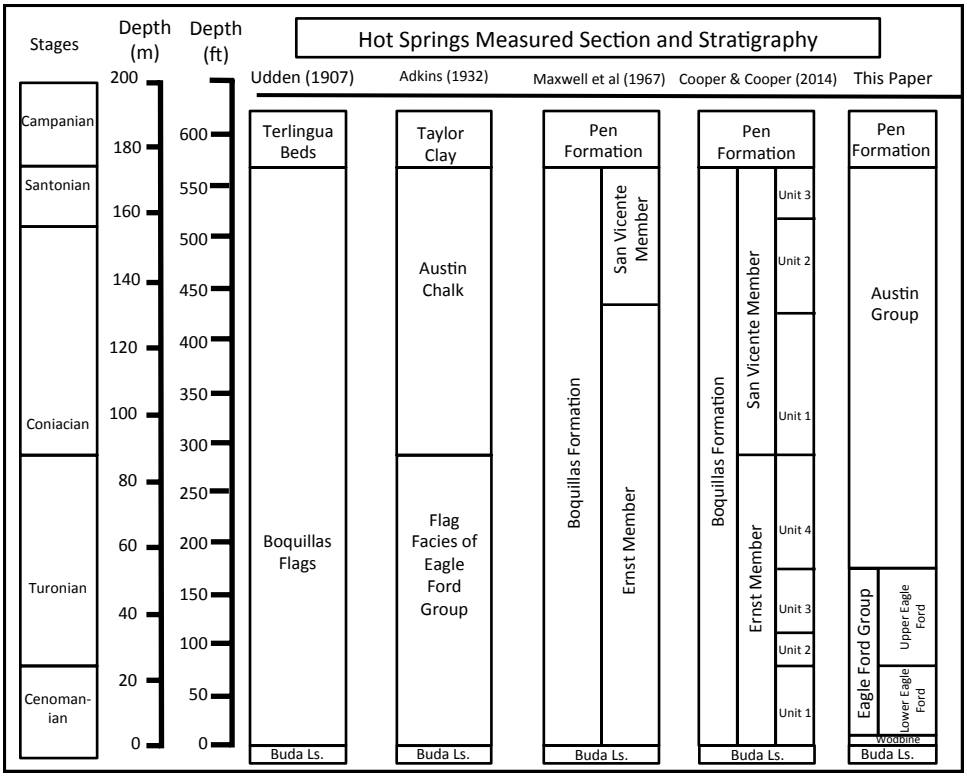

Figure 3.8: Comparison of the stratigraphic nomenclature for the Upper Cretaceous stratigraphic units in the Big Bend area in Brewster County, Trans-Pecos, Texas.

Ford Group. Maxwell et al. (1967), however, rejected Adkins (1932) proposed (Eagle Ford/Austin) nomenclature for the Big Bend Region and named Udden's Boquillas Flags, the Boquillas Formation. He also divided his Boquillas Formation into a lower Ernst Member and an upper San Vicente Member. The contacts of these formations, however, differed from the Eagle Ford/Austin contact proposed by Adkins (1932). Cooper et al. (2007), however, redefined the San Vicente Formation, and used the *Allocrioceras hazzardi* beds to define its base (Fig. 3.8). In this updated framework, Adkins (1932) Eagle Ford and Austin groups equated respectively to the new Ernst and San Vicente members of Boquillas Formation as defined byCooper et al. (2007) .

3.2.2 Previous work: south and west Texas

In the subsurface of South Texas, strata between the Buda and Austin are referred to as the Eagle Ford Group (e.g. Fig. 3.5). The base of the Eagle Ford is marked by a distinct gamma ray (GR) increase driven by an increase in U, as well as Th and K content, along with an increase in total organic content (TOC) content, and decrease in carbonate content. The base of the overlying Austin is typically marked by a change from a funnel- to blocky-GR profile driven by a drop in U, K, and Th content, along with a drop in clay and slight increase in carbonate and quartz content (Fig. 3.5). Biostratigraphically, the classic base of the Coniacian also marks the base of the Austin.

The Eagle Ford Group, in turn, is commonly divided into two formations: an organic-rich Lower Eagle Ford Formation and an upper (carbonate-rich) Upper Eagle Ford Formation (Fig. 3.5). The base of the Upper Eagle Ford is marked by a distinct GR drop, driven by a major decrease in U content, and the onset of a blocky GR profile. In the subsurface of South Texas, the geochemical proxy for the OAE2 (the positive δ^{13}C isotope excursion) occurs at the base of the Upper Eagle Ford Formation.

Texas to the Lozier Canyon outcrops of West Texas (Fig. 3.5). Like the subsurface of South Texas, the Eagle Ford Group in outcrop is bounded by the Buda Formation below and by the Austin Group above (Fig. 3.6). In outcrop, like the subsurface, the base of the Eagle Ford is marked by a distinct GR increase driven by an increase in U, as well as Th and K content. Above the boundary an increase in TOC, clay, and quartz content occurs, as well as a decrease in carbonate content. Lithologically, the Buda/Eagle Ford boundary is marked by a sharp change from wackstones below, to interbedded grainstone beds and carbonate mudstones above. Similar to the subsurface, the base of the Austin Group is

marked by a change from a funnel to blocky GR profile driven by a drop in U, K, and Th content. Lithologically, the boundary is marked by a sharp change from interbedded grainstones and carbonate mudstones below to carbonate mudstones (chalks) above. Rip-up clasts of underlying Eagle Ford are also locally observed in the basal Austin (Donovan et al., 2015b). Biostratigraphically, the classic base of the Coniacian also marks the base of the Austin.

Within the Eagle Ford Group (Fig. 3.6) an organic-rich, higher-GR Lower Eagle Ford Formation and carbonate-rich, lower-GR Upper Eagle Ford Formation can also be defined. A distinct GR drop driven by a major drop-off in U-content marks the base of the Upper Eagle Ford. In the Lozier Canyon outcrops, as in the subsurface of South Texas, the geochemical proxy for the OAE2 also occurs in the basal portions of the Upper Eagle Ford Formation (Figs. 3.5 and 3.6).

3.3 Methods

3.3.1 Introduction

This paper follows a modified version of Gradstein et al. (2012) time scale (Fig. 3.7). We use the classic (pre-2012) boundary for the base of the Coniacian, which corresponds to the base of the Austin Group throughout Texas. The ammonite groups that were traditionally included in the basal Coniacian, now uppermost Turonian, are highlighted in yellow (Fig. 3.7). It should be noted that the *Allocriocreas hazardi* beds essentially correspond to the new proposed base of Coniacian, the *Cremnoceramus deformis erectus/Scaphites preventricosus* (inoceramid/ammonite biozone pair) biozone. The association of the *A. hazzardi* biozone with the *C. deformis erectus* biozone was confirmed by Hancock and Walaszczyk (2004). For comparing ammonite/inoceramid biozonation of the Western Interior Seaway

(WIS) and the local ammonite/inoceramid biozonation, we used Cobban et al. (2006) and Cobban et al. (2008), respectively.

For naming sequences and comparison with previously published works on Eagle Ford Group in West Texas, the naming system for sequences uses an alpha-numeric scheme where the first letter is for geologic period (in this case, K is for Cretaceous), then the two numeric digits are assigned in ascending order from base of the Cretaceous series, and the final two letters are modifiers that indicate the type of sequence stratigraphic surface. For instance, sb is for sequence boundary and ts is for transgressive sequences. This naming scheme has been used in many previous publications (Donovan and Staerker, 2010; Donovan et al., 2012; Gardner et al., 2013).

3.3.2 Measured section

For this study, the Hot Springs section was measured at the location near the section reported by Miller (1990) at coordinates, 29.182447°N and 102.993501°W, just 100 ft (35m) from Hot Spring Trail (Fig. 3.9). This location is 0.22 mi (0.36 km) from the section proposed as the type section for Ernst Member of the Boquillas Formation (Cooper et al., 2007). The outcrop was measured from 6 ft (2 m) below the Buda-Boquillas contact up to 41 ft (12.5 m) above the *A. hazzardi* bed that has been noted by all previous workers, including Udden (1907). A bed-by-bed description was made and the beds were classified using Dunham's classification. A total of 172 hand-sized samples were taken from the outcrop with a mean sample interval of 2 ft (60 cm). While in the field, a handheld gamma-ray scintillometer was used to acquire spectral gamma ray data (U, Th, and K content) at 30 cm (1 ft) intervals. The scintillometer is a Terraplus RS-230 Gamma Ray Spectrometer. The total gamma ray (TGR) in API units is estimated using the formula of

Herron and Herron (1996). For 48 of the 172 hand-size samples, a total of 50 thin sections were made for confirmation of lithology and allochem type. When petrographic observations are noted, the lithology is reported using Folk's classification since that is ideal for petrography.

3.3.3 Geochemistry

All 172 hand-sized specimens were analyzed with energy-dispersive x-ray fluorescence (ED-XRF) for major and trace element concentrations. The ED-XRF data were acquired using a Thermo Scientific Niton XL3t 950 GOLDD+ Analyzer (up to 36 elements are detected using the Cu/Zn filter). The XRF analyzer was calibrated using the method described by Rowe et al. (2012). For stable isotope analysis (δ^{13}C and δ^{18}O) 53 of the 172 samples were analyzed using a Thermo Scientific Kiel IV Automated Carbonate Device coupled to a Thermo Scientific MAT 253, which reside at the Stable Isotope Geoscience Facility at Texas A&M University. The mean interval between isotope samples was 6.3 ft (1.9 m).

3.3.4 Paleontology

The work of Cobban et al. (2008) has a good summary of the ammonite zones reported from the Big Bend National Park area, mostly from the Hot Springs area. The following ammonite biozones were reported. In the basal 16 inches (0.5 m) above the top of the Buda, an *Acompsoceras inconstans* fauna (early Cenomanian) is indicated by the presence of *Moremanoceras bravoense* and *Euhystrichoceras adkinsi*. About 10 ft (3.5 m) above the top of Buda, an *Acanthoceras bellense* fauna of the middle Cenomanian is suggested by *Inoceramus arvanus*, a mollusc. Cobban et al. (2008) suggests that an ammonite reported by Cooper et al. (2008) as *Calycoceras sp*. at 12 ft (4 m) above the top of Buda

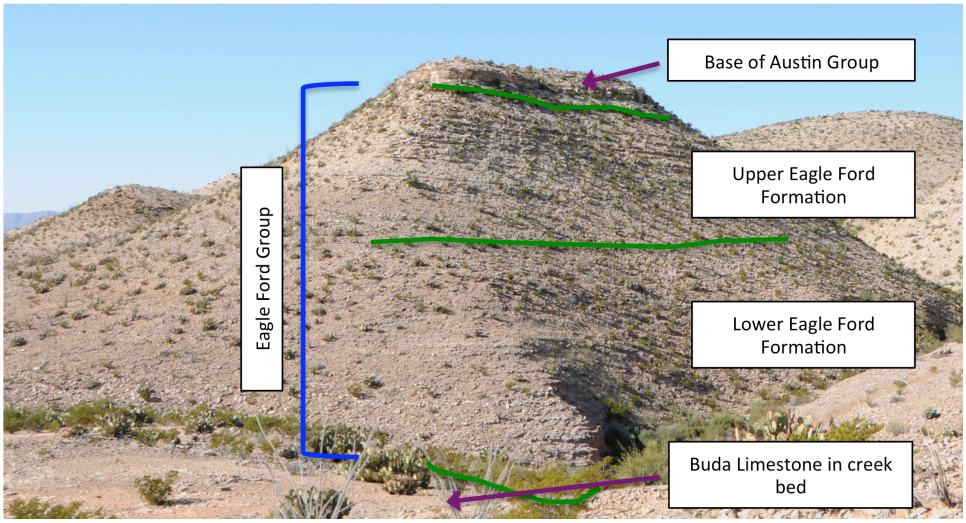

Figure 3.9: Photo of the Hot Springs Outcrop site measured for this study. The blue bracket marks the vertical extent of allostratigraphic Eagle Ford Group; the green lines delineate the alloformations: Upper Eagle Ford and Lower Eagle Ford.

is actually *A. bellense*. At about 17 ft (5 m), a collection of *Ostrea beloiti*, *Tarrantoceras sellardsi*, and *Turrilites acutus* suggests an *A. amphibolum* biozone. Now the following biozones were reported by Cobban et al. (2008) along with Cooper and Cooper (2014), but their data cannot be reliably matched to the Hot Springs measured section of this study: *Metoicoceras mosbyense*, *Euomphaloceras septemseriatum*, *Pseudaspidoceras flexuosum*, *Collignoniceras woollgarii*, *Prionocyclus hyatti*, *P. novimexicanus*, *P. quadratus*, *P. germari*, *Forresteria peruana*, and *Allocrioceras hazzardi*. The last one, *A. hazzardi*, was confirmed from 289 ft (88m) at Hot Springs.

For this study, Jim Pospichal of BugWare, Inc. did a quantitative assessment of 41 of the 172 hand-sized samples for calcareous nannofossil biostratigraphy. Sampling range for nannofossil biostratigraphy ranges from 3 ft (1 m) below the Buda-Eagle Ford contact through 289 ft (88 m) above the Buda-Eagle Ford contact within, which is 99 ft (33 m) above the Eagle Ford-Austin boundary.

3.4 Big Bend lithostratigraphic interpretation

The lithologic and geochemical data collected for the Hot Springs locality at BBNP are presented in Figures 3.5 and 3.6. Similar to the subsurface of South Texas and Lozier Canyon in West Texas, the top of the Buda is marked by a distinct GR increase, driven by an increase in U, Th, and K content. Lithologically it is marked by a sharp change from wackestones (below) to interbedded grainstones and mudstones (above). One hundred and eighty-five feet above the top of the Buda, a distinct geochemical and petrophysical change, similar to the change at the base of the Austin Group chalks in South Texas and Lozier Canyon in Terrell County in West Texas was noted. At this proposed boundary, the GR profile becomes distinctly blocky, due to low U, Th, and K content. At this boundary, a change from more variable to low carbonate, silica, and aluminum (Al) content occurs. Lithologically, a change from interbedded carbonate grainstones and mudstones below, to carbonate mudstones above occurs. Furthermore, classic Late Turonian (Eagle Ford Group equivalent) through earliest Coniacian (Austin Group equivalent) inoceramids of the respective *Inoceramus perplexus* and *Mytiloides scupini* zones (Fig. 7) were reported between 183 ft and 194 ft (55.8 m and 59 m, respectively) at this locality Cobban et al. (2008). Based on these various criteria, the Eagle Ford/Austin contact is placed 185 ft (56.5 m) above the top of the Buda at the Hot Springs locality (Figs. 3.10 and 3.11). In general, this position corresponds to the boundary between units 3 and 4 of Cooper and Cooper (2014) Ernst Member of the Bouquillas Formation (Fig. 3.8).

Within the newly defined Eagle Ford Group at Hot Springs, a distinct GR drop due to a major decrease in U, Th, and K occurs at 99 ft (33 m) above the top of the Buda (Fig. 3.10). A major increase in carbonate content and decrease in silica content also occurs at

this point. Based on these criteria, the contact between the Lower and Upper Eagle Ford formations is placed at this distinct geochemical boundary. For historical context Cooper and Cooper (2014) placed the boundary of units 2 and 3 of their Ernst Formation at this same position. It should be noted however, that the geochemical proxy for the OAE2, the δ^{13}C positive isotope excursion was not observed at the Hot Springs locality (Fig. 3.10).

Figure 3.12 is a lithostratigraphic correlation between Hot Springs, Lozier Canyon, and the Swift Fasken #1 well in Webb County. The thicknesses of the Eagle Ford Group and the internal formations similar at Hot Springs and Lozier Canyon: 175 ft (53 m) at Lozier and 185 ft (56.5 m) at Hot Springs. At Lozier, the Lower Eagle Ford is 96 ft (32 m) thick vs. 99 ft (33 m) at Hot Springs. The Upper Eagle Ford is 79 ft (24 m) thick at Lozier Canyon, while it is 85 ft (26 m) thick at Hot Springs. This suggests a similar deposition setting on the flooded Comanche Platform for the Eagle Ford Group at both Hot Springs and Lozier Canyon. This is in contrast to Swift Fasken in Webb County, which is substantially thicker at about 170 ft (52 m) for Lower Eagle Ford and 212 ft (65 m) for Upper Eagle Ford.

3.5 Big Bend insights into the Upper Cretaceous sequence stratigraphy of Texas

3.5.1 Overview

Based on work on the outcrops and subsurface across Texas, Donovan et al. (2015a,b) concluded that both the Woodbine and Eagle Ford were unconformity-bounded depositional sequences (Fig. 3.7). They outlined that the Woodbine was an early Cenomanian siliciclastic-dominated sequence whose present distribution was primarily restricted to East and Central Texas. In terms of the surfaces defined, they placed their K60sb at its base and K63sb at its top (Fig. 3.7). The Eagle Ford was outlined as a middle Cenomanian to late Turonian organic-rich sequence, which changed from more siliciclastic-rich to the

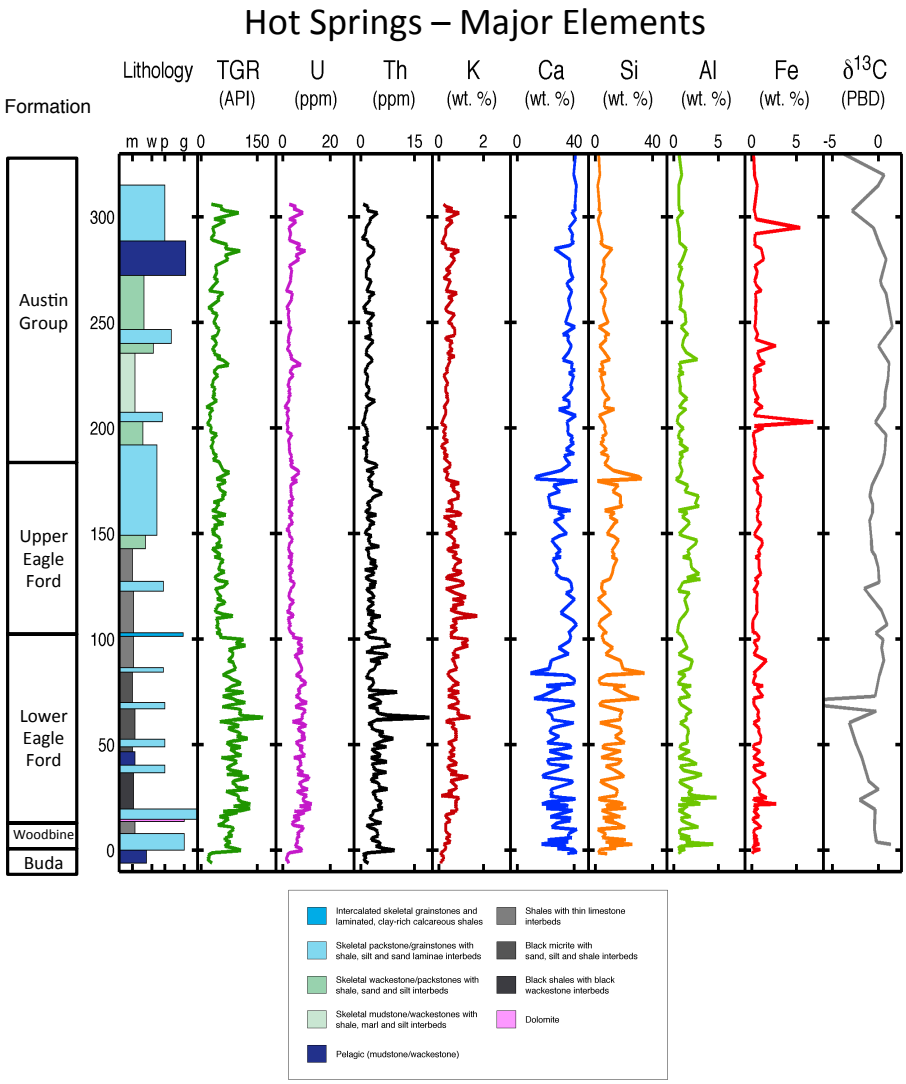

Figure 3.10: The lithostratigraphy combined with spectral gamma ray logs (U, Th, and K) and selected major elements from XRF (Ca, Si, Al, Fe) for the Hot Springs outcrop in Big Bend National Park, Brewster County, Texas. The curve labeled TGR is the total gamma ray in API units as estimated using the formula of Herron and Herron (1996). Also a bulk carbonate δ^{13}C curve is included. The combination of these curves shows bulk geochemistry (proxying for bulk mineralogy) associated with the spectral gamma ray curves and as well as comparison with the bulk lithology as determined from field observation. The bulk carbonate δ^{13}C curve does not preserve an obvious isotopic excursion (had been predicted to at 100 ft or 33 m) as initially expected at the beginning of the study.

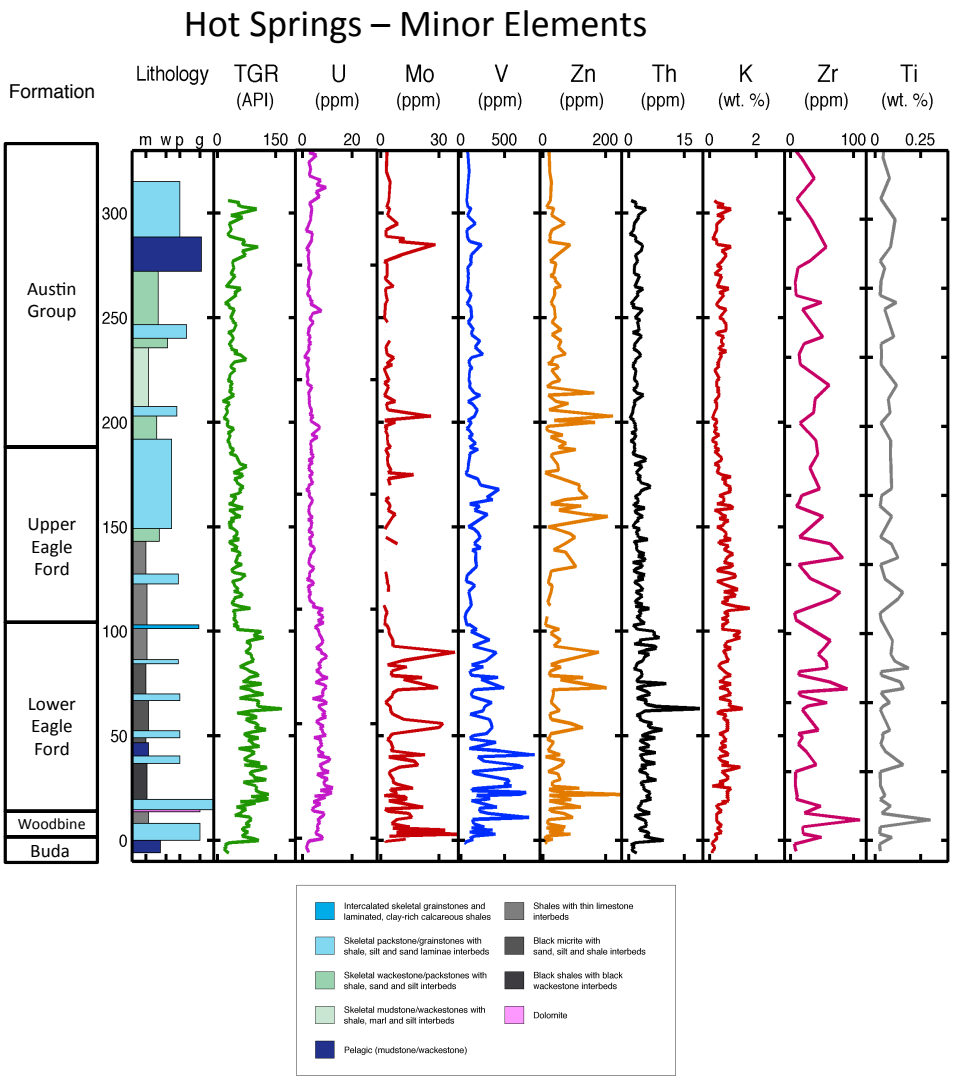

Figure 3.11: For the Hot Springs outcrop in Big Bend National Park, the lithostratigraphy and total gamma ray (TGR) are displayed with the following trace elements obtained from XRF: Mo, V, Zn, Zr, and Ti. The elements, U, Th, and K are the from the handheld spectral gamma ray log. The elements are arranged by proxy type. The redox elements are grouped together: U, Mo, V, and Zn. The terrestrial and/or detrital elemental proxies are Th, K, Zr, and Ti.

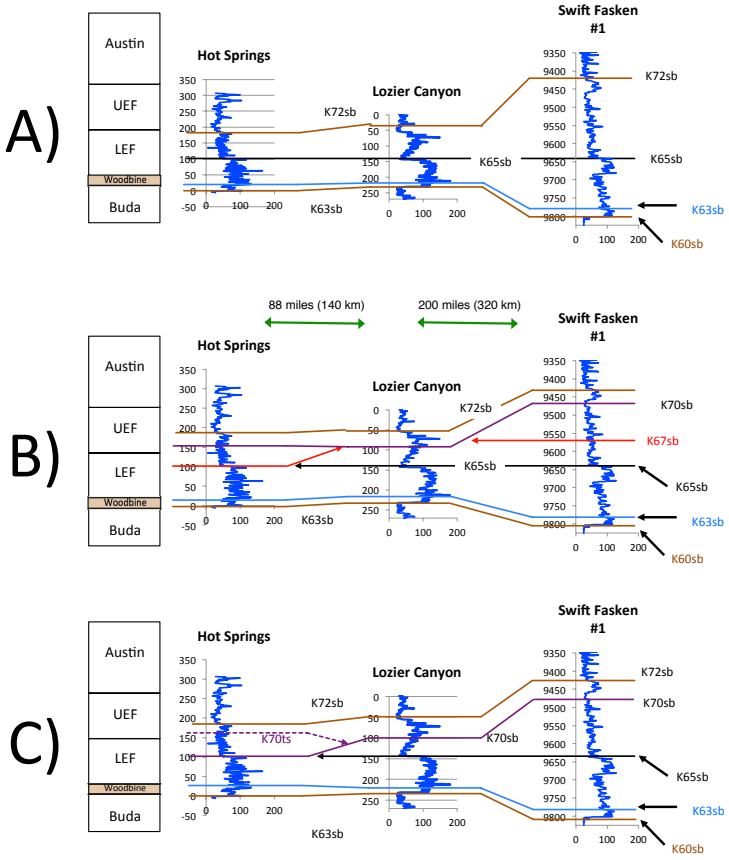

Figure 3.12: A correlation diagram showing three interpretations of the sequence stratigraphy for Hot Springs in Big Bend Nation Park, Lozier Canyon in Terrell County, and Swift Fasken #1 in Webb County. The first scenario (correlation A) is that the isotope signal is obscured by weathering and poor outcrop preservation. The second scenario (correlation B) that there is a previously unknown sequence preserved at Hot Springs that is between K65 and K70 sequences. The third scenario (correlation C) has the Hot Springs section containing an expanded K70 sequence that has the lowstand section not normally preserved in previously studied outcrops. The thin brown layer is the early Cenomanian section that is time-equivalent to Woodbine Group of East Texas Basin.

northeast to more carbonate-prone towards the southwest across Texas. In terms of the surfaces defined, they placed their K63sb at its base and K72sb at its top (Fig. 3.7).

Donovan et al. (2015a, 2012), Gardner et al. (2013), and Donovan (2016) also divided the Eagle Ford into four high-frequency sequences, two in the Lower Eagle Ford Formation, and two in the Upper Eagle Ford Formation (Fig. 3.7). They referred to these sequences as the K63, K64, K65, and K70 sequences. The K63 Sequence, which was also referred to as Lower (Lozier Canyon) Member of the Lower Eagle Ford Formation, was described as a middle Cenomanian organic-rich sequence. The K64 Sequence, which was also referred to as the Upper (Antonio Creek) Member of the Lower Eagle Ford Formation, was defined as a late Cenomanian uranium- and thorium- (bentonite) rich and organic-poor sequence. The K65 Sequence, which was also referred to as the Lower (Scott Ranch) Member of the Upper Eagle Ford Formation, was defined as a latest Cenomanian to middle Turonian carbonate-rich sequence, characterized by the presence of the OAE2, and its associated positive δ^{13}C isotope excursion, at its base. The K70 Sequence, which was also referred to as the Upper (Langtry) Member of the Upper Eagle Ford Formation was defined as late middle to late Turonian sequence characterized by the presence of abundant burrows, hard-bodied fossils, and distinct bentonite beds. Each of the four defined sequences also had distinct mappable maximum flooding surfaces defined respectively from the base up as the K63mfs, K64mfs, K65mfs, and the K70mfs.

3.5.2 Woodbine remnant?

At the Hot Springs locality, the basal 10 ft (3.3m) of the section measured above the Buda Formation, consists of medium-bedded, hummocky-stratified packstones to grainstones, locally interbedded with very thin carbonate mudstone or bentonite beds (Fig.

3.13). These strata are overlain by a succession of more distinctly interbedded packstones and carbonate mudstones (Fig. 3.13). The sedimentary structures are suggestive of shallow storm-dominated settings as previously interpreted by Wehner et al. (2015) for basal Eagle Ford outcrops in West Texas. As illustrated on Figure 3.14, a slight drop in uranium and thorium content also occurs above the contact between the two different facies at 10 ft (3.3 m) on the measured section. Interestingly, Cobban et al. (2008) reported the ammonites *Moremanoceras bravoensis* and *Euhystrichoceras adkini*, which were collected in the grainstone beds approximately 1.5 ft (0.5 m) above the top of Buda at Hot Springs. These early Cenomanian ammonites of the *A. inconstans* ammonite biozone are also present in outcrops of the Woodbine Group along the west flank of the East Texas Basin (Cobban and Kennedy, 1989). Cobban et al. (2008) also reported *Inoceramus arvanus*, which appear to have been collected in the basal portions of the overlying interbedded packestone and carbonate mudstone succession at Hot Spring. They also stated that this inoceramid species is a good marker for the middle Cenomanian *Acanthoceras bellense* biozone, which is also present in the basal portions of the Eagle Ford Group on the western flank of the East Texas Basin (Cobban and Kennedy, 1989). Based on these lithostratigraphic and biostratigraphic relationships, it likely that: 1) the proper placement of the K63sb marking the base of the Eagle Ford Group is 10 ft (3.3 m) above the top of the Buda at the Hot Springs locality; 2) the K60sb, marking the base of the Woodbine Group occurs at 0 ft (0 m) on the measured section coinciding with the top of the Buda at the Hot Springs locality; and 3) the interval between 0 ft (0 m) and 10 ft (3.3 m) on the measured section at Hot Springs represents strata which are coeval to the Woodbine Group in the East Texas Basin.

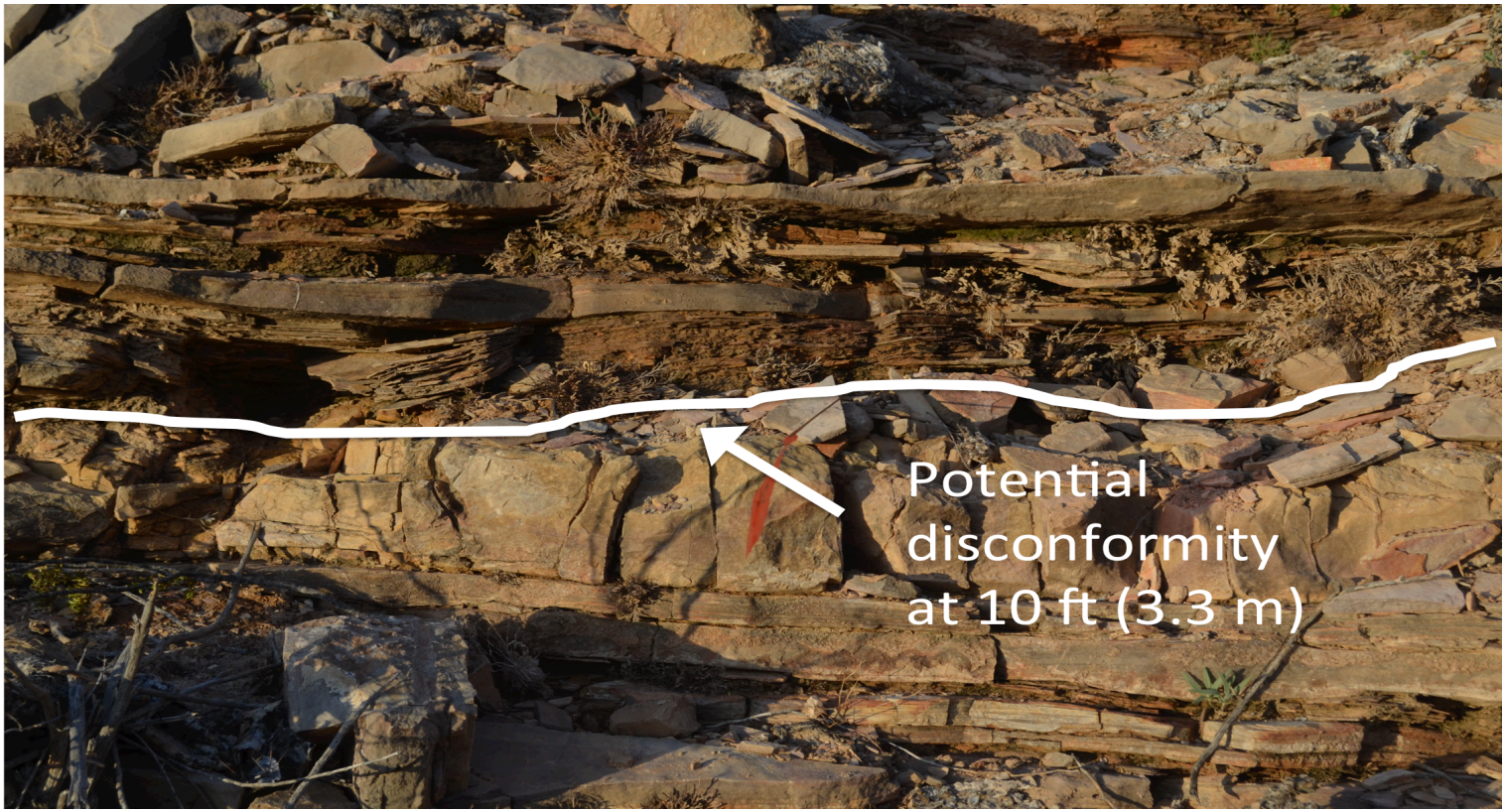

Figure 3.13: An outcrop image of the 10 ft (3.3 m) proposed contact between the Woodbine Group equivalent and Eagle Ford Group at the Hot Springs locality.

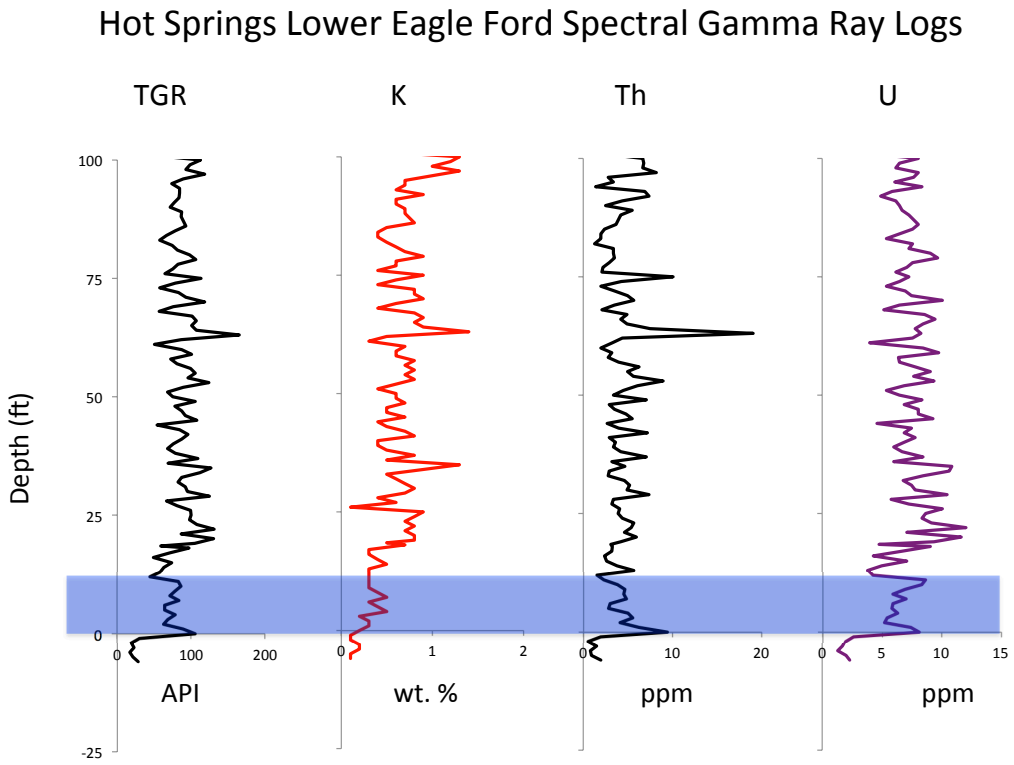

Figure 3.14: A close up of the lower 100 ft (33 m) of the Hot Springs handheld spectral gamma ray logs to show the basal 10 ft (3.3 ft) section that is distinct from the other 90 ft (27 m) by a discontinuity. This break in the spectral gamma ray logs is most apparent in the uranium log and total gamma ray log. The blue-purplish rectangle highlights the interval interpreted in this paper as Woodbine Group equivalent.

3.5.3 Eagle Ford sequence stratigraphy

Based on the various criteria outlined by Donovan et al. (2015a,b) for the depositional sequences within the Eagle Ford in the outcrops from the eastern portions of West Texas (Lozier Canyon), as well as the subsurface of South Texas the following sequence stratigraphic interpretations are made for the Hot Springs locality (Figs. 3.10 and 3.11). Although TOC analysis was not conducted on the samples taken at Hot Springs section, the organic-rich K63 depositional sequence or the Lower Member of the Lower Eagle Ford Formation is interpreted from 10 ft (3.3 m) to 50 ft (15 m) on the measured section at Hot Springs. The interval between 50 ft (15 m) and 99 ft (33 m) at the Hot Springs locality is interpreted as the bentonite-, thorium-, and uranium-rich and organic-poor K64 depositional sequence.

As mentioned previously, the interval between 99 ft (33 m) and 185 ft (56.5 m) is interpreted as the Upper Eagle Ford Formation. Like of Lozier Canyon, and the subsurface of South Texas, a sharp GR drop drive driven by a decrease in uranium content occurs above this contact followed by an overall blocky GR log pattern (Fig. 3.10). While the log character of this boundary and overlying strata are similar at the Hot Springs locality, the specific depositional sequence present at the base of the Upper Eagle Ford Formation at the Hot Springs locality is open to debate (Fig. 3.12).

At Lozier Canyon and the subsurface of South Texas the K65 depositional sequence occurs at the base of the Upper Eagle Ford Formation. This carbonate-prone sequence is characterized by the presence of the OAE2 interval, whose geochemical proxy is a distinct positive δ^{13}C isotope excursion (Figure 3.6). This positive δ^{13}C isotope excursion was not observed at the Hot Springs section at the base of the interpreted Upper Eagle Ford

Formation. As outlined on Figure 3.12, there are at least 3 possible reasons for this.

The first possible solution, as illustrated on Figure 3.12a is that the K65 and K70 depositional sequences are both present, but the K65 sequence is simply missing its classic δ^{13}C positive isotope excursion due to weathering and the failure to collect fresh samples. We have observed this happening at another locality in West Texas, where the excursion was absent in a roadcut along Highway 90 in Val Verde County, but reported in a borehole adjacent to the site (Eldrett et al., 2015b). Denne et al. (2016) predicted this scenario and hinted at earlier by Frush and Eicher (1975). A second possible solution is that another (middle Turonian) depositional sequence (the K67?), which has not previously been identified in our work in West Texas, marks the base of the Upper Eagle Ford at Hot Springs (Fig. 3.12b). In this scenario, a new K67 depositional sequence is interpreted from 99 ft (33 m) to 160 ft (49 m) on the measured section overlain from 160 ft to 185 ft (49 m and 56.5 m, respectively) by the K70 Sequence, or the Upper Member of the Upper Eagle Ford. A third possible solution is that the entire Upper Eagle Ford succession at Hot Springs represents an expanded K70 Sequence or the Upper Member of the Upper Eagle Ford Formation (Fig. 3.12c). In this scenario, 99 ft (33 m) to 160 ft (49 m) on the measured section would be interpreted as the K70 lowstand, while 160 ft to 185 ft (49 m and 56.5 m, respectively) would represent the K70 transgressive and highstand deposits. Clearly additional biostratigraphic and/or chronostratigraphic (absolute age dating) work needs to be conducted at the Hot Springs locality to properly constrain the various interpretations.

3.6 Conclusion

Correlations from Lozier Canyon in Terrell County (West Texas) revealed that the Boquillas Formation at Hot Springs in Brewster County (West Texas) is equivalent to both the

Eagle Ford and Austin groups as presently defined in the Lozier Canyon region of West Texas. The Eagle Ford Group defined herein at Hot Springs is equivalent to strata previously referred to as Units 1 to 3 of the Ernst Member of the Boquillas Formation (Cooper and Cooper, 2014). Our work also suggests that Unit 1 of the Ernst Member at Hot Springs is equivalent to the Lower Eagle Ford in Lozier Canyon, while Units 2 and 3 of the Ernst Member at Hot Springs is equivalent to the Upper Eagle Ford at Lozier Canyon. As defined in our work the new Eagle Ford/Austin contact proposed at Hot Springs is coeval to the Eagle Ford/Austin contact as defined in Lozier Canyon, as well as in the subsurface of West Texas. The contact occurs at the classic (pre-2012) base of the Turonian stage. The newly proposed (Gradstein et al., 2012) base Coniacian occurs well above the base of the Austin Chalk in both Terrell and Brewster counties. At Hot Springs, the basal 10 ft (3.3 m) succession, directly overlying the Buda, contains hummocky stratified grainstones (Pope et al., 2017), which contains an early Cenomanian fauna near its base. This 10 ft (3.3 m) interval is interpreted as the K60 depositional sequence, which is coeval to the Woodbine Group in the East Texas Basin. The K63sb, marking the base of the Eagle Ford Group, is placed at 10 ft (3.3 m) in the Hot Springs section, and the K72sb marking the base of the Austin Group is placed at 185 ft (56.5m) in the Hot Springs section. A distinct GR drop, driven by a decrease in uranium content, which also corresponds to a distinct increase in carbonate content, at 99 ft (30 m) on the measured section, is picked as the contact between the Lower Eagle Ford Formation and the Upper Eagle Ford Formation. Within the Lower Eagle Ford Formation, the K63 and K64 Depositional Sequences defined in Lozier Canyon appear also to be present at Hot Springs. Within the Upper Eagle Ford Formation, the characteristic positive δ^{13}C isotope excursion that typically marks the base of the Upper Eagle Ford, as well as the K65 Sequence, the Lower (Scott Ranch) Member of the Upper Eagle Ford Formation, was not observed at Hot Springs. This may be due to: 1) weathering, 2) the presence of a new (previously unidentified) depositional sequence at the

base of the Upper Eagle Ford Formation at Hot Springs, or 3) the presence of an expanded K70 Sequence, the Upper (Langtry) Member of the Upper Eagle Ford Formation.

4. EUXINIA, ORGANIC CARBON AND SULFUR IN THE EAGLE FORD GROUP AND ITS TIME-EQUIVALENT UNITS IN THE TRANS-PECOS, WEST TEXAS

4.1 Introduction

4.1.1 Paleogeographic and stratigraphy

West Texas lies is at the convergence of several key geologic features, including the southern opening of the Western Interior Seaway (WIS), the epicontinental seaway that formed in the central USA for most of the Upper Cretaceous, and the western edge of the Comanche Platform, a largely passive, lower Cretaceous carbonate platform that stopped growing by the early Cenomanian (Fig. 4.1). Additionally, west of the Comanche Platform and the WIS, lay the land area of Laramidia, formed by the Sevier and Laramide orogenies. Flexural warping of the continent east of the orogenies allowed the WIS to remain flooded while Laramidia experienced mountain-building (Kauffman and Caldwell, 1993; Pang and Nummedal, 1995). It should be noted that Mexico, which lay to the southwest, during was composed of multiple microcontinent blocks that depending on the basement composition and orientation of stress field either formed troughs or uplifts (Martini and Ortega-Gutiérrez, 2017; Shepard and Walper, 1982).

Eagle Ford Group sediments, mostly organic-rich mudstone (mixed siliciclastic and carbonate fine-graineed units) are well studied from the East Texas Basin region down to the Maverick Basin adjacent to the US-Mexico border (Hentz and Ruppel, 2010; Tian et al., 2012). However, the Eagle Ford Group sediments in west Texas have not been integrated with correlative sediments in the East Texas and Maverick Basins. Ammonite and inoceramid biostratigraphy and lithostratigraphy have been used to correlate equivalent-aged sediments in West Texas. Challenges that prevent the correlation of Eagle Ford Group

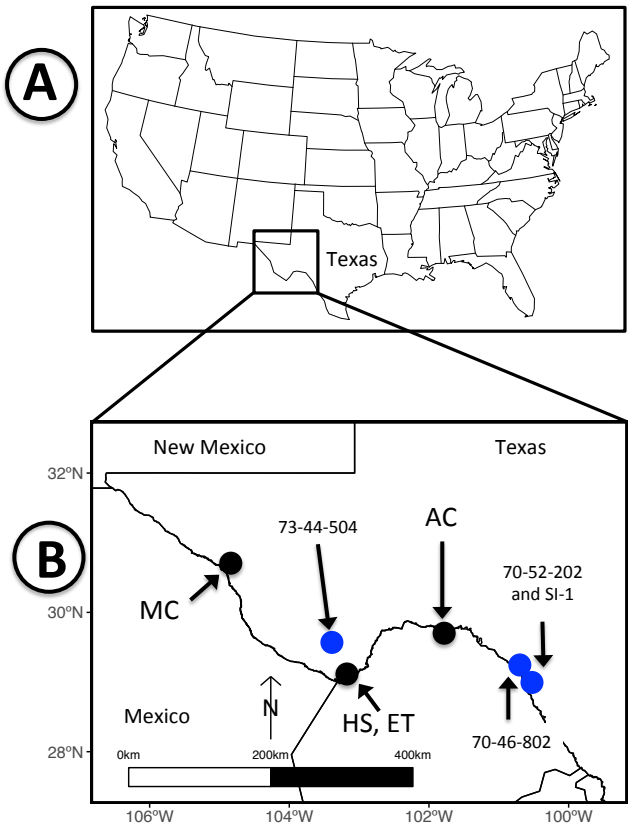

Figure 4.1: Map showing the locations of the outcrops and wells used in this study. The study area is in west Texas (Trans-Pecos) area and is both south and west of the Permian Basin. Part A shows the Trans-Pecos area in context of the whole USA; part B shows outcrop and well locations in the Trans-Pecos region. Black dots are outcrop locations and blue dots are wells.

sediments are at least three-fold. One, there is a lack of well-vetted and stable correlation between the biostratigraphic data (i.e. ammonite biozones with nannofossil biozones). Two, there is a lack of outcrop data that can be directly compared to subsurface data (i.e. gamma ray, resistivity, and porosity logs). And three, there are inconsistencies in the lithostratigraphic nomenclature of Eagle Ford Group sediments in west Texas (Trans-Pecos). At least three formations appear to be equivalent or partially equivalent to Eagle Ford Group: Boquillas, Chispa Summit, and Ojinaga (Cooper and Cooper, 2014; Maxwell et al., 1967; McNulty et al., 1985; Wehner et al., 2017).

Two relatively new techniques enable us to integrate outcrop and core data in stratigraphic correlation: handheld gamma-ray scintillometers passively measure gamma radiation from rock in outcrop producing data exactly analogous to the gamma ray well log common in the petroleum exploration industry; handheld x-ray fluoresence (ED-XRF) spectrometry yields a wealth of elemental data tied to trends in mineralogy, lithology, and sedimentary geochemistry, and has been used to reconstruct the redox chemistry of ancient oceans (Rowe et al., 2012, 2008). The use of stable isotopes to build high-resolution stratigraphy is a well-established procedure that works well in carbonate sections and not as well in siliciclastic sections. Regional and continental correlations using stable isotopes during the Cenomanian and Turonian are common (Jarvis et al., 2016). Some stable isotope data for Eagle Ford are available but as now no attempt has been made for a regional correlation in Eagle Ford, particularly in West Texas (Donovan et al., 2012; Eldrett et al., 2014; Fairbanks, 2012; Jenkyns et al., 2016; Phelps et al., 2015). Also the stable data is are variable quality and type (i.e. bulk carbon isotopes vs. organic carbon isotopes). Nannofossil and microfossil biostratigraphy has matured as alternate biostratigraphic methodologies to ammonite and molluscan biostratigraphy. In this contribution, we use gamma radiation and handheld ED-XRF data gathered from outcrops to correlate Eagle Ford Group

sediments across the Trans-Pecos region of west Texas to the south Texas, extending the sequence stratigraphic model developed for Eagle Ford Group sediments in East Texas to the Trans-Pecos area (Donovan et al., 2012; Gardner et al., 2013; Wehner et al., 2017). We use isotope stratigraphy to tie West Texas biostratigraphic correlations based on ammonites and inoceramids to south Texas correlations based on nannofossils. Analysis of the new data also provides insight into the paleogeography and redox chemistry during the deposition of the Eagle Ford Group, which was near the south end of the Western Interior Seaway, during the Cenomanian and Turonian.

4.1.2 XRF geochemistry

The development of portable energy-dispersive x-ray fluorescence (ED-XRF) devices resulted in two major advantages: the simplification of sample preparation (Hou et al., 2004) and the ability to generate large datasets (e.g. Weltje and Tjallingii 2008, Rowe et al. 2012). ED-XRF data have been used to interpret paleoredox conditions or to discriminate between "chemofacies" using elemental combinations/ratios within a stratigraphic framework.

Algeo and Tribovillard (2009) used cross-plots of Mo/Al and U/Al enrichment factors, normalized to continental values, generated by ED-XRF to identify euxinic conditions in ancient seas.Algeo and Rowe (2012) observed that the marine water renewal rate (effectively a measure of basin restriction) correlates with Mo/TOC. Integrating ED-XRF data with TOC or Rock-eval data types provides new insight into the paleogeography and redox chemistry of ancient marine basins.

4.2 Locations

4.2.1 Field observations and measurements

Five outcrops of the Eagle Ford Group formations (Fig. 4.1) were surveyed by the Eagle Ford Research group at Texas A&M University (Table 4.1). For this study four wells were included (Table 4.1 and Fig. 4.1). The Antonio Creek composite site consists of two nearby outcrops, one in Lozier Canyon, the other in Antonio Creek, and a research well drilled in 2013 a few 10's of meters behind the Lozier Canyon outcrop (Donovan, 2016; Donovan and Staerker, 2010; Donovan et al., 2016, 2012; Gardner et al., 2013). To reiterate, for the purpose of this paper, both the Lozier Canyon well and Lozier Canyon outcrop will be considered a composite section for now called Antonio Creek composite site.

Lozier Canyon is a well-known outcrop of Boquillas Formation now considered to belonging to the Eagle Ford Group (Wehner et al., 2017). Here, we will consider Lozier Canyon along with BP/SLB Lozier Canyon #1 and Antonio Creek to be part of a composite section. Four additional wells enable us to extend correlations developed for the Lozier Canyon composite site to the west: three with gamma-ray logs from Brewster and Kinney counties; and a Shell research well with isotope stratigraphy (Table 4.1). The high-resolution isotope data from this well, presented by Eldrett and colleagues as a good reference curve for the middle Cenomanian through early Coniacian interval in the Western Interior Seaway, appears to be a relatively complete section (Eldrett et al., 2015a,b, 2014; Jenkyns et al., 2016).

We made measured and described five sections bed-by-bed and the carbonate rocks were classified using Dunham's (1962) classification. While measuring each section, we passively acquired spectral gamma ray data using a handheld Terraplus RS-230 Gamma Ray

Study Locations	Abbrev.	Lat	Long	County
Mule Canyon	MC	30.81011	-105.21166	Hudspeth
Hot Springs	HS	29.18776	-102.99451	Brewster
Ernst Tinaja	ET	29.25581	-103.01312	Brewster
Lozier Canyon*	LC			Terrell
Antonio Creek*	AC	29.84766	-101.78947	Terrell
Lozier Canyon #1	BP/SLB LC1			Terrell
Wells				
73-44-504		29.32750	-103.55556	Brewster
70-46-802		29.28056	-100.32306	Kinney
70-52-202		29.22944	-100.56083	Kinney
Shell Iona #1	SI-1	29.22517	-100.74150	Kinney

Table 4.1: A list of locations of Eagle Ford sections used in this project. The sections marked with an asterisk (*) are combined into a composite section called Antonio Creek Composite.

Spectrometer. We processed these data to calculate the uranium (U), potassium (K), and thorium (Th) content at 1ft (30 cm) intervals and estimated the total gamma ray value the formula of Herron and Herron (1996). Graphically, the results of the scintillometer are plotted in the same manner as gamma ray logs generated by downhole tools common in the petroleum and water exploration industry. The use of scintillometer data allows direct comparison of outcrop stratigraphy and data with well log patterns well known from subsurface wells (Ettensohn et al., 1979; Hampson et al., 2005; Myers and Wignall, 1987; Schwalbach and Bohacs, 1992).

4.3 Methods

4.3.1 Sequence stratigraphy and isotope chemostratigraphy

The sequence stratigraphy and isotope chemostratigraphy of the Eagle Ford Group used in this contribution integrates direct outcrop observations of disconformities and hiatal sur-

faces, digitalized gamma-ray logs, foraminiferal and nannofossil biostratigraphic data, and U-Pb zircon ash bed dates (Deluca, 2016; Donovan et al., 2015a; Moore, 2016; Peavey, 2017; Wehner et al., 2017). In addition legacy ammonite data from published were integrated (Cobban et al., 2008; Cobban and Kennedy, 1989; Cobban et al., 2006; Cooper and Cooper, 2014; Kennedy and Cobban, 1993). Our regional correlation of the Eagle Ford Group also incorporates gamma-ray logs from water wells in Brewster and Kinney counties.

We used bulk δ^{13}C isotopic data of selected intervals to identify OAE2 in Eagle Ford Group sections, supplemented by organic δ^{13}C isotopic data for the Mule Canyon section. The bulk carbonate stable isotopes (δ^{13}C and δ^{18}O) for the Hot Springs (50 samples) and Antonio Creek (90 samples) sections were measured using a Thermo Scientific Kiel IV Automated Carbonate Device coupled to a Thermo Scientific MAT 253 at the Stable Isotope Geoscience Facility, a multi-disciplinary facility at Texas A&M University. However, the isotope samples from Mule Canyon (27 samples), while meausured at the same facility, were measured using a Carlo Erba NA1500 elemental analyzer (EA) coupled with a Thermo Finnigan Delta XP isotope ratio mass spectrometer (IRMS). The average outcrop/core sample spacing between measures was variable from section to section, but typically was 3-6 ft (1-2 m), except for Antonio Creek where the sample spacing was 0.5 ft (0.15 m). All carbon isotope values are in VPDB scale. Also we extend our isotopic results with the published carbon isotopic curves of Eldrett et al. (2015a,b, 2014) Eldrett and collaborators (2014, 2015a, 2015b).

Study Locations	Abbrev.	XRF	Stable isotopes	TOC	XRD
Mule Canyon	MC	x	x	x	
Hot Springs	HS	x	x		
Ernst Tinaja	ET	x	x	x	
Lozier Canyon*	LC	x			
Antonio Creek*	AC	x	x	x	
Lozier Canyon #1	BP/SLB LC1	x	x		x
Wells					
73-44-504					
70-46-802					
70-52-202					
Shell Iona #1	SI-1		x		

Table 4.2: A list of data types available for the Eagle Ford sections and water wells used in this project. The sections marked with an asterisk are combined into a composite section called Antonio Creek Composite.

4.3.2 Geochemistry

This study included geochemistry data from four different methods for five sections. The available geochemistry data types are: energy-dispersive x-ray fluorescence (ED-XRF), stable isotopes (carbon and oxygen), total organic content (TOC), and mineralogy via XRD. Not all outcrop sections have all the geochemistry data (Table 4.2).

The ED-XRF work was acquired using a Thermo Scientific Niton XL3t 950 GOLDD+ XRF Analyzer (up to 36 elements are detected using the Cu/Zn filter) and was calibrated using the method described by Rowe et al. (2012) as well as using the calibration samples made by Dr. Harry Rowe, formerly of Bureau of Economic Geology.

The TOC data available for the Antonio Creek outcrop was measured by Geomark along with calcimetry. Unfortunately, TOC data is not currently available for the other Trans-

Pecos Eagle Ford outcrops. However, at Antonio Creek there is TOC data that can be compared with iron and sulfur concentration from XRF.

XRD data was available from the BP/SLB Lozier Canyon #1 core and can be considered representative of the mineralogy in the nearby Antonio Creek outcrop section (8 km).

4.3.3 Molybdenum (Mo) and uranium (U) concentration

Two elements are key for analyzing anoxia and particularly euxinic conditions: molybdenum (Mo) and uranium (U). In this study, U and Mo data are from the Thermo Scientific Niton XL3t 950 GOLDD+ XRF Analyzer, described in the previous paragraph. As an initial criteria to see if euxinia is likely, checked the Mo levels; if Mo concentrations exceed 25 ppm then euxinia may be a factor (Dahl et al., 2013). The second criteria is the examination of the cross-plot of Mo and U, but the concentration of Mo and U first must be processed to calculate the corresponding enrichment factors, as proposed by Brumsack (2006). The method is a cross-plot of molybdenum (Mo) and uranium (U), each normalized by aluminum content. Then the normalized ratio is divided by the continental value of the element with Al. The formula for both Mo and U enrichment factors are as follows:

$$\mathrm{EF_{Mo}} = (\mathrm{Mo/Al})_{\mathrm{sample}}/(\mathrm{Mo/Al})_{\mathrm{continental}} \tag{4.1}$$

$$\mathrm{EF_{U}} = (\mathrm{U/Al})_{\mathrm{sample}}/(\mathrm{U/Al})_{\mathrm{continental}} \tag{4.2}$$

On each cross-plot, two lines are plotted: a brown and blue one. The brown line represents global, continental basement value based on the measurements of McLennan (2001) and the blue line represents the wt.% ratio of Mo/Al vs. U/Al of modern seawater (3.2).

The way to interpret these plots is that values that values that are close to the brown line are those enriched by Mo and U reduced from the sediment itself during subsea anoxic conditions. This is in contrast to those that are near or above the blue line. Values are this part of the compositional space have Mo and U in proportion similar to that of the ocean, suggesting that the reduction of these elements occurred within the water column (euxinia).

4.3.4 Bioturbation

A bioturbation dataset using a 0 - 5 scale (Droser and Bottjer, 1986) was acquired for the Antonio Creek outcrop. 0 is no detectable bioturbation and 5 is completely mixed and homogenized sediment by bioturbation. For this study 59 samples were examined and visually assigned an index value, using the 0 - 5 scale.

4.4 Results

4.4.1 Sequence stratigraphy and isotope chemostratigraphy

The Eagle Ford Group in west Texas has four depositional sequences (Donovan, 2016; Donovan et al., 2015a,b; Wehner et al., 2017). A fifth sequence consisting of dolomitic marlstone with comparably high levels of trace elements (e.g. Sr, Zr, and Rb) occurs at the base of Eagle Ford sections in the Trans-Pecos (Wehner et al., 2017). Based on published ammonite data and updated ammonite zonation, this fifth sequence is time equivalent to part of the Woodbine Group. A key result of Eagle Ford sequence stratigraphic studies is that many sections are incomplete and some sequence boundaries are difficult to identify in outcrop and core (Fig. 4.2).

The bulk carbon isotopic data (bulk δ^{13}C) with stratigraphic depth confirm key isotopic

events (Fig. 4.3). The Mule Canyon carbon isotope values vary between -0.32 and 1.59 ‰; it does not have unusually anomalous values. The most evidence feature of the carbon isotope curve is a spike at 51 ft (15.5 m). A similar spike is also seen in the organic carbon isotopes available for the Mule Canyon section. Hot Springs has a δ^{13}C range of -9.93 to 1.52 ‰ but most are between -3 and 1 ‰. The bulk carbon isotopes values between 19.5 ft (5.9 m) and 83 ft (25.3 m) tend to be low and contain some anomalously low values. The data resolution at Antonio Creek is considerably higher than the previously described sections at every 2 ft (0.6 m). The bulk carbon isotope ratio varies from -4.93 to 2.21‰ with the majority of the values between -3 and 1 ‰. Between the top of Buda and 60 ft above Buda (18.3 m), the bulk δ^{13}C values oscillate between -1.75 to 0.75 ‰ while the interval between 60 and 114 ft (18.3 and 34.8 m) has two zones with low bulk isotopes values in the range of -1 to -5 ‰. In the interval between 114 and 137 ft (34.8 to 41.8 m), there is a notable positive anomaly in a tight range of 1.25 to 2.25 ‰.

The fourth carbon isotope curve in the stratigraphic cross-section is a isotopic curve published for a research well (Shell Iona #1) in Kinney County east of Antonio Creek Eldrett et al. (2015a,b, 2014). The maximum range of values is -5.2 to 3.75 ‰ however the vast majority of the values are between 0 and 2 ‰. Some anomalously negative anomalies exist but these do detract from the observation of positive anomalies at 471 ft (143.6 m), 304-342 ft (92.7-104.2 m), and 233 ft (71 m). The identification of carbon isotopic events in Shell Iona #1 is well established by a suite of independent measures (radiometric dating, nannofossil and foraminiferal biostratigraphy, and palynology).

The carbon isotope curves had one initial result that was counterintuitive: the OAE2 anomaly is not associated with the high TOC content of Lower Eagle Ford as originally expected. A second result was the absence of the OAE2 in the Hot Springs, suggesting

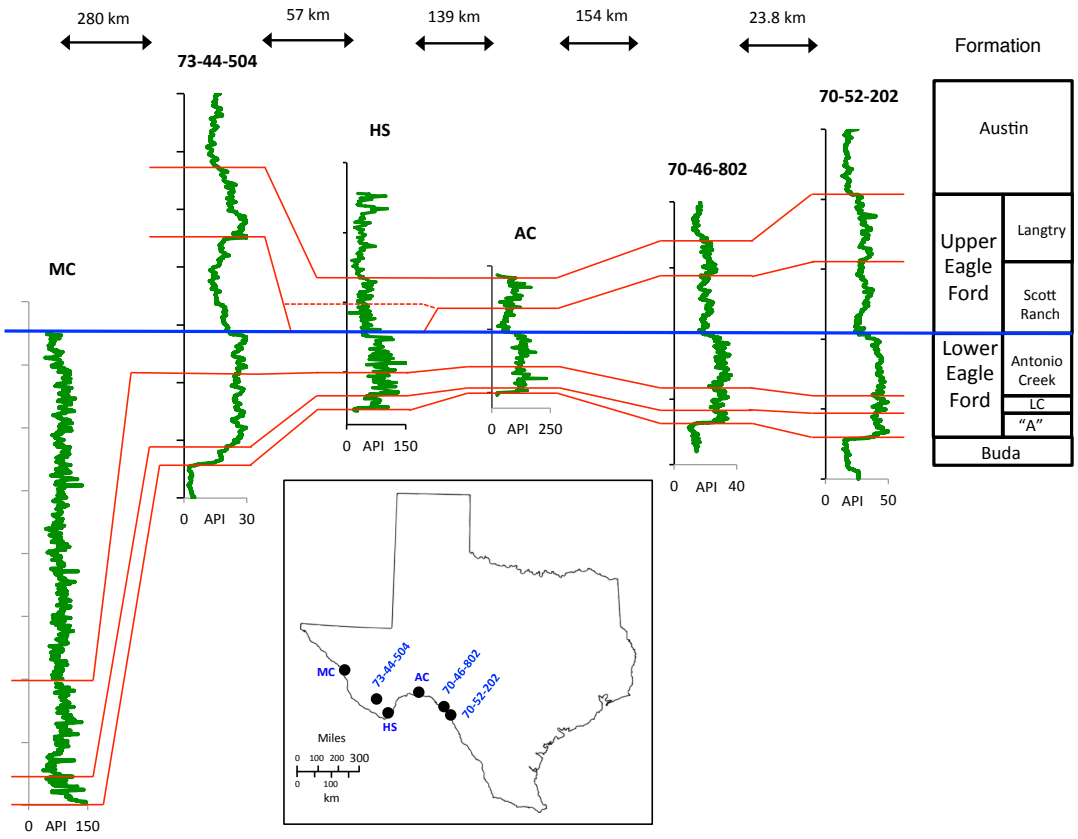

Figure 4.2: A gamma-ray log correlation of outcrops and wells in the Trans-Pecos area, extending the Eagle Ford Group correlation westward from Lozier Canyon to Hot Springs in Big Bend National Park (Brewster County) and Mule Canyon in Hudspeth County. The gamma ray values for outcrops were determined using concentration values for K, U, and Th obtained from the Terraplus RS-230 Gamma Ray Spectrometer and the total gamma ray values calculated using the formula of Herron and Herron (1996). The vertical (depth) scale is uniform for all sections in this figure. The sections are hung on the sequence boundary (horizontal blue line) that separates Upper Eagle Ford Formation from Lower Eagle Ford Formation, called K65sb in a number of works (e.g. Donovan 2016). The red lines are interpreted sequence boundaries within each formation. In the Hot Springs section (HS), there is a dotted line that separates an interpreted sequence that cannot be easily correlated into the adjacent sections.

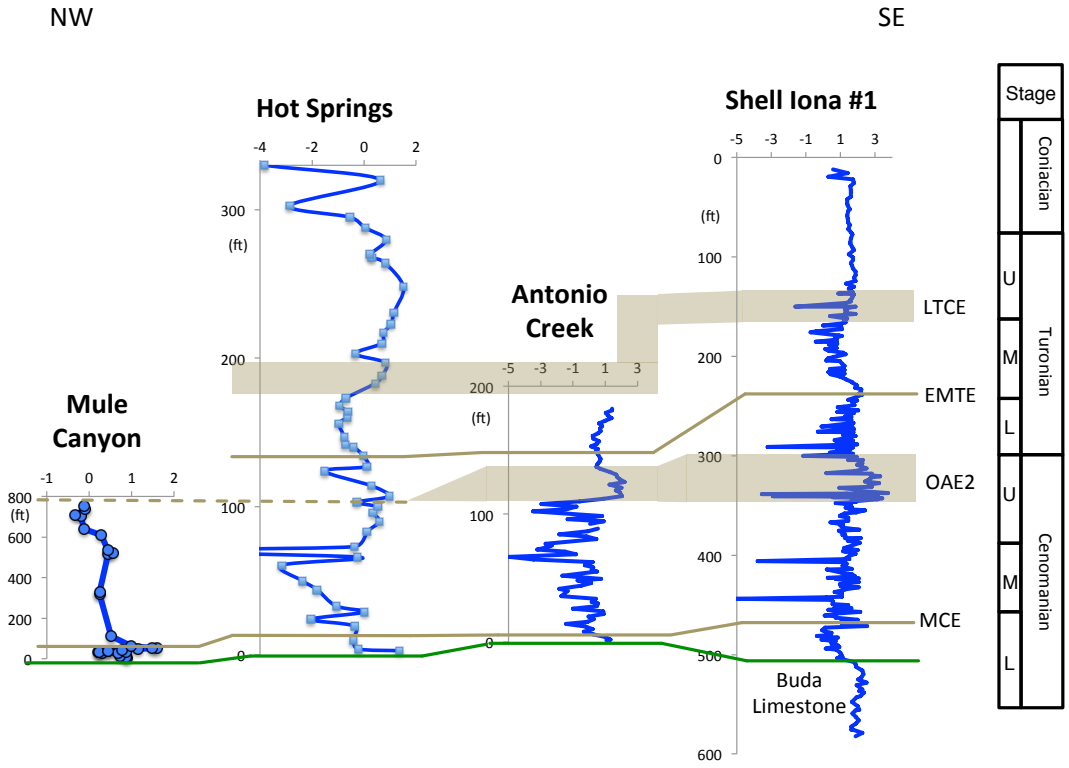

Figure 4.3: Bulk carbon isotope chemostratigraphy correlation for four outcrop sections in the Trans-Pecos area. The sections are in a transect that trends from northwest in Hudspeth County to Lozier Canyon in Terrell County and southeast towards Shell Iona #1 and water well 70-52-202 (Texas Water Development Board designation). The correlations are constrained by biostratigraphic and ash-bed chronology (Deluca, 2016; Donovan et al., 2015a; Lowery et al., 2014; Peavey, 2017). The data constrains for Shell Iona #1 come from Eldrett et al. (2015a,b). The depth scales are not uniformly scaled and the sections are hung on the OAE2 isotopic event. The unexpected result is that OAE2 isotope anomaly is difficult to correlate on a regional scale in Eagle Ford Group while the other isotopic events like MCE and LTCE may be easier to detect in the more consistently preserved sequences. The green line is the top of the Buda Limestone, which underlies Eagle Ford Group and in some places the Woodbine Group equivalent sediments.

that the OAE2 is not recorded or preserved in some sections. Based on biostratigraphic data (micro- and nannofossils), little or no Upper Eagle Ford formation was measured at the Mule Canyon site in Hudspeth County, so this section does not provide an opportunity to compare its OAE2 anomaly to the other sections.

4.4.2 Bioturbation indices and distribution of Mo-U values

Bioturbation indices for the Lower Eagle Ford range from 0 to 1, with bioturbation in the Lower Eagle Ford confined to the top of a few rippled grainstone beds. Otherwise, the Lower Eagle Ford is barren of bioturbation. In Upper Eagle Ford, bioturbation indices range from 1 to 5, but most values are either 4 or 5 meaning that the sediments were completely homogenized.

High levels of Mo (> 25 ppm) and Mo/U enrichment factors ratio > 3.2 have been used to identify euxinia in the rock record (e.g Algeo and Tribovillard 2009). High Mo/U enrichment factors occurred at Mule Canyon, in the basal 21 m of the outcrop, which is likely equivalent of the most basal portion of the Lower Canyon Member of the Lower Eagle Ford Formation, and the basal Woodbine Group in East Texas Basin (Wehner et al., 2017). At Hot Springs and Ernst Tinaja, the Mo/U enrichment factor ratio seldom passed the 3.2 seawater Mo/Al enrichment factor ratio (Fig. 4.4 and 4.5). Nonetheless, field observations of laminated sediments, interrupted by occasional thin bioturbated events with abundant molluscs, suggest that anoxia prevailed during the deposition except for some minor oxygenation events.

The cross-plots of Mo/Al and U/Al enrichment factors show that accumulations of Mo and U tend to be consistent with reported average continental values for Hot Springs and

Ernst Tinaja (McLennan 2001: Fig. 4.5). At Antonio Creek, high Mo/U enrichment factor ratios, frequently exceeding the seawater ratio of 3.2, occurred during the Lozier Canyon sequence and continued throughout the Antonio Creek sequence, up to the end of the Lower Eagle Ford at the base of Upper Eagle Ford (Fig. 4.5). Mule Canyon has an enrichment factor distribution that is similar to Antonio Creek except the proportion that exceed 3.2 vs. those that do not is likely skewed since sampling interval averages about every 10 ft (3.3 m).

4.4.3 Iron-sulfur-organic carbon (Fe-S-TOC) relations in Eagle Ford

Figures 4.6 and 4.7 show the amount of iron, sulfur, and TOC with depth at Antonio Creek. In Figure 4.6, the ternary diagram reveals the relationship between Fe, S, and TOC in the Lower and Upper Eagle Ford formations. The pyrite line (blacked dashed line in Figure 4.6 and 4.7) reflect the stoichiometric ratio between Fe and S for pyrite and if all Fe and S in the sediments formed pyrite, the values would fall on this line. A high percentage of Lower Eagle Ford samples fall below and parallel to the pyrite line, indicating that these samples contain excess sulfur (i.e. more sulfur than predicted, assuming all available Fe is contained in pyrite). These samples tend to have TOC values in excess of 2 wt. %. Upper Eagle Ford samples show no relationship between Fe, S, and TOC.

Figure 4.7 shows the Fe/S, TOC, and BI values of Antonio Creek samples with stratigraphic depth. Fe/S values lower than the pyrite stoichiometric ratio of 0.87 commonly occurs in the Lower Eagle Ford. In these samples, low Fe/S ratios appear inversely correlated with TOC. Further, these samples tend to have low bioturbation indices. In the Upper Eagle Ford Formation, the Fe/S ratio is well in excess of 0.87 and sometimes can approach 10. In the Scott Ranch Member of Upper Eagle Ford, there is still moderate to

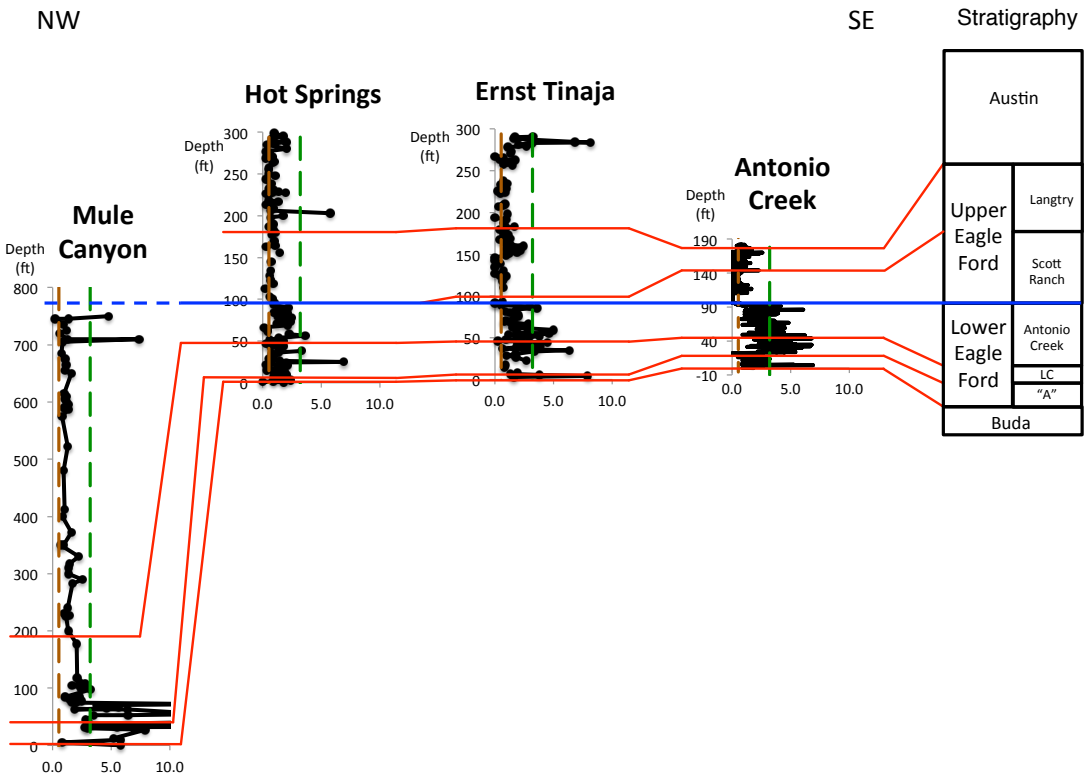

Figure 4.4: Stratigraphic plots of molybdenum-uranium enrichment factor ratios (Mo/U) arranged as in a NW - SE transect from Mule Canyon in Hudspeth County to Antonio Creek in eastern Terrell County. The Mo/U ratio in the Mule Canyon does reach about 21 about 33 ft (7 - 10 m) above the top of Buda Formation. The scale is in ft and the sections are all to scale. The sections are hung on the sequence boundary (blue line) that separate Upper from Lower Eagle Ford formations. The red lines are the sequence boundaries within the formations.

high TOC but abundant authigenic pyrite that are visible to the naked eye even in outcrops, as well moderate-to-high bioturbation (BI = 2-4). The Langtry sequence has low TOC (in the 0.1-0.5 wt. % range) and high Fe/S values up to 10 suggesting that pyrite is not the main host of iron in this unit.

XRD data for the Langtry Member from the BP/Schlumberger #1 core, just 8 km from An-

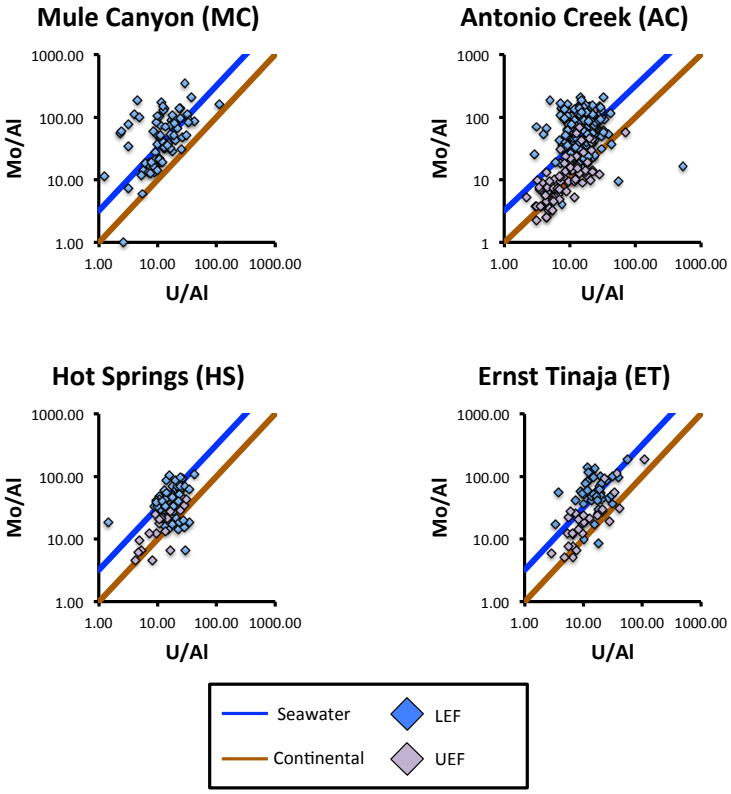

Figure 4.5: Molybdenum-uranium (Mo-U) covariation cross-plots for four locations in west Texas (Trans-Pecos) from the calibrated XRF data. The Mo-U values were transformed using the enrichment factor equation of Brumsack (2006) and the average shale values from McLennan (2001). The blue line is the average seawater ratios of Mo/Al and U/Al while the red line is the Mo/Al and U/Al ratios for average shale (Algeo and Tribovillard, 2009; Tribovillard et al., 2012). Values that are close to blue line indicate euxinia and those near the red line did not experience sulfur-reduction until after being buried by accumulating sediments (pore water sulfur-reduction). The abundance of values, particularly those from Lower Eagle Ford (LEF), at or above blue line suggests that euxinia was common during deposition of LEF.

tonio Creek, shows that the Langtry sequence has elevated levels of ankerite and chlorite, compared to the rest of Eagle Ford Group. The stoichiometry of iron content in ankerite and chlorites is not fixed, but these minerals can host large quantities of iron as Fe^{2+}. Ankerite can contain a mixture of iron, magnesium, and manganese while chlorite clays

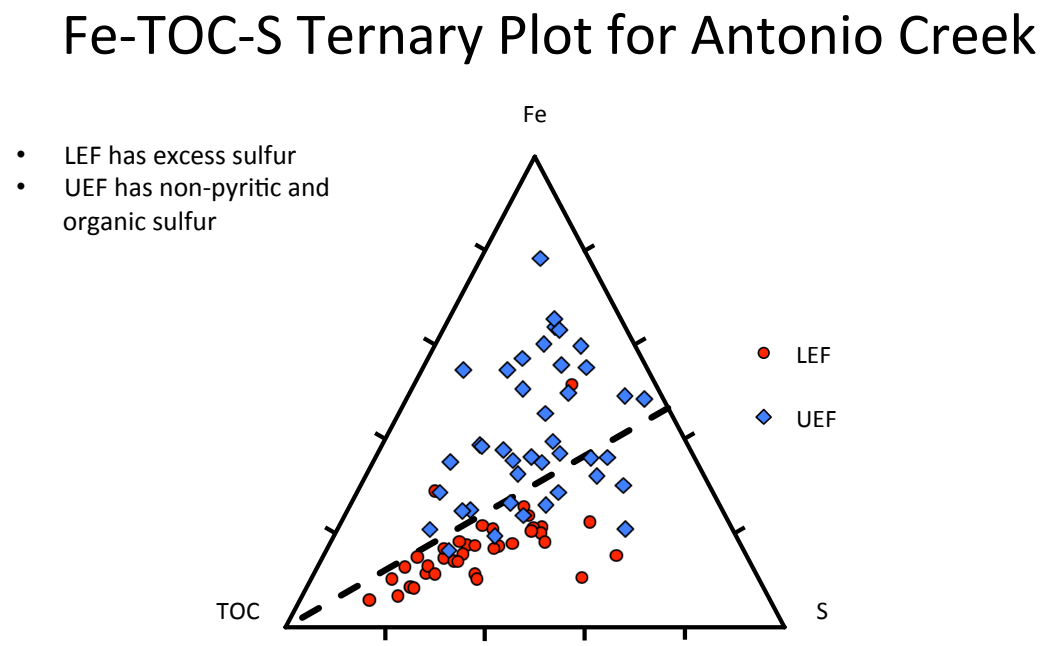

Figure 4.6: Fe-S-TOC ternary diagram for the Antonio Creek outcrop in Terrell County. The red dots are from the Lower Eagle Ford Formation (LEF) and the blue diamonds are from the Upper Eagle Ford Formation (UEF). The dashed line is the stoichiometric pyrite line where Fe/S is 0.87 for all values of TOC. When TOC exceeds 40 % of the Fe-S-TOC composition (usually a red dot from LEF), the Fe/S becomes less than 0.87 yet parallels the pyrite possibly because of the co-occurrence of pyritic sulfur with the excess sulfur. The latter is hypothesize to be held in kerogen and hydrocarbons. The majority of the UEF samples do not show any significant trend since it is likely that much of the iron is held neither in TOC or pyrite. XRD suggests that iron could be held in carbonates (e.g. dolomite) and clay minerals (e.g. chlorites). The tick marks are spaced at 20 %. The template for the ternary diagram is based on the version, called Ternplot, published by Marshall (1996).

have two common end-members: chamosite (Fe end-member) and clinochlore (Mg end-member). Chamosite is commonly reported from shale (e.g. Sheppard and Hunter 1960; Schieber and Riciputi 2004) and likely occurs in the Eagle Ford Group although it is likely reported under the more generic name of chlorite clay.

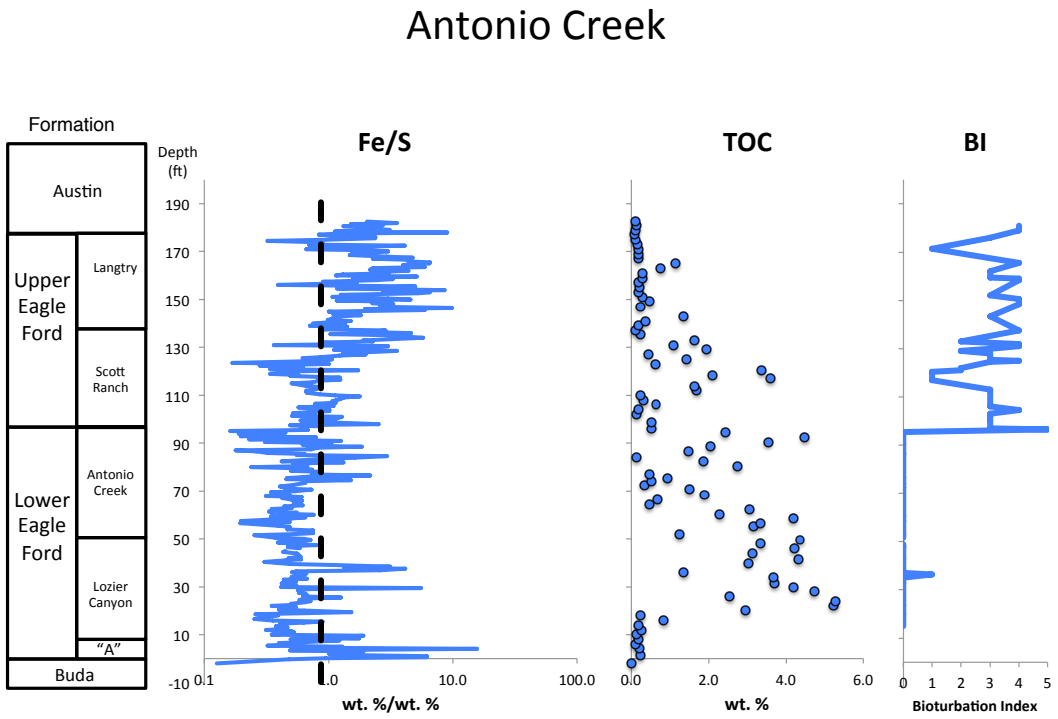

Figure 4.7: This stratigraphic plot compares the stratigraphic distribution of Fe/S ratio (the vertical dashed line is the stoichiometric ratio 0.87 for pyrite), TOC, and bioturbation index (BI) where 0 means no bioturbation and 5 means the sediments were 100% bioturbated. There is covariation between Fe/S, TOC, and BI. TOC values decrease while both Fe/S and BI increase.

4.5 Discussion

4.5.1 Carbon isotope chemostratigraphy, biostratigraphy, and sequence stratigraphy

The carbon isotope chemostratigraphy presented here encompasses most of the Trans-Pecos area of Texas and builds on on previously published chrono- and biostratigraphies The Hot Springs sequence is notable because it does not appear to preserve an OAE2 in-

terval (Wehner et al., 2017). Peavey (2017) reported a possible sliver of OAE2; however if OAE2 occurs in this section, it may be narrower than the sampling interval used in this study, which is about a meter). The westernmost outcrop in this study, Mule Canyon, exposes only the Lower Eagle Ford Formation and early Cenomanian sediments equivalent to the Woodbine Group. A comparison of both organic and bulk carbon isotopes from the Mule Canyon section suggests that the Mid-Cenomanian Event (MCE: see also Eldrett et al. (2015a,b)) is recorded there. We were not able to identify the MCE isotopic event in the Hot Springs section; however Fry (2015) may have captured this event in her data. Our sampling resolution may have been too coarse; in addition organic carbon isotopes might be needed since there is some evidence of late diagenesis as evidenced by liesengang banding surrounding fractures at Hot Springs. Likewise, the MCE may be preserved at Antonio Creek. Using the published isotopic reference curves of Eldrett et al. (2015a,b) it is possible to identify the early-middle Turonian Event (EMTE), the middle Turonian event (MTE), and the Late Turonian-Coniacian Event (LTCE) in the Shell Iona #1 core. It is possible to correlate the LTCE and EMTE (Fig.4.3) into Antonio Creek and Hot Springs, using the biostratigraphic, legacy ammonite/inoceramid data, and U-Pb zircon ash beds as constraints.

In Figure 4.3, the thickness of the interval between MCE and OAE2 for Shell Iona #1, Antonio Creek, and Hot Springs are similar (90-120 ft). However, the interval between OAE2 and EMTE is quite variable, with different amounts of time missing in different sections. This suggests that the mechanisms responsible for non-deposition and erosion were not necessarily widespread. Pope et al. (2017) suggested that the variance in preserved strata/time could relate to a number of factors including changes in marine circulation patterns (i.e. currents) and cryptic hiatuses (unconformities formed or enhanced by forebulge migration: see also White et al. 2002).

At Hot Springs, the detailed nannofossil biostratigraphy does confirm the apparent absence of OAE2. None of the nannofossil indicators for the calcareous nannofossil datums for UC4, UC5, and UC6 were found. These nannofossil biozones include the time during which OAE2 occurred. The interval of time missing based on the absence of the above mentioned calcareous nannofossil biozones is on the order of 1 million years and happens to missing at the contact between Lower and Upper Eagle Ford formations. This supports the statement that most or all of the OAE2 interval is missing at Hot Springs, which also implies that most of the Scott Ranch sequence is missing.

4.5.2 Shallow-water euxinia?

The spatio-temporal distribution of euxinia suggests that euxinia was diachronous (Fig. 4.4). At Mule Canyon, the westernmost section in our study area euxinia occurred sporadically in the early Cenomanian and the first part of the middle Cenomanian. In the Lozier Canyon composite section to the east, euxinia occurred throughout the upper Cenomanian. In the Big Bend area to the south, we documented four euxinic events in the upper Cenomanian, occurred, within the upper Lozier Canyon sequence and the lower part of the Antonio Creek sequence.

In general, euxinia seems associated with the mudstones (compositionally marlstones) between foraminiferal grainstone limestone beds that are frequently contain hummocky cross-stratification (HCS) and wave ripples, although often these limestone beds are converted to cement and other diagenetic processes that destroy internal stratification. These grainstones form thin (approximately 30 cm thick) amalgamated limestone beds that are latereally continuous on the scale of hundreds of meters. These bedforms are most abun-

dant at the Lozier Canyon composite section and become lest frequent going westward. This would appear to be consistent with the possilibility that the Eagle Ford Group sediments Lozier Canyon composite section and the Shell Iona #1 were deposited on a shallow shelf, a paleotopographic high. This area is a known topographic high during the early Cretaceous called Devils River Uplift (e.g. Donovan 2010). We interpret these limestone beds as shallow water features based on the abundance of wave ripple sedimentary structures at locations like Antonio Creek (Donovan and Staerker, 2010; Trevino, 1988; Wehner et al., 2015). We interpret the surrounding fine-grained sediments as euxinic based on the high molybdenum content (concentration > 25 ppm) and Mo/U enrichment factor ratio frequently exceeds 3.2, the seawater ratio of molybdenum and uranium. The latter implies that molybdenum and uranium reduction was occurring within the water column, which is possible under euxinic conditions. Reported biomarker data from gas chromatography mass spectrometry (GC-MS) data for samples from the Maverick Basin revealed that aryl isoprenoids are present in the preserved organic matter of Lower Eagle Ford Formation (Maulana, 2016). Aryl isoprenoids is regarded as a proxy for the presence of photic-zone sulfur-reducing bacteria and thus can be regarded as a type of evidence for euxinia (Koopmans et al., 1996; Summons and Powell, 1986). The juxtaposition of fine-grained euxinic sediments with shallow water grainstones suggests euxinia in the Eagle Ford Group was shallow water and occurred during flooding of the Comanche Platform in the early Cenomanian, and continued through the Late Cenomanian at Lozier Canyon. The observation of shallow-water biomarkers in Eagle Ford sediments reported by Maulana (2016) supports our interpretation of shallow water euxinia. Eagle Ford euxinia may have been tied to low sea level, splitting the Comanche Platform into isolated silled basins. As sea level rose, euxinia became less frequent and for the most part disappeared in Upper Eagle Ford sediments. Sageman (1996) interpreted grainstone beds from shales that are age-equivalent to the Eagle Ford Group as shallow water features and the interbedded fine-grained sedi-

ments as deep-water facies. However, this explanation would require repeated, significant sea-level change on the order of 10-100 m, within relatively short timescales, almost in the eccentricity cycle range. Tinnin and Darmaoen (2016) invoked the oxygen minimum zone to explain euxinia in the Eagle Ford. In modern settings, oxygen minimum and upwelling zones create anoxic conditions in deep settings, about 500-2000 m in depth. However, this seems inconsistent with the correlation between shallow-water bedforms and euxinia and the presence of shallow-water indicators of euxinia in the Eagle Ford Group (Lyon, 2015; Wehner et al., 2015).

4.5.3 Use of iron/sulfur ratio for sulfurized organic matter

The Fe/S ratio may serve as a proxy for TOC enrichment in the Eagle Ford Group. In the ternary diagram showing the Fe, S and TOC content of Eagle Ford sediments from Antonio Creek, the Lower Eagle Ford samples plotted below the pyrite line, suggesting that these samples contain excess sulfur. Further, the amount of excess S correlates positively with TOC. When TOC accounted for greater than half of the iron-sulfur-TOC composition, almost all examples showed excess sulfur (Fig. 4.5). This suggests that there could some association of excess sulfur with high TOC levels. Sun et al. (2016) reported that kerogen/hydrocarbons in Eagle Ford have significant sulfur content, with kerogen sulfur contents ranging from 7 to 12 wt. %. One of the organofacies of oil from the Eagle Ford is characterized by high sulfur content (up to 2 wt. % of produced oils: Zumberge et al. 2016). This organofacies occurs in areas that are up-dip areas away from basin centers and paleo-reef margins (Zumberge et al., 2016). Their examples show that the carbonate shale has a combination of higher API gravity (meaning lighter, less dense oil) and high sulfur content compared to oils produced from more argillaceous Eagle Ford. At the outcrop sections, the kerogen is immature and likely has produced little oil (Ro = 0.6 for Lozier

Canyon/Antonio Creek and a Rock-Eval derived Ro value of about 0.45 for Shell Iona #1).

Excess sulfur in the Eagle Ford sediments is likely hosted by kerogen and other hydrocarbons. Sulfurized organic materials (including organosulfur) in shale are reported from a number of places (Bottcher et al., 2006; Hartgers et al., 1997; Tribovillard et al., 2004; van Kaam-Peters, 1997). Extensive evaporite minerals, like gypsum or polyhalite, within the shale could cause excess sulfur however sulfate minerals were not detected in any of the 101 XRD samples from the Lozier Canyon Composite Section (sampled in the BP/SLB Lozier Canyon #1 core).

There is some debate about whether the sulfur is primary or diagenetic in sulfurized organic carbon. Sulfur is thought to be in the form of organosulfur compounds. This is how the Fe/S ratio could be inversely correlated with TOC content in the Eagle Ford Group as observed and any other organic-rich shale that has similar geochemical conditions.

One interesting implication for situations where excess sulfur is held in TOC is that the alternate way to estimate DOP (degree of pyritization) from iron and sulfur as proposed by Algeo and Maynard (2004) will exceed 1 (DOP > 1), which is an absurd result because according the definition of Raiswell and Berner (1985) this would mean pyrite iron is greater than total iron. The issue here is because of the assumption that all sulfur is associated with pyrite, which may work for some rocks but does not in Eagle Ford and some other shales. This is not to suggest that one should not use Fe and S to estimate DOP, but merely we are suggesting some caution in interpreting estimated DOP values estimated from elemental iron and sulfur alone. One could also choose to interpret a result of DOP > 1 as indicating the abundance of organic sulfur.

4.5.4 Fe/S ratios in Cretaceous Western Interior Seaway

Multiple cores from Western Interior Seaway (WIS) have existing XRF data, acquired with the same Thermo Scientific Niton XL3t 950 analyzer used in this study (Nakamura, 2015; Nakamura et al., 2013). Nakamura (2015)provides a Fe-S-TOC dataset from the Noble Aristocrat 11-07 well from Weld County, Colorado, acquired using Leco and ICP. From the ICP data, iron is reported as Fe_2O_3 and transformed to elemental iron using a conversion factor. Regardless, the resulting ternary diagram, where Fe and S are from ICP (Fig. 4.8), the data from the Noble Aristocrat 11-07 well suggests that none of the samples have excess sulfur. However, if one plots Fe/S stratigraphically from the XRF data (as we did for the Eagle Ford samples in Figure 4.6), some samples have excess sulfur, but this was not seen in the ICP data. Nakamura (2015) did not provide details about the ICP preparation procedure, but if the ICP preparation procedure did not utilize a microwave digestion it could be that the ICP results are not including trace elements and organosulfur hosted by kerogen and hydrocarbons. However, the low Fe/S ratios in the Aristocrat 11-07 are not extreme or as common as those in found in Lower Eagle Ford.

When the same Fe/S data (from XRF) from Noble Aristocrat 11-07 was plotted against stratigraphic depth (Fig. 4.9), it becomes clear that some stratigraphic intervals do indeed have Fe/S values < 0.87, which could suggest the presence of sulfurized organic matter. A comparison of the same Fe/S plot next to TOC seems to suggest that the excess sulfur phenomena in the Noble Aristocrat 11-07 well is confined to the Niobrara Formation and not present in the adjacent units: Pierre Shale, Hartland Shale, and Lincoln Limestone. These adjacent units have TOC > 2.0 wt. %, but the Bridge Creek Member has TOC in the 0.5-1.5 wt. % range. Also the Hartland Shale, despite having TOC > 1.5 wt. %, does not appear to have excess sulfur, so it is likely that the TOC is not extensively sulfurized. This

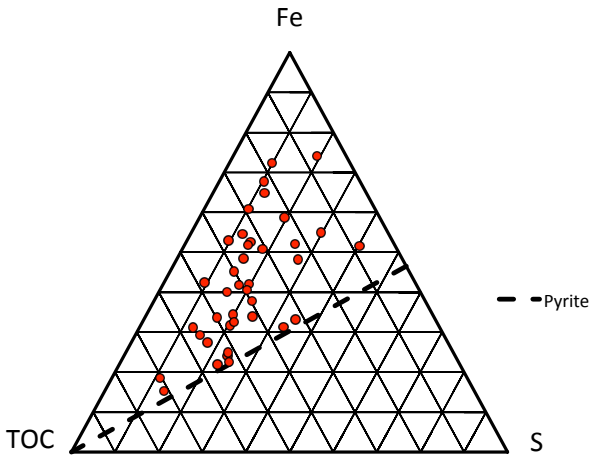

Figure 4.8: Ternary plot of Fe, S, and TOC for the Noble Aristocrat 11-07 well from Weld County, Colorado. The majority of the values are not even close to the pyrite line (where Fe/S =0.87), suggesting that much iron in the majority of the section is not held in pyrite or sulfurized organics and could be in a variety of other minerals, like clays or carbonates. The data used to make this figure is derived from supplemental material for Nakamura (2015).

means that not all high-TOC shales are going to have low Fe/S values, but for the ones that do Fe/S values appears to clearly identify the sulfurized high-TOC zones.

4.6 Conclusion

Geochemical tool are applied to examine geologic outcrops and/or cores in greater detail and at greater spatial resolution in the hope to better understand controls on heterogeneity,

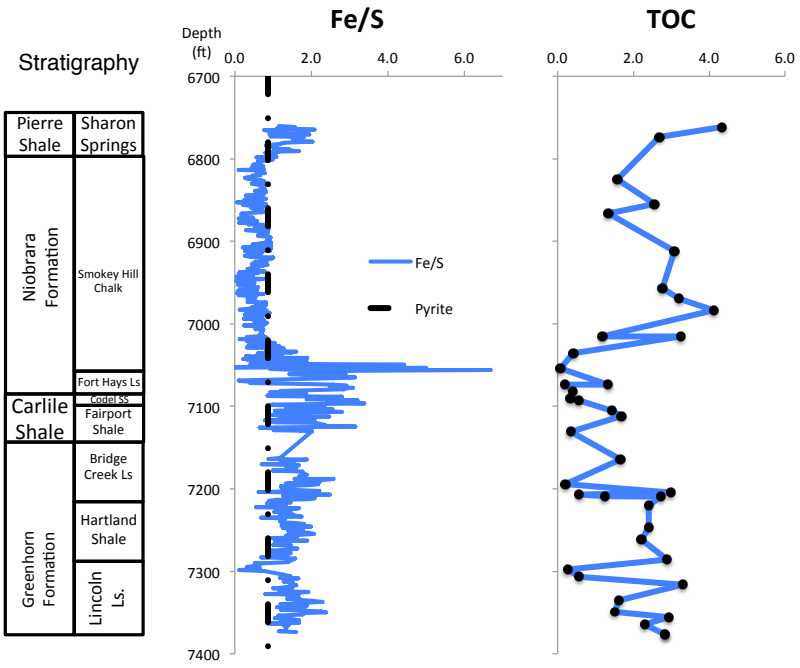

Figure 4.9: Stratigraphic plot of Fe/S and TOC for the Noble Aristocrat 11-07 well from Weld County, Colorado. The interval of low Fe/S values (<0.87) is within the Smokey Hill Chalk Member of the Niobrara Formation, which is similar to what is seen in Lower Eagle Ford in Texas but not as extreme. However, the second interval of high TOC (excess of 2.5 wt. %) in the Hartland Shale has high values of Fe/S (excess of 2), which suggest that the TOC in Hartland Shale is not sulfurized. The data used to make this figure is derived from supplemental material for Nakamura (2015).

etc. The Eagle Ford Group sequence stratigraphy and chronostratigraphy are improved by integrating biostratigraphy and ash-bed geochronology. We extended the sequence stratigraphy and chronostratigraphy to five outcrops and several well logs in the Trans-Pecos area of West Texas. Based on that correlation, a carbon isotope stratigraphy for the same region was presented. The stratigraphy of the Eagle Ford Group in the Trans-Pecos area appears to have been complicated by variable hiatuses whose cause and distribution has yet to be completely understood. Euxinia (using Mo/U enrichment factor ratio from XRF data) has a diachronous distribution within sequence stratigraphy and chronostratigraphic framework. Euxinia appears to be associated and most persistent in shallow-water sections and paleotopographic highs (e.g. Devils River Uplift). The high TOC content in Eagle Ford Group appears to be in the intervals where the Fe/S < 0.87, suggesting an excess of sulfur that is not in pyrite and may be associated with TOC as organosulfur. Furthermore, the use of Fe/S may aide the identification of sulfurized TOC-rich intervals in some shales.

5. SUMMARY

5.1 Summary for first paper: shallow-water photic-zone anoxia in Eagle Ford Group mudstones

Many new quantitative tools exist for analysis of organic-rich mudstone, however a wide range of applications are possible with x-ray fluorescence (XRF), not just as a stand-alone tool but in integration with tradtional and non-tradtional data types. This dissertation consists of three projects that utilize XRF in different ways for the Eagle Ford Group mudstones of Texas. The first one, used XRF to make inferences about paleoredox conditions, specifically I showed that in Eagle Ford Shale, euxinia frequently dominated redox conditions using molybdenum and uranium ratios as proxies. This observation combined with the biomarkers for photic-zone sulfur-reducing bacteria and sedimentary structures made by waves (i.e hummocky cross-stratification, wave ripples, amalgamated beds of ripples) suggests that the depositional environment of Eagle Ford can be characterized as shallow-water (< 100 m), storm-dominated, photic-zone, episodically euxinic. Oxygenation events were brief in Lower Eagle Ford Formation as shown by shallow burrowing on the tops of some of the wave ripples.

5.2 The Eagle Ford Group returns to Big Bend National Park, Brewster County, Texas

The second and final project sought to use integrated petrophysical and chemostratigraphy data to extend the sequence stratigraphy of the Eagle Ford Group as defined from the type section at Lozier Canyon, Terrell County to Hot Springs in Big Bend Nation Park, Brewster County, Texas. Using handheld gamma ray spectrometry (petrophysical data), XRF and stable isotopes (chemostratigraphy), and integrated it with nannofossil biostratigraphy

acquired for the project as well previously published macrofossil biostratigraphic data revealed stratigraphic complications that had only been suspected. Basically, at Hot Springs the following stratigraphic observations were made: one, there is a thin interval (10 ft or 3.3 m) that is early and middle Cenomanian in age that is older than Eagle Ford Group and could be regarded as time-equivalent to Woodbine Group. Based on the new dataset, I was able to pick the boundary between the Eagle Ford and Austin groups; it is not at the *Allocrioceras hazzardi* beds (basal Coniacian according to the 2012 Geologic TIme Scale), but in the *Inoceramus perplexus* (*Prionocyclus novimexicanus* ammonite zone) in Upper Turonian. This implies that there is Austin Group sediments in the Big Bend area not preserved in the type section of Austin Chalk in central Texas and also that there is Austin Group sediments that are late Turonian. The final puzzling observation is that the entire OAE2 interval is missing at Hot Springs, however most of this interval is preserved in the Lozier Canyon outcrop 80 miles NE of Hot Springs. One possible hypothesis for this is a tectonically-induced diachronous unconformity resulting from a migrating forebulge as the foreland basin in the western part of the Western Interior Seaway is filled from the west, shifting the warping of the lithosphere eastward. There are also alternatives that invoke other mechanisms such as thermal expansion/contraction of seawater, but it is still unresolved which process(es) dominant the sea-level changes during the Cretaceous since the use of modern processes (expansion/contraction of continental ice sheets) appear to have less significant during the Cretaceous.

5.3 Euxinia, organic carbon and sulfur in the Eagle Ford Group and its time-equivalent units in the Trans-Pecos, west Texas

For the third and final project, we extended the sequence stratigraphy and chronostratigraphy of Eagle Ford Group into west Texas (Trans-Pecos area) from Lozier Canyon in

Terrell County all the way to Hudspeth County. After that, we built a correlated carbon isotope chemostratigraphy using the bulk carbon isotope data from three sections (Mule Canyon, Hot Springs, and Antonio Creek) and compared them to a published curve from Shell Iona #1 well in Kinney County about 76 mi (123 km) to the southeast. The following isotopic events were identified and correlated: MCE (Mid-Cretaceous Event), OAE2 (Ocean Anoxic Event 2), EMTE (early to mid Turonian Event), and LTCE (Late Turonian-Coniacian Event). Then we used the XRF data to infer about the occurrence of euxinia by using the enrichment factor ratios of the covariation of molybdenum (Mo) and uranium (U). Based on the chronostratigraphy model, euxinia was present in the west part of the study area (Mule Canyon) only during the early to mid Cenomanian. However, euxinia rarely occurred in Hot Springs. Yet it was persistent throughout the late Cenomanian at Antonio Creek in Terrell County, which is in the eastern part of the study area. This combined with the sedimentological evidence seems to suggest that euxinia may have been most persistent in areas that were shallower and subject to more persistent basin restriction. Another application of the XRF data involved comparing the iron-sulfur rations with organic carbon (TOC) for Antonio Creek. A ternary plot of iron, sulfur, and organic carbon shows that the relations of iron, sulfur, and organic carbon (TOC) are different for Lower Eagle Ford and Upper Eagle Ford. In the Lower Eagle Ford Formation, for increasing TOC, the Fe/S ratio parallels the stoichiometric ratio of pyrite yet is below the pyrite line, implying that there is more sulfur in the rocks than would be predicted than if all sulfur was in pyrite. This is interpreted that some of the sulfur is in the organic carbon (e.g. kerogen, hydrocarbons). Yet in the Upper Eagle Ford Formation, no clear relationship is observed for iron, sulfur, and organic carbon (TOC) and the XRD data suggests that several minerals potentially contain abundant iron are present in Upper Eagle Ford. These minerals include chlorite clays and dolomite. So the results suggests that the Fe/S ratio can be used to detect high TOC in shale that contains sulfurized organic matter (TOC).

REFERENCES

Adams, R. L. and Carr, J. P. (2010). Regional depositional systems of the Woodbine, Eagle Ford, and Tuscaloosa of the U.S. Gulf Coast. *Gulf Coast Association of Geological Societies Transactions*, 60:3–27.

Adkins, W. S. (1932). The Mesozoic systems in Texas. In Sellards, E. H., Adkins, W. S., and Plummer, F. B., editors, *The Geology of Texas*, University of Texas Bulletin No. 3232, pages 239–518. Bureau of Economic Geology, Austin, Texas.

Aigner, T. (1982). Calcareous tempestites: storm-dominated stratification in Upper Muschelkalk Limestones (Middle Trias, SW-Germany). In Einsele, G. and Seilacher, A., editors, *Cyclic and Event Stratification*, pages 180–198. Springer-Verlag, Berlin.

Aigner, T. (1985). *Storm Depositional Systems: Dynamic Stratigraphy in Modern and Ancient Shallow-marine Sequences*. Lecture Notes in Earth Sciences No. 3s. Springer-Verlag, Berlin.

Algeo, T. J. and Maynard, J. B. (2004). Trace-element behavior and redox facies in core shales of Upper Pennsylvanian Kansas-type cyclothems. *Chemical Geology*, 206(3-4):289–318.

Algeo, T. J. and Rowe, H. D. (2012). Paleoceanographic applications of trace-metal concentration data. *Chemical Geology*, 324-325:6–18.

Algeo, T. J. and Tribovillard, N. (2009). Environmental analysis of paleoceanographic systems based on molybdenum–uranium covariation. *Chemical Geology*, 268(3-4):211–225.

Bottcher, M. E., Hetzel, A., Brumsack, H.-J., and Schipper, A. (2006). Sulfur-iron-carbon geochemistry in sediments of the Demarara Rise. *Proceedings of the Ocean Drilling Project*, 207:1–23.

Bowman, T. D. (2014). Understanding and updating the Eagle Ford East–Eaglebine. In *Unconventional Resources and Technology Conference*, Denver, Colorado. URTeC1922762.

Brumsack, H.-J. (2006). The trace metal content of recent organic carbon-rich sediments: Implications for Cretaceous black shale formation. *Palaeogeography, Palaeoclimatology, Palaeoecology*, 232(2-4):344–361.

Cobban, W. A., Hook, S. C., and McKinney, K. C. (2008). Upper Cretaceous molluscan record along a transect from Virden, New Mexico, to Del Rio, Texas. *New Mexico Geology*, 30:75–92.

Cobban, W. A. and Kennedy, W. J. (1989). *Acompsoceras inconstans* zone, a lower Cenomanian marker horizon in Trans-Pecos, Texas. *Neues Jahrbuch fur Geologie un Palaontologie, Abhandlungen*, 178(2):133–145.

Cobban, W. A., Walaszczyk, I., Obradovich, J. D., and McKinney, K. C. (2006). A USGS zonal table for the Upper Cretaceous middle Cenomanian-Maastrichtian of the Western Interior of the United States based on ammonites, inoceramids, and radiometric ages. Technical Report Open-File Report 2006-1250, USGS, Washington, D.C.

Collinson, J., Mountney, N., and Thompson, D. (2006). *Sedimentary Structures*. Terra Publishing, Edinburgh, 3rd edition.

Cooper, D. A. R., Cooper, R. W., Stevens, J. B., and Stevens, M. S. (2007). The Hot Springs Trail reference section (Cenomanian-Turonian-Coniacian), Ernst Member, Boquillas Formation, Big Bend National Park, Texas. *Geological Society of America Abstracts with Programs*, 39(6):635.

Cooper, R. W. and Cooper, D. A. (2014). *Field Guide to Late Cretaceous Geology of the Big Bend Region*. A Houston Geological Society Field Guidebook. Houston Geological Society, Houston.

Cooper, R. W., Cooper, D. A., Stevens, J. B., and Stevens, M. S. (2008). Geology of the

Hot Springs Trail area, Ernst and San Vicente members of the Boquillas Formation. In Cooper, D. A., editor, *The Southern Extension of the Western Interior Seaway: Geology of Big Bend National Park and Trans-Pecos, Texas: Field Trip Guidebook for the 2008 Joint Annual Meeting of the Geological Society of America (Boulder, Colorado) and the Houston Geological Society (Texas)*, pages 24–33. Geological Society of America and the Houston Geological Society.

Corbett, M. J. and Watkins, D. K. (2013). Calcareous nannfossil paleoecology of the mid-Cretaceous Western Interior Seaway and evidence of oligotrophic surface waters during OAE2. *Palaeogeography, Palaeoclimatology, Palaeoecology*, 392:510–523.

Corbett, M. J., Watkins, D. K., and Posphical, J. J. (2014). A quantitative analysis of calcareous nannofossil bioevents of the Late Cretaceous (Late Cenomanian-Coniacian) Western Interior Seaway and their reliability in established zonation schemes. *Marine Micropaleontology*, 109:30–45.

Cusack, C., Beeson, J., Stoneburner, D., and Robertson, G. (2010). The discovery, reservoir attributes, and significance of the Hawkville Field and Eagle Ford Shale Trend, Texas. *Gulf Coast Association of Geological Societies Transactions*, 60:165–179.

Dahl, T. W., Ruhl, M., Hammarlund, E. U., Canfield, D. E., Rosing, M. T., and Bjerrum, C. J. (2013). Tracing euxinia by molybdenum concentrations in sediments using hand-held x-ray fluorescence spectroscopy (HHXRF). *Chemical Geology*, 360-361:241–251.

Dawson, W. C. (1997). Limestone microfacies and sequence stratigraphy: Eagle Ford Group (Cenomanian-Turonian) north-central Texas outcrops. *Gulf Coast Association of Geological Societies Transactions*, 47:99–106.

Deluca, M. J. (2016). Ash Bed Analysis of the Cretaceous Eagle Ford Shale Using ID-TIMS U/Pb Methods: Implications for Biostratigraphic Refinement and Correlations Within the Western Interior Seaway. Master's thesis, Texas A&M University.

Denne, R. A., Breyer, J. A., Kosanke, T. H., Spaw, J. M., Callender, A. D., Hinote, R. E.,

Kariminia, M., Tur, M., Kita, Z., Lees, J. A., and Rowe, H. (2016). Biostratigraphic and geochemical constraints on the stratigraphy and depositional environments of the Eagle Ford and Woodbine groups of Texas. In Breyer, J. A., editor, *The Eagle Ford Shale–a Renaissance in U.S. Oil Production*. AAPG Memoir 110, Tulsa, OK.

Donovan, A. D. (2010). The sequence stratigraphy family tree: understanding the portfolio of sequence methodologies. In Ratcliffe, K. T. and Zaitlin, B. A., editors, *Application of Modern Stratigraphic Techniques: Theory and Case Histories*. SEPM Special Publication 94.

Donovan, A. D. (2015). Chronostratigraphic relationships of the Woodbine and Eagle Ford Groups across Texas. *Houston Geological Society Bulletin*, 57(8):37–41.

Donovan, A. D. (2016). Making outcrops relevant for an unconventional source rock play: an example from the Eagle Ford Group of Texas. In Bowman, M., Smyth, H. R., Passey, S. R., Hirst, J. P. P., and Jordan, C. J., editors, *The Value of Outcrop Studies in Reducing Subsurface Uncertainty and Risk in Hydrocarbon Exploration and Production*, pages 193–206. Geological Society, London, Special Publications, London, UK.

Donovan, A. D., Gardner, R. D., Pramudito, A., Staerker, T. S., Wehner, M., Corbett, M. J., Lundquist, J. J., Romero, A. M., Henry, L. C., Rotzien, J. R., and Boling, K. (2015a). Chronostratigraphic relationships of the Woodbine and Eagle Ford groups across Texas. *GCAGS Journal*, 4:67–87.

Donovan, A. D. and Staerker, T. S. (2010). Sequence stratigraphy of the Eagle Ford (Boquillas) Formation in the subsurface of south Texas and outcrops of west Texas. *Gulf Coast Association of Geological Societies Transactions*, 60:861–899.

Donovan, A. D., Staerker, T. S., Gardner, R., Pope, M. C., Pramudito, A., and Wehner, M. (2016). Findings from the Eagle Ford outcrops of west Texas and implications to the subsurface of south Texas. In Breyer, J. A., editor, *The Eagle Ford Shale–a Renaissance in U.S. Oil Production*, pages 301–336. AAPG Memoir 110, Tulsa, OK.

Donovan, A. D., Staerker, T. S., Gardner, R. D., Pope, M. C., and Wehner, M. (2015b). Making outcrops relevant to the subsurface: learnings from the Eagle Ford of west Texas. In *Unconventional Resources Technology Conference*, San Antonio, TX. URTeC 2154599.

Donovan, A. D., Staerker, T. S., Pramudito, A., Li, W., Corbett, M. J., Lowery, C. M., Romero, A. M., and Gardner, R. D. (2012). The Eagle Ford outcrops of west Texas: a laboratory for understanding heterogeneities within unconventional mudstone reservoirs. *GCAGS Journal*, 1:162–185.

Droser, M. L. and Bottjer, D. J. (1986). A semiquantitative field classification of ichnofabric. *Journal of Sedimentary Research*, 56(4):558–559.

Dumas, S. and Arnott, R. W. C. (2006). Origin of hummocky and swaley cross-stratification–the controlling influence of unidirectional current strength and aggradation rate. *Geology*, 34(12):1073–1076.

Dumas, S., Arnott, R. W. C., and Southard, J. B. (2005). Experiments on oscillatory-flow and combined-flow bed forms: implications for interpreting parts of the shallow-marine sedimentary Record. *Journal of Sedimentary Research*, 75(3):501–513.

Dunham, R. J. (1962). Classification of carbonate rocks according to depositional texture. In *Classification of Carbonate Rocks - A Symposium*, pages 108–121. AAPG Memoir 1, Tulsa, OK.

Ehlers, E. G. and Blatt, H. (1982). *Petrology: Igneous, Sedimentary, and Metamorphic*. W. H. Freeman and Company, New York.

Einsele, G. and Seilacher, A. (1991). Distinction of tempestites and turbidites. In Einsele, G., Ricken, W., and Seilacher, A., editors, *Cycles and Events in Stratigraphy*, pages 377–382. Springer-Verlag, Berlin.

Elder, W. P. (1989). Molluscan extinction patterns across the Cenomanian-Turonian stage boundary in the Western Interior of the United States. *Paleobiology*, 15(3):299–320.

Elder, W. P. and Kirkland, J. I. (1994). Cretaceous paleogeography of the southern Western Interior Region. In *Mesozoic Systems of the Rocky Mountain Region, USA*, pages 415–440. The Rocky Mountain Section SEPM, Tulsa, OK.

Eldrett, J. S., Ma, C., Bergman, S. C., Lutz, B., Gregory, F. J., Dodsworth, P., Phipps, M., Hardas, P., Minisini, D., Ozkan, A., Ramezani, J., Bowring, S. A., Kamo, S. L., Ferguson, K., Macaulay, C., and Kelly, A. E. (2015a). An astronomically calibrated stratigraphy of the Cenomanian, Turonian and earliest Coniacian from the Cretaceous Western Interior Seaway, USA: implications for global chronostratigraphy. *Cretaceous Research*, 56(C):316–344.

Eldrett, J. S., Ma, C., Bergman, S. C., Ozkan, A., Minisini, D., Lutz, B., Jackett, S.-J., Macaulay, C., and Kelly, A. E. (2015b). Origin of limestone-marlstone cycles: astronomic forcing of organic-rich sedimentary rocks from the Cenomanian to early Coniacian of the Cretaceous Western Interior Seaway, USA. *Earth and Planetary Science Letters*, 423(C):98–113.

Eldrett, J. S., Minisini, D., and Bergman, S. C. (2014). Decoupling of the carbon cycle during the Ocean Anoxic Event 2. *Geology*, 42(7):567–570.

Ettensohn, F. R., Fulton, L. P., and Kepferle, R. C. (1979). Use of scintillometer and gamma-ray logs for correlation and stratigraphy in homogeneous black shales: summary. *Geological Society of America Bulletin*, 90(5):421–423.

Fairbanks, M. D. (2012). *High Resolution Stratigraphy and Facies Architecture of the Upper Cretaceous (Cenomanian-Turonian) Eagle Ford Group, Central Texas*. PhD thesis, University of Texas, Austin, Texas.

Ferrill, D. A., Morriss, A. P., Wigginton, S. S., Smart, K. J., McGinnis, R. N., and Lehrmann, D. (2016). Deciphering thrust fault nucleation and propagation and the importance of footwall synclines. *Journal of Structural Geology*, 85(C):1–11.

Frush, M. P. and Eicher, D. L. (1975). Cenomanian and Turonian foraminifera and pale-

oenvironments in the Big Bend region of Texas and Mexico. *The Geological Association of Canada Special Paper*, 13:277–301.

Fry, K. O. (2015). Lithofacies, Biostratigraphy, Chemostratigraphy, and Stratal Architecture of the Boquillas Formation and Eagle Ford Group: a Comparison of Outcrop and Core Data from Big Bend National Park to Maverick Basin, Southwest Texas, USA. Master's thesis, University of Texas at Austin.

Gardner, R. D., Pope, M. C., Wehner, M., and Donovan, A. D. (2013). Comparative stratigraphy of the Eagle Ford Group strata in Lozier Canyon and Antonio Creek, Terrell County, Texas. *GCAGS Journal*, 2:42–52.

Gradstein, F. M., Ogg, J. G., Schmitz, M., and Ogg, G. (2012). *The Geologic Time Scale*. Elsevier B. V., Amsterdam, The Netherlands.

Hampson, G. J., Davies, W., Davies, S. J., Howell, J. A., and Adamson, K. R. (2005). Use of spectral gamma-ray data to refine subsurface fluvial stratigraphy: late Cretaceous strata in the Book Cliffs, Utah, USA. *Journal of the Geological Society*, 162(4):603–621.

Hancock, J. M. and Walaszczyk, I. (2004). Mid-Turonian to Coniacian changes of sea level around Dallas, Texas. *Cretaceous Research*, 25(4):459–471.

Harms, J. C., Southard, J. B., Spearing, D. R., and Walker, R. G. (1975). *Depositional Environments as Interpreted From Primary Sedimentary Structures and Stratification Sequences*. SEPM Short Course No. 2, Tulsa, OK.

Hartgers, W. A., Lopez, J. F., Sinninghe Damsté, J. S., Reiss, C., Maxwell, J. R., and Grimalt, J. O. (1997). Sulfur-binding in recent environment: II. Speciation of sulfur, iron and implications for the occurrence of organo-sulfur compounds. *Geochimica et Cosmochimica Acta*, 61(22):4769–4788.

Hentz, T. F., Ambrose, W. A., and Smith, D. (2015). Eaglebine play of the southwestern East Texas Basin: stratigraphic and depositional framework of the Upper Cre-

taceous (Cenomanian-Turonian) Woodbine and Eagle Ford groups. *AAPG Bulletin*, 98(12):2551–2580.

Hentz, T. F. and Ruppel, S. C. (2010). Regional lithostratigraphy of the Eagle Ford Shale: Maverick Basin to East Texas Basin. *Gulf Coast Association of Geological Societies Transactions*, 60:325–337.

Herron, S. L. and Herron, M. M. (1996). Quantitative lithology: an application for open and cased hole spectroscopy. In *SPWLA 37th Annual Logging Symposium*, pages 1–14, New Orleans, Louisiana.

Hou, X., He, Y., and Jones, B. T. (2004). Recent advances in portable x-ray fluorescence spectrometry. *Applied Spectroscopy Reviews*, 39(1):1–25.

Jarvis, I., Trabucho Alexandre, J., Grocke, D. R., Uličný, D., and Laurin, J. (2016). Intercontinental correlation of organic carbon and carbonate stable isotope records: evidence of climate and sea-level change during the Turonian (Cretaceous). *The Depositional Record*, 1(2):53–90.

Jenkyns, H. C., Dickson, A. J., Ruhl, M., and van den Boorn, S. H. J. M. (2016). Basalt-seawater interaction, the Plenus Cold Event, enhanced weathering and geochemical change: deconstructing Oceanic Anoxic Event 2 (Cenomanian-Turonian, Late Cretaceous). *Sedimentology*, 64(1):16–43.

Kauffman, E. G. and Caldwell, W. G. E. (1993). The Western Interior Basin in space and time. *The Geological Association of Canada Special Paper*, 39:1–30.

Kennedy, W. J. and Cobban, W. A. (1990). Cenomanian ammonite faunas from the Woodbine Formation and lower part of the Eagle Ford Group, Texas. *Palaeontology*, 33:75–154.

Kennedy, W. J. and Cobban, W. A. (1993). Lower Cenomanian *Forbesiceras brundrettei* zone ammonite fauna in Texas U.S.A. *Neues Jahrbuch fur Geologie un Palaeontologie, Abhandlungen*, 188(3):327–344.

Kennedy, W. J., Walaszczyk, I., and Cobban, W. A. (2005). The global boundary stratotype section and point for the base of the Turonian stage of the Cretaceous: Pueblo, Colorado, U.S.A. *Episodes*, 28(2):93–104.

Koopmans, M. P., Schouten, S., Kohnen, M. E., and Sinninghe Damste, J. S. (1996). Restricted utility of aryl isoprenoids as indicators for photic zone anoxia. *Geochimica et Cosmochimica*, 60(23):4873–4876.

Lock, B. E. and Peschier, L. S. (2006). Boquillas (Eagle Ford) upper slope sediments, west Texas: outcrop analogs for potential shale reservoirs. *Gulf Coast Association of Geological Societies Transactions*, 56:491–508.

Loucks, R. G., Reed, R. M., Ruppel, S. C., and Hammes, U. (2012). Spectrum of pore types and networks in mudrocks and a descriptive classification for matrix-related mudrock pores. *AAPG Bulletin*, 96(6):1071–1098.

Lowery, C. M., Corbett, M. J., Leckie, R. M., Watkins, D. K., Romero, A. M., and Pramudito, A. (2014). Foraminiferal and nannofossil paleoecology and paleoceanography of the Cenomanian–Turonian Eagle Ford Shale of southern Texas. *Palaeogeography, Palaeoclimatology, Palaeoecology*, 413:49–65.

Lyon, T. S. (2015). Determining the Depositional Environment of the Lower Eagle Ford in Lozier Canyon, Antonio Creek, and Osman Canyon, Texas: an Outcrop Study of Bedding Features at Outcrop Scale. Master's thesis, Texas A&M University.

Marshall, D. (1996). Ternplot: an Excel spreadsheet for ternary diagrams. *Computers & Geosciences*, 22(6):697–699.

Martini, M. and Ortega-Gutiérrez, F. (2017). Tectono-stratigraphic evolution of eastern Mexico during the break-up of Pangea: a review. *Earth-Science Reviews*. In press.

Maulana, I. (2016). Basin Geochemical Evolution of the Eagle Ford and Effects on Trace Element Release. Master's thesis, Texas A&M University.

Maxwell, R. A., Lonsdale, J. T., Hazzard, R. T., and Wilson, J. A. (1967). *Geology of Big*

Bend National Park, Brewster County, Texas. The University of Texas Publication No. 6711. Bureau of Economic Geology, Austin, TX.

McLennan, S. M. (2001). Relationships between trace element compositions of sedimentary rocks and upper crust. *Geochemistry, Geophysics, Geosystems*, 2:1–24. doi: 10.1029/2000GC000109.

McNulty, C. L., Neybert, D. S., and Reaser, D. F. (1985). Foraminifers of the Lower Ojinaga Formation (Cretaceous), Southern Quitman Mountains, Hudspeth County, Texas. *Gulf Coast Association of Geological Societies Transactions*, 35:467–472.

Meyers, S. R., Sageman, B. B., and Arthur, M. A. (2012). Obliquity forcing of organic matter accumulation during Oceanic Anoxic Event 2. *Paleoceanography*, 27(3). doi: 10.1029/2012PA002286.

Miller, R. W. (1990). The Stratigraphy and Depositional Environment of the Boquillas Formation of Southwest Texas. Master's thesis, University of Texas at Arlington.

Moore, B. T. (2016). A Stratigraphic and Geochemical Analysis of the Ojinaga Formation, West Texas. Master's thesis, Texas A&M University.

Myers, K. J. and Wignall, P. B. (1987). Understanding Jurassic organic-rich mudrocks-new concepts using gamma-ray spectrometry and palaeoecology: examples from the Kimmeridge Clay of Dorset and the Jet Rock of Yorkshire. In *Marine Clastic Sedimentology: Concepts and Case Study*, pages 172–189. Graham and Trotman, London, UK.

Nakamura, K. (2015). *Chemostratigraphy of the Late Cretaceous Western Interior (Greenhorn, Carlile, and Niobrara Formations), Denver Basin, CO, U.S.A.* PhD thesis, Colorado School of Mines.

Nakamura, K., Humphrey, J., Stout, L., and Canter, K. L. (2013). High-resolution carbon isotope and elemental chemostratigraphy of the Greenhorn, Carlile and Niobrara formations, Denver Basin, CO. In *Unconventional Resources Technology Conference*, pages

1–5, Denver, CO. URTeC 1619340.

Ogg, J. G., Hinnov, L. A., and Huang, C. H. (2012). Cretaceous. In Gradstein, F. M., Ogg, J. G., Schmitz, M., and Ogg, G., editors, *The Geologic Time Scale 2012*, pages 793–843. Elsevier, Amsterdam, Netherlands.

Pang, M. and Nummedal, D. (1995). Flexural subsidence and basement tectonics of the Cretaceous Western Interior basin, United States. *Geology*, 23(2):173.

Peavey, E. J. (2017). A New Chronostratigraphic Framework for Eagle Ford- and Austin Chalk-equivalent Strata in West Texas: Implications for Basin Evolution and Diachroneity in Unconventional Reservoirs. Master's thesis, Texas A&M University.

Phelps, R. M., Kerans, C., Da Gama, R. O. B. P., Jeremiah, J., Hull, D. C., and Loucks, R. G. (2015). Response and recovery of the Comanche carbonate platform surrounding multiple Cretaceous oceanic anoxic events, northern Gulf of Mexico. *Cretaceous Research*, 54(C):117–144.

Pope, M., Wehner, M. P., Peavey, E., Conte, R., Tice, M. M., and Donovan, A. (2017). Surface to subsurface correlation of Eagle Ford equivalent strata from west to south Texas. In *Unconventional Resources Technology Conference*, Austin, Texas. American Association of Petroleum Geologists. URTeC 2716442.

Pratt, L. M. and Threlkeld, C. N. (1984). Stratigraphic significance of 13C/12C ratios in mid-Cretaceous rocks of the Western Interior, U.S.A. *Canadian Society of Petroleum Geologists Memoir*, 9:305–312.

Raiswell, R. and Berner, R. A. (1985). Pyrite formation in euxinic and semi-euxinic sediments. *American Journal of Science*, 285:710–724.

Rowe, H. D., Hughes, N., and Robinson, K. (2012). The quantification and application of handheld energy-dispersive x-ray fluorescence (ED-XRF) in mudrock chemostratigraphy and geochemistry. *Chemical Geology*, 324:122–131.

Rowe, H. D., Loucks, R. G., Ruppel, S. C., and Rimmer, S. M. (2008). Mississippian

Barnett Formation, Fort Worth Basin, Texas: bulk geochemical inferences and Mo–TOC constraints on the severity of hydrographic restriction. *Chemical Geology*, 257(1-2):16–25.

Sageman, B. B. (1996). Lowstand tempestites: depositional model for Cretaceous skeletal limestones, Western Interior Basin. *Geology*, 24(10):888–892.

Schieber, J. and Riciputi, L. (2004). Pyrite ooids in Devonian black shales record intermittent sea-level drop and shallow-water conditions. *Geology*, 32(4):305.

Schwalbach, J. R. and Bohacs, K. M. (1992). Field Investigation Techniques for Analysis of the Monterey Formation. In *Sequence Stratigraphy in Fine-grained Rocks: Examples From the Monterey Formation*, pages 21–29. Pacific Section of SEPM, Tulsa, OK.

Scotese, C. R. (1999). Paleomap project: Continental drift (0-750 million years). University of Texas at Arlington. CD-ROM.

Selley, R. C. (1998). *Elements of Petroleum Geology*. Academic Press, Waltham, MA, 2nd edition.

Selley, R. C. (2012). UK shale gas: the story so far. *Marine and Petroleum Geology*, 31:100–109.

Shepard, T. M. and Walper, J. L. (1982). Tectonic evolution of Trans-Pecos, Texas. *Gulf Coast Association of Geological Societies Transactions*, 32:165–172.

Sheppard, R. A. and Hunter, R. E. (1960). Chamosite oolites in the Devonian of Pennsylvania. *Journal of Sedimentary Petrology*, 30(4):585–588.

Sloss, L. L. (1963). Sequences in the cratonic interior of North America. *Geologic Society of America Bulletin*, 74:93–114.

Summons, R. E. and Powell, T. G. (1986). Chlorobiaceae in Palaezoic seas revealed by biological markers, isotopes and geology. *Nature*, 319:763–765.

Sun, X., Zhang, T., Sun, Y., Milliken, K. L., and Sun, D. (2016). Geochemical evidence of organic matter source input and depositional environments in the lower and upper Eagle

Ford Formation, south Texas. *Organic Geochemistry*, 98(C):66–81.

Tian, Y., Ayers, W. B., and McCain, W. D. D. (2012). Regional analysis of stratigraphy, reservoir characteristics, and fluid phases in the Eagle Ford Shale, south Texas. *Gulf Coast Association of Geological Societies Transactions*, 62:471–483.

Tinnin, B. M. and Darmaoen, S. T. R. (2016). Chemostratigraphic variability of the Eagle Ford Shale, south Texas: insights into paleoredox and sedimentary facies changes. In Breyer, J. A., editor, *The Eagle Ford Shale–a Renaissance in U.S. Oil Production*, pages 259–283. AAPG Memoir 110, Tulsa, OK.

Trevino, R. H. (1988). Facies and Depositional Environments of the Boquillas Formation, Upper Cretaceous of Southwest Texas. Master's thesis, Texas A&M University.

Tribovillard, N., Algeo, T. J., Baudin, F., and Riboulleau, A. (2012). Analysis of marine environmental conditions based on molybdenum–uranium covariation—applications to Mesozoic paleoceanography. *Chemical Geology*, 324-325:46–58.

Tribovillard, N., Riboulleau, A., Lyons, T., and Baudin, F. (2004). Enhanced trapping of molybdenum by sulfurized marine organic matter of marine origin in Mesozoic limestones and shales. *Chemical Geology*, 213(4):385–401.

Udden, J. A. (1907). A sketch of the geology of the Chisos country, Brewster County, Texas. *University of Texas Bulletin*, 93:29–33.

van Kaam-Peters, H. M. E. (1997). *The Depositional Environment of Jurassic Organic-rich Sedimentary Rocks in NW Europe. A Biomarker Approach*. PhD thesis, University of Utrecht.

Wehner, M., Gardner, R. D., Pope, M. C., and Donovan, A. D. (2017). The Eagle Ford Group returns to Big Bend National Park, Brewster County, Texas. *GCAGS Journal*, 6:161–176.

Wehner, M., Gardner, R. D., Tice, M. M., Pope, M. C., Donovan, A. D., and Staerker, T. S. (2015). Anoxic, storm dominated inner carbonate ramp deposition of Lower Eagle

Ford Formation, west Texas. In *Unconventional Resources Technology Conference*, San Antonio, Texas. URTeC 2154667.

Weltje, G. J. and Tjallingii, R. (2008). Calibration of XRF core scanners for quantitative geochemical logging of sediment cores: theory and application. *Earth and Planetary Science Letters*, 274(3-4):423–438.

White, T., Furlong, K., and Arthur, M. (2002). Forebulge migration in the Cretaceous Western Interior basin of the central United States. *Basin Research*, 14:43–54.

Wignall, P. B. and Newton, R. (2001). Black shales on the basin margin: a model based on examples from the Upper Jurassic of the Boulonnais, northern France. *Sedimentary Geology*, 144:335–356.

Zumberge, J., Illich, H., and Waite, L. (2016). Petroleum geochemistry of the Cenomanian-Turonian Eagle Ford oils of south Texas. In Breyer, J. A., editor, *The Eagle Ford Shale–a Renaissance in U.S. Oil Production*, pages 135–165. AAPG Memoir 110, Tulsa, OK.

APPENDIX A

SAMPLE LOCATIONS

The slabbed images shown in this appendix, as explained in the contributors page, were kindly provided by Trey Lyon (class of 2015 at Texas A&M), a fellow classmate and colleague. The samples he used in his thesis, I assisted with collection of the samples, however he did the rock cutting, slabbing, and photography himself. Further details of his are in his thesis (Lyon, 2015). All the sedimentary structure measurement data I collected.

This appendix contains additional data about sedimentary structures that supports the interpretation that sediments in the Eagle Ford Group, especially in west Texas, were deposited in storm-influenced, shallow-water, photic zone anoxia depositional environment as described in Chapter 2 of this dissertation. The majority of the samples are units A and B from both Lozier Canyon and Antonio Creek localities in Terrell County, Texas. Five images are provided. For the first four images, blocks containing entire hummocks were recovered from the field, slabbed with a set of polished surfaces perpendicular to each other, and the images of the two sides of each hummock were placed side-by-side for a composite image (Lyon, 2015). Criteria for identification of HCS, SCS, and wave ripples are described in the following works: (Aigner, 1982, 1985; Einsele and Seilacher, 1991; Harms et al., 1975). Field measurements of ripples as defined by Collinson et al. (2006) indicates that many sedimentary structures in Unit A, a few in unit B, and some in unit E are consistent with those of wave-dominated or combined flow regimes. The ripple symmetry index (RSI) has a mean of 1.23, which is nearly symmetric and a ripple index (RI) of 5.99, which corrected for compaction would be much smaller (assuming a compaction ratio ~ 0.6 would give an RI of about 3.6) and is consistent with a combined flow regime.

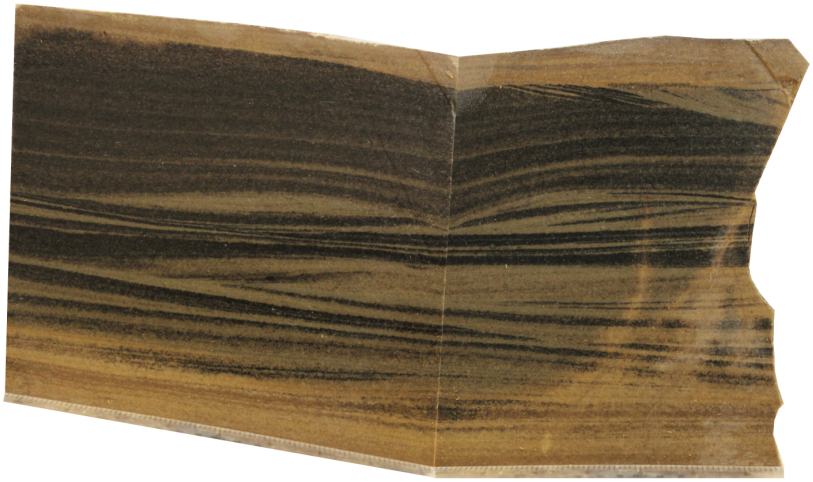

Figure A.1: Slabbed low-angle hummocky-cross stratification (HCS).

Figure A.2: Lens-shaped ripple with internal low-angle stratification and symmetric scouring. The image is a composite of two polished surfaces of a hummock that was slabbed. The 3-D nature of the sedimentary structures precludes it being an antidune. The two rulers at the bottom of each slabbed surface are 15 cm (6 inches).

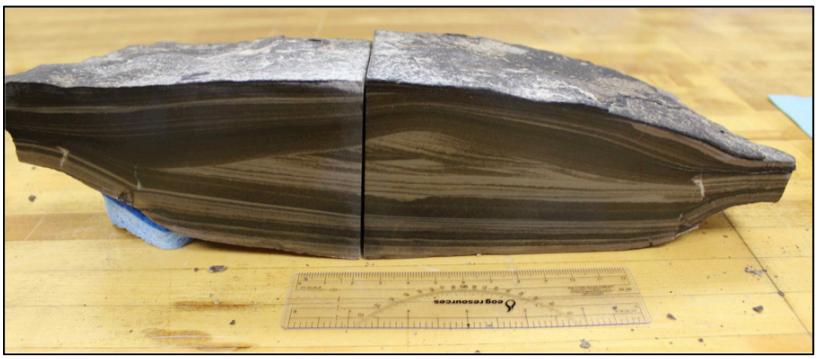

Figure A.3: Another view of the slab shown in Fig. A.2 of this data supplement. The 3-D symmetry is clear from comparing this view with the view in Fig. A.2. Also the thinning at the edge is not due to compaction as some have hypothesized for lense-shaped beds that are frequently cemented.

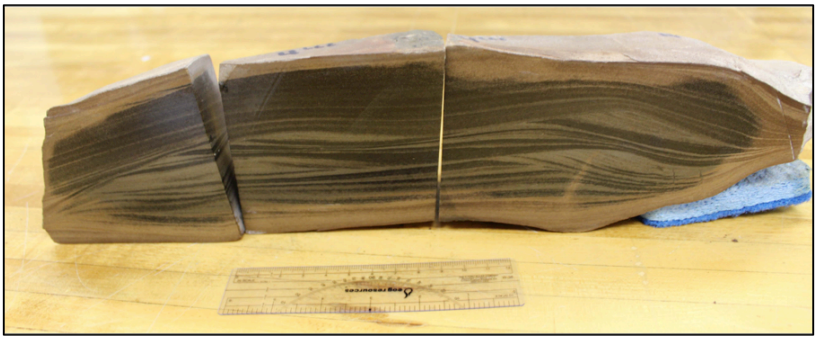

Figure A.4: Another example of HCS from unit A of Lozier Canyon, Texas. This one is amalgamated by stacked scouring and filling, much like the HCS shown in Dumas and Arnott (2006).

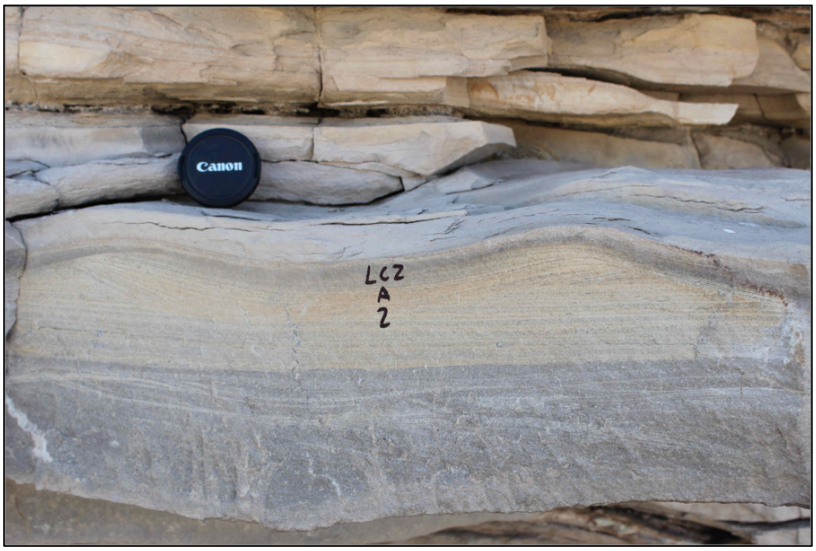

Figure A.5: Examples of wave ripples from unit A, Lower Eagle Ford Formation at Lozier Canyon, Terrell County, Texas. The symmetry of these ripples suggests that waves sculpted these ripples

APPENDIX B

GEOCHEMISTRY

B.1 Geochemistry: organic geochemistry

Ivan Maulana, my colleague, as part of his master's thesis acquired GC-MS data from the Swenson #1-H core (Maulana, 2016). This well is in McMullen County, Texas. The core was donated to Dr. Michael Tice by Comstock Oil & Gas. The Pr/Ph ratio is the ratio of the organic molecules, pristane (Pr) over phytane (Ph), which can distinguish between a reducing and oxidizing environment. The quantity, AIR, is the aryl isoprenoid ratio and are biomarkers for photic-zone sulfur-reducing marine bacteria. If the AIR is > 2, this is interpreted as indicating episodic photic zone euxinia. The organic geochemistry used in this dissertation is listed in Table B.1.

The data shown in Figure 2.4 is from two datasets. The data from BP/Schlumberger #1 well (annotated as LC/AC in Figure 2.4) is from the XRF data I acquired. I also have comparable data for the Swenson #1 core (SW), but an ICP-MS dataset was also made available for the figure graphic. For both sections (LC/AC and SW), I have an XRF dataset. The quantities in the following tables marked with the subscript EF refers to something called the Enrichment Factor. It is intended to calculate the relative enrichment of a trace element over aluminum as compared to something called "average shale" or "average upper crustal value" (Brumsack, 2006). In this project, we used the upper crustal values of McLennan (2001) as the standard value for the EF equation given by Brumsack (2006).

B.2 Geochemistry: uranium and molybdenum

Depth (ft)	Pr/Ph	AIR
10391.10	0.45	1.83
10389.97	0.38	1.68
10407.35	0.60	1.98
10417.52	0.57	2.95
10424.09	0.46	3.43
10428.68	0.40	2.15
10438.85	0.31	2.46
10471.33	0.50	3.22
10473.94	0.45	3.10

Table B.1: Table of pristane/phytane ratios and aryl isoprenoids ratio (AIR). The data in this table can be found in (Maulana, 2016).

Swenson #1 data (ICP-MS)								
Depth (ft)	U^{238} ppm	Mo^{98} ppm	Al^{27} ppm	Mo/Al	U/Al	U_{EF}	Mo_{EF}	Unit
10378	1.48	1.93	23013	8.39E-05	6.42E-05	1.84	4.50	UEF
10379	1.88	2.18	26833	8.11E-05	7.00E-05	2.01	4.35	UEF
10380	2.04	1.48	25417	5.84E-05	8.02E-05	2.30	3.13	UEF
10381	2.70	1.98	42705	4.63E-05	6.33E-05	1.82	2.48	UEF
10382	2.55	1.22	12039	1.01E-04	2.12E-04	6.08	5.42	UEF
10382.5	0.27	0.35	21014	1.69E-05	1.27E-05	0.36	0.90	UEF
10384	1.51	1.51	58922	2.56E-05	2.56E-05	0.74	1.37	UEF
10384.5	3.73	7.43	89162	8.34E-05	4.18E-05	1.20	4.47	UEF
10385.5	4.39	20.52	54070	3.79E-04	8.12E-05	2.33	20.34	LEF
10387	5.03	307.50	46930	6.55E-03	1.07E-04	3.08	351.21	LEF
10387.5	4.13	20.84	56968	3.66E-04	7.24E-05	2.08	19.61	LEF
10388	4.20	20.63	53054	3.89E-04	7.91E-05	2.27	20.84	LEF

Continued on next page

Depth (ft)	U^{238} ppm	Mo^{98} ppm	Al^{27} ppm	Mo/Al	U/Al	U_{EF}	Mo_{EF}	Unit
10390	5.46	29.16	45619	6.39E-04	1.20E-04	3.44	34.27	LEF
10391	3.99	16.44	48306	3.40E-04	8.27E-05	2.37	18.24	LEF
10392	4.55	19.29	23162	8.33E-04	1.97E-04	5.65	44.63	LEF
10393	3.59	22.53	51464	4.38E-04	6.98E-05	2.00	23.46	LEF
10394	3.86	13.93	63028	2.21E-04	6.12E-05	1.76	11.85	LEF
10395	4.32	21.14	63446	3.33E-04	6.81E-05	1.96	17.86	LEF
10396	1.56	4.77	9227	5.17E-04	1.69E-04	4.86	27.73	LEF
10396.5	0.95	2.83	9239	3.06E-04	1.03E-04	2.96	16.40	LEF
10397.5	4.32	23.95	32685	7.33E-04	1.32E-04	3.80	39.27	LEF
10399	5.36	25.54	52789	4.84E-04	1.01E-04	2.91	25.93	LEF
10400	3.90	15.10	35803	4.22E-04	1.09E-04	3.13	22.60	LEF
10401	5.74	29.21	44085	6.63E-04	1.30E-04	3.74	35.52	LEF
10402	4.47	20.91	51373	4.07E-04	8.71E-05	2.50	21.82	LEF
10403	1.88	6.36	16037	3.96E-04	1.17E-04	3.37	21.25	LEF
10404	3.71	20.84	28558	7.30E-04	1.30E-04	3.73	39.11	LEF
10405	5.46	35.35	39979	8.84E-04	1.37E-04	3.92	47.40	LEF
10406	5.15	22.40	38279	5.85E-04	1.34E-04	3.86	31.36	LEF
10407	3.27	10.61	41758	2.54E-04	7.82E-05	2.25	13.61	LEF
10408	4.91	20.29	24481	8.29E-04	2.01E-04	5.76	44.43	LEF
10409	4.90	22.20	51723	4.29E-04	9.47E-05	2.72	23.00	LEF
10409.5	4.26	24.47	20976	1.17E-03	2.03E-04	5.84	62.53	LEF
10411	5.51	33.03	23663	1.40E-03	2.33E-04	6.69	74.81	LEF

Continued on next page

Depth (ft)	U^{238} ppm	Mo^{98} ppm	Al^{27} ppm	Mo/Al	U/Al	U_{EF}	Mo_{EF}	Unit
10412	4.17	21.37	46145	4.63E-04	9.03E-05	2.59	24.82	LEF
10413	3.81	23.06	26349	8.75E-04	1.45E-04	4.16	46.91	LEF
10414	3.38	18.20	15245	1.19E-03	2.22E-04	6.37	64.00	LEF
10415	3.75	16.56	23404	7.08E-04	1.60E-04	4.60	37.92	LEF
10416	1.14	3.89	5970	6.51E-04	1.92E-04	5.51	34.89	LEF
10417	4.89	23.97	35384	6.77E-04	1.38E-04	3.96	36.30	LEF
10418	3.59	23.15	34698	6.67E-04	1.03E-04	2.97	35.76	LEF
10420	3.17	23.38	21171	1.10E-03	1.50E-04	4.30	59.20	LEF
10422	5.39	33.37	18264	1.83E-03	2.95E-04	8.48	97.94	LEF
10423	4.79	42.50	20119	2.11E-03	2.38E-04	6.84	113.23	LEF
10424	1.68	5.29	7360	7.19E-04	2.28E-04	6.55	38.52	LEF
10425	3.40	30.32	20740	1.46E-03	1.64E-04	4.71	78.36	LEF
10426	3.73	30.73	22816	1.35E-03	1.64E-04	4.70	72.19	LEF
10427	6.99	39.57	21100	1.88E-03	3.31E-04	9.51	100.53	LEF
10428	1.77	4.92	4754	1.04E-03	3.73E-04	10.71	55.49	LEF
10429	4.32	32.14	21345	1.51E-03	2.02E-04	5.81	80.71	LEF
10430	0.65	4.02	4614	8.71E-04	1.42E-04	4.07	46.66	LEF
10431	3.84	33.54	44270	7.58E-04	8.68E-05	2.49	40.60	LEF
10432	5.91	34.22	40217	8.51E-04	1.47E-04	4.22	45.60	LEF
10433	4.97	34.09	29042	1.17E-03	1.71E-04	4.91	62.91	LEF
10434	6.69	42.62	36018	1.18E-03	1.86E-04	5.34	63.42	LEF
10436	2.47	17.78	17234	1.03E-03	1.43E-04	4.11	55.29	LEF

Continued on next page

Depth (ft)	U^{238} ppm	Mo^{98} ppm	Al^{27} ppm	Mo/Al	U/Al	U_{EF}	Mo_{EF}	Unit
10437	5.03	26.65	18521	1.44E-03	2.72E-04	7.80	77.11	LEF
10438	6.62	42.96	28912	1.49E-03	2.29E-04	6.57	79.65	LEF
10439	5.98	39.67	24806	1.60E-03	2.41E-04	6.92	85.72	LEF
10440	5.78	29.46	36554	8.06E-04	1.58E-04	4.54	43.19	LEF
10441	6.25	42.90	33988	1.26E-03	1.84E-04	5.28	67.65	LEF
10443	2.14	16.16	11429	1.41E-03	1.87E-04	5.38	75.79	LEF
10444	4.33	35.96	25839	1.39E-03	1.68E-04	4.81	74.59	LEF
10445	3.40	23.95	19443	1.23E-03	1.75E-04	5.03	66.01	LEF
10446	6.41	42.03	27509	1.53E-03	2.33E-04	6.69	81.89	LEF
10447.5	7.03	32.37	25952	1.25E-03	2.71E-04	7.78	66.85	LEF
10448	3.08	29.77	27490	1.08E-03	1.12E-04	3.22	58.04	LEF
10450	5.44	24.86	27378	9.08E-04	1.99E-04	5.70	48.66	LEF
10451	3.40	21.84	21160	1.03E-03	1.61E-04	4.62	55.32	LEF
10452	3.58	29.06	30419	9.55E-04	1.18E-04	3.38	51.21	LEF
10453	1.64	8.15	21887	3.73E-04	7.48E-05	2.15	19.97	LEF
10454	2.38	21.25	25854	8.22E-04	9.21E-05	2.64	44.05	LEF
10455	3.83	23.87	29688	8.04E-04	1.29E-04	3.71	43.10	LEF
10456	3.46	29.13	32886	8.86E-04	1.05E-04	3.02	47.48	LEF
10457	2.29	23.64	46281	5.11E-04	4.95E-05	1.42	27.38	LEF
10458	5.72	34.40	24593	1.40E-03	2.33E-04	6.68	74.97	LEF
10459	2.64	21.29	34438	6.18E-04	7.68E-05	2.20	33.14	LEF
10460	3.14	30.23	38293	7.90E-04	8.20E-05	2.35	42.32	LEF

Continued on next page

Depth (ft)	U^{238} ppm	Mo^{98} ppm	Al^{27} ppm	Mo/Al	U/Al	U_{EF}	Mo_{EF}	Unit
10462	2.71	10.36	12812	8.08E-04	2.11E-04	6.07	43.33	LEF
10463	3.02	30.40	28296	1.07E-03	1.07E-04	3.06	57.58	LEF
10464	4.60	19.08	30070	6.34E-04	1.53E-04	4.39	34.00	LEF
10466	2.73	25.20	26787	9.41E-04	1.02E-04	2.93	50.43	LEF
10467	2.65	16.83	21812	7.72E-04	1.21E-04	3.48	41.36	LEF
10468	1.24	7.76	8319	9.33E-04	1.48E-04	4.26	50.03	LEF
10469	2.73	19.53	19184	1.02E-03	1.42E-04	4.09	54.56	LEF
10470	3.24	27.84	36786	7.57E-04	8.80E-05	2.53	40.56	LEF
10471	2.59	25.45	35677	7.13E-04	7.25E-05	2.08	38.24	LEF
10472	4.56	27.76	32959	8.42E-04	1.38E-04	3.97	45.15	LEF
10473	6.95	54.82	56638	9.68E-04	1.23E-04	3.52	51.88	LEF
10474	3.19	34.19	34579	9.89E-04	9.23E-05	2.65	52.99	LEF
10476	3.59	33.83	34788	9.72E-04	1.03E-04	2.96	52.12	LEF
10477	7.38	45.77	24433	1.87E-03	3.02E-04	8.67	100.42	LEF
10477	4.01	26.06	38079	6.84E-04	1.05E-04	3.02	36.69	LEF
10478	4.30	9.54	56936	1.67E-04	7.55E-05	2.17	8.98	LEF
10479	4.26	17.00	38368	4.43E-04	1.11E-04	3.19	23.75	LEF
10480	4.97	21.50	68640	3.13E-04	7.24E-05	2.08	16.79	LEF
10481	3.94	20.29	19142	1.06E-03	2.06E-04	5.91	56.80	LEF
10482	1.38	5.92	9267	6.39E-04	1.49E-04	4.27	34.24	LEF
10483	2.48	12.60	13406	9.40E-04	1.85E-04	5.32	50.37	LEF
10484	3.90	52.32	35001	1.49E-03	1.11E-04	3.20	80.12	LEF

Continued on next page

Depth (ft)	U^{238} ppm	Mo^{98} ppm	Al^{27} ppm	Mo/Al	U/Al	U_{EF}	Mo_{EF}	Unit
10485	3.67	52.58	38086	1.38E-03	9.63E-05	2.76	74.00	LEF
10486	4.46	35.84	38875	9.22E-04	1.15E-04	3.29	49.42	LEF
10487	3.41	30.11	42481	7.09E-04	8.02E-05	2.30	38.00	LEF
10488	1.70	11.64	7048	1.65E-03	2.41E-04	6.91	88.50	LEF
10489	5.18	57.80	28468	2.03E-03	1.82E-04	5.22	108.82	LEF
10490	4.94	28.07	32457	8.65E-04	1.52E-04	4.37	46.35	LEF
10491	3.54	36.19	38317	9.44E-04	9.23E-05	2.65	50.62	LEF
10492	5.09	33.87	38229	8.86E-04	1.33E-04	3.82	47.49	LEF
10493	3.13	12.53	14412	8.69E-04	2.17E-04	6.23	46.60	LEF
10494	1.83	7.34	7590	9.67E-04	2.41E-04	6.92	51.85	LEF
10495	4.40	11.82	41266	2.86E-04	1.07E-04	3.06	15.36	LEF
10496	3.17	10.53	28539	3.69E-04	1.11E-04	3.19	19.77	LEF
10497	3.82	20.64	39790	5.19E-04	9.60E-05	2.76	27.81	LEF
10498	5.00	25.79	27278	9.45E-04	1.83E-04	5.26	50.67	LEF
10499	2.97	25.72	21747	1.18E-03	1.37E-04	3.93	63.40	LEF
10500	3.43	14.24	17435	8.17E-04	1.97E-04	5.65	43.78	LEF
10501	5.59	29.81	56578	5.27E-04	9.87E-05	2.84	28.24	LEF
10502	4.06	24.23	21360	1.13E-03	1.90E-04	5.45	60.80	LEF
10503	2.81	18.42	18426	9.99E-04	1.52E-04	4.38	53.57	LEF
10504	1.93	9.67	12046	8.03E-04	1.61E-04	4.61	43.03	LEF
10505	3.34	26.13	29369	8.90E-04	1.14E-04	3.27	47.70	LEF
10506	4.64	39.06	34620	1.13E-03	1.34E-04	3.85	60.47	LEF

Continued on next page

Depth (ft)	U^{238} ppm	Mo^{98} ppm	Al^{27} ppm	Mo/Al	U/Al	U_{EF}	Mo_{EF}	Unit
10507	5.59	35.28	37040	9.53E-04	1.51E-04	4.33	51.06	LEF
10508	2.40	13.67	19024	7.18E-04	1.26E-04	3.62	38.51	LEF
10509	3.54	23.69	30535	7.76E-04	1.16E-04	3.33	41.58	LEF
10510	6.47	43.76	30079	1.45E-03	2.15E-04	6.18	77.99	LEF
10511	5.59	29.16	21632	1.35E-03	2.59E-04	7.42	72.25	LEF
10512	2.54	12.59	15363	8.20E-04	1.66E-04	4.75	43.94	LEF
10513	2.64	9.88	11525	8.57E-04	2.29E-04	6.59	45.94	LEF
10514	2.20	8.52	9890	8.62E-04	2.23E-04	6.39	46.18	LEF
10515	3.60	26.13	27556	9.48E-04	1.31E-04	3.75	50.82	LEF
10516	3.68	21.38	29422	7.27E-04	1.25E-04	3.59	38.94	LEF
10517	2.12	8.57	14061	6.10E-04	1.51E-04	4.33	32.68	LEF
10518	2.26	11.30	16240	6.96E-04	1.39E-04	4.00	37.30	LEF
10519	3.62	34.62	36526	9.48E-04	9.91E-05	2.85	50.81	LEF
10520	3.67	30.18	36322	8.31E-04	1.01E-04	2.90	44.54	LEF
10521	4.56	30.56	39535	7.73E-04	1.15E-04	3.31	41.43	LEF
10522	2.87	17.92	25834	6.93E-04	1.11E-04	3.20	37.17	LEF
10523	3.73	25.62	37053	6.91E-04	1.01E-04	2.89	37.06	LEF
10524	2.16	10.58	19582	5.40E-04	1.10E-04	3.17	28.96	LEF
10525	5.85	38.60	50655	7.62E-04	1.16E-04	3.32	40.85	LEF
10527	7.75	19.26	39837	4.83E-04	1.95E-04	5.59	25.91	LEF
10529	9.58	17.29	74125	2.33E-04	1.29E-04	3.71	12.50	Buda
10530	20.44	9.38	56547	1.66E-04	3.61E-04	10.38	8.89	Buda

Continued on next page

Depth (ft)	U^{238} ppm	Mo^{98} ppm	Al^{27} ppm	Mo/Al	U/Al	U_{EF}	Mo_{EF}	Unit

Table B.2: ICP-MS data for selected samples for Swenson #1 well.

BP/Schlumberger Lozier #1 data (XRF)								
Depth (ft)	U ppm	Mo ppm	Al ppm	Mo/Al	U/Al	U_{EF}	Mo_{EF}	Unit
65.77	3.5	2.36	2588	9.12E-04	1.35E-03	26.19	48.88	Austin
69.71	5.06	1.4	4547	3.08E-04	1.11E-03	8.84	16.50	Austin
72.20	4.81	2.76	3238	8.52E-04	1.49E-03	24.47	45.68	Austin
75.20	4	2.1	2156	9.74E-04	1.86E-03	27.97	52.21	Austin
78.90	8.37	5.12	18812	2.72E-04	4.45E-04	7.82	14.59	UEF
81.58	4.78	1.63	12981	1.26E-04	3.68E-04	3.61	6.73	UEF
83.50	6.08	3.35	18474	1.81E-04	3.29E-04	5.21	9.72	UEF
85.13	4.82	3.09	23099	1.34E-04	2.09E-04	3.84	7.17	UEF
86.80	3.88	1.58	15813	9.99E-05	2.45E-04	2.87	5.36	UEF
91.14	6.42	2.64	11330	2.33E-04	5.67E-04	6.69	12.49	UEF
92.91	3.78	1.57	8401	1.87E-04	4.50E-04	5.37	10.02	UEF
98.64	5.3	1.89	27671	6.83E-05	1.92E-04	1.96	3.66	UEF
99.26	5.07	2.21	10811	2.04E-04	4.69E-04	5.87	10.96	UEF
100.91	3.76	1.58	12287	1.29E-04	3.06E-04	3.69	6.89	UEF
103.78	5.55	2.46	13139	1.87E-04	4.22E-04	5.38	10.04	UEF
107.13	8.74	10.79	20889	5.17E-04	4.18E-04	14.83	27.69	UEF
109.15	4.76	1.31	16161	8.11E-05	2.95E-04	2.33	4.34	UEF
113.15	6.61	2.67	13452	1.98E-04	4.91E-04	5.70	10.64	UEF
115.14	4.09	1.08	6687	1.62E-04	6.12E-04	4.64	8.66	UEF
116.89	4.24	1.45	14853	9.76E-05	2.85E-04	2.80	5.23	UEF
120.89	4.4	1.58	11185	1.41E-04	3.93E-04	4.06	7.57	UEF

Continued on next page

Depth (ft)	U ppm	Mo ppm	Al ppm	Mo/Al	U/Al	U_{EF}	Mo_{EF}	Unit
124.75	3.36	1.79	9969	1.80E-04	3.37E-04	5.16	9.62	UEF
126.70	3.11	1.85	15405	1.20E-04	2.02E-04	3.45	6.44	UEF
129.14	4.24	2	9965	2.01E-04	4.26E-04	5.76	10.76	UEF
131.14	2.67	2.85	27141	1.05E-04	9.84E-05	3.02	5.63	UEF
133.14	2.22	1.52	6086	2.50E-04	3.65E-04	7.17	13.39	UEF
135.00	2.67	1.94	10090	1.92E-04	2.65E-04	5.52	10.31	UEF
153.70	2.31	1.95	9949	1.96E-04	2.32E-04	5.63	10.51	UEF
154.39	14.72	9.46	14585	6.49E-04	1.01E-03	18.62	34.77	UEF
157.48	9.76	22.9	16186	1.41E-03	6.03E-04	40.62	75.83	UEF
159.40	8.46	14.13	10866	1.30E-03	7.79E-04	37.34	69.70	UEF
161.38	10	26.91	12828	2.10E-03	7.80E-04	60.24	112.44	UEF
163.15	5.21	22.96	13355	1.72E-03	3.90E-04	49.37	92.15	UEF
165.40	11.17	25.51	8221	3.10E-03	1.36E-03	89.10	166.32	UEF
167.31	12.33	21.01	5983	3.51E-03	2.06E-03	100.83	188.21	UEF
169.45	14.09	19.04	5266	3.62E-03	2.68E-03	103.81	193.78	UEF
171.20	15.84	27.26	11411	2.39E-03	1.39E-03	68.60	128.05	UEF
173.17	18.52	21.9	26949	8.13E-04	6.87E-04	23.33	43.56	LEF
174.92	10.54	19.78	6620	2.99E-03	1.59E-03	85.79	160.14	LEF
176.93	14.62	22.87	20301	1.13E-03	7.20E-04	32.35	60.38	LEF
179.43	5.44	4.45	8949	4.97E-04	6.08E-04	14.28	26.65	LEF
181.26	14.39	23.95	15267	1.57E-03	9.43E-04	45.05	84.09	LEF
183.11	10.58	25.55	8981	2.85E-03	1.18E-03	81.69	152.49	LEF

Continued on next page

Depth (ft)	U ppm	Mo ppm	Al ppm	Mo/Al	U/Al	U_{EF}	Mo_{EF}	Unit
185.66	18.9	12.97	64904	2.00E-04	2.91E-04	5.74	10.71	LEF
187.20	10.91	25.57	7056	3.62E-03	1.55E-03	104.05	194.24	LEF
188.91	11.32	23.7	14293	1.66E-03	7.92E-04	47.61	88.87	LEF
190.92	10.65	16.92	7366	2.30E-03	1.45E-03	65.96	123.12	LEF
193.15	12.08	18.15	26261	6.91E-04	4.60E-04	19.85	37.05	LEF
194.90	5.42	8.8	1952	4.51E-03	2.78E-03	129.46	241.66	LEF
197.13	12.8	27.7	11296	2.45E-03	1.13E-03	70.42	131.44	LEF
199.14	12.91	41.06	11195	3.67E-03	1.15E-03	105.31	196.58	LEF
201.12	13.94	45.22	15348	2.95E-03	9.08E-04	84.60	157.92	LEF
203.15	10.11	31.84	10699	2.98E-03	9.45E-04	85.45	159.51	LEF
205.23	9.22	22.36	7523	2.97E-03	1.23E-03	85.34	159.30	LEF
207.37	7.07	23.71	11978	1.98E-03	5.90E-04	56.84	106.10	LEF
208.80	13.84	30.01	7445	4.03E-03	1.86E-03	115.75	216.07	LEF
211.14	10.52	27.25	12927	2.11E-03	8.14E-04	60.53	112.99	LEF
213.50	9.71	38.93	15470	2.52E-03	6.28E-04	72.26	134.89	LEF
215.13	7.97	33.93	10614	3.20E-03	7.51E-04	91.79	171.34	LEF
217.15	9.33	24.09	10133	2.38E-03	9.21E-04	68.26	127.42	LEF
219.07	12.59	24.87	12420	2.00E-03	1.01E-03	57.50	107.33	LEF
221.14	13.4	20.89	10615	1.97E-03	1.26E-03	56.51	105.49	LEF
222.13	14.59	10.58	23679	4.47E-04	6.16E-04	12.83	23.95	LEF
222.30	25.05	22.12	7996	2.77E-03	3.13E-03	79.43	148.27	LEF
224.20	23.71	44.3	25204	1.76E-03	9.41E-04	50.47	94.21	LEF

Continued on next page

Depth (ft)	U ppm	Mo ppm	Al ppm	Mo/Al	U/Al	U_{EF}	Mo_{EF}	Unit
226.70	18.33	12.68	11021	1.15E-03	1.66E-03	33.04	61.67	LEF
228.60	7.48	5.99	4333	1.38E-03	1.73E-03	39.70	74.10	LEF
228.80	28.98	46.09	13259	3.48E-03	2.19E-03	99.81	186.32	LEF
230.80	30.17	56.79	16089	3.53E-03	1.88E-03	101.36	189.20	LEF
233.20	7.45	2.7	9170	2.94E-04	8.12E-04	8.45	15.78	LEF
234.30	28.84	52.49	22068	2.38E-03	1.31E-03	68.30	127.49	LEF
236.70	18.87	71.12	23728	3.00E-03	7.95E-04	86.07	160.66	LEF
238.90	21.29	21.78	35075	6.21E-04	6.07E-04	17.83	33.28	LEF
239.92	5.69	5.19	8458	6.14E-04	6.73E-04	17.62	32.89	LEF
240.30	3.24	3.09	2058	1.50E-03	1.57E-03	43.12	80.48	Buda
271.13	2.16	1.38	9455	1.46E-04	2.28E-04	4.19	7.82	Buda
276.56	4.04	1.6	23784	6.73E-05	1.70E-04	1.93	3.61	Buda

Table B.3: XRF data for the BP/Schlumberger Lozier #1 well in Terrell County, Texas.

APPENDIX C

STRATIGRAPHIC SAMPLE LOCATIONS

All samples collected for these studies were labeled with a prefix (e.g. HS for Hot Springs) and a number that was the measured stratigraphic depth above the top of Buda Limestone. The prefixes are as follows: AC (Antonio Creek), HS (Hot Springs), MC (Mule Canyon). The attached figures are strat columns with the sample depths marked with blue dots. The captions specify the prefix associated with the strat column. The annotated strat columns are arranged in the following order: Antonio Creek, Hot Springs, and Mule Canyon.

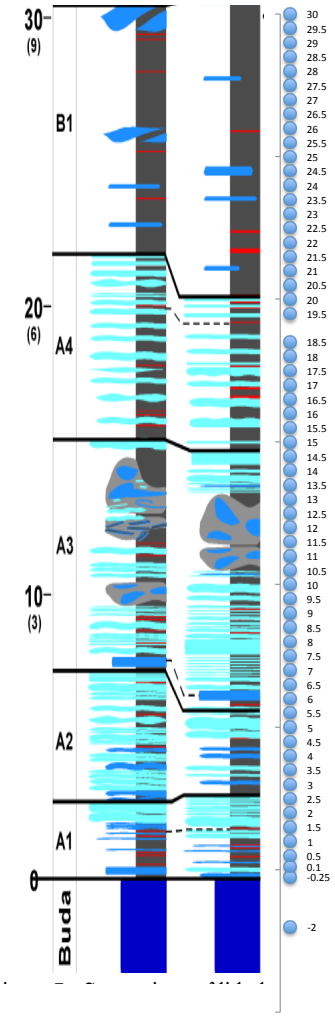

Figure C.1: Antonio Creek (prefix AC) part 1 from -5 ft to 30 ft. Samples are numbered by depth above Buda and have AC for prefix

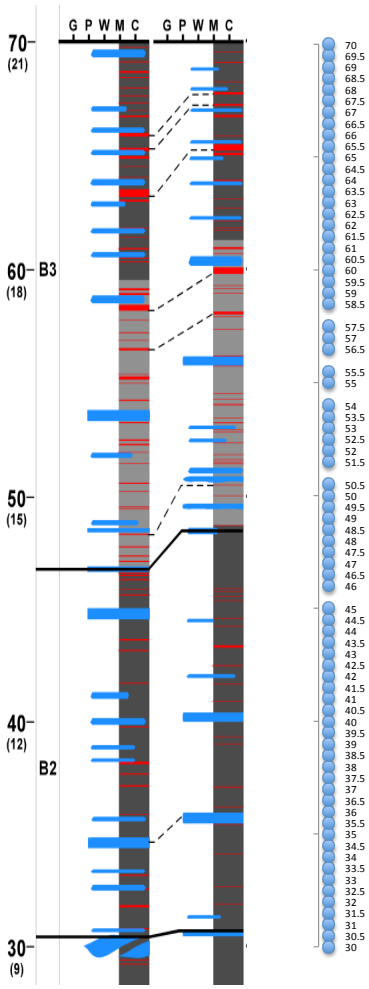

Figure C.2: Antonio Creek (prefix AC) part 2 from 30 ft to 70 ft. Samples are numbered by depth above Buda and have AC for prefix

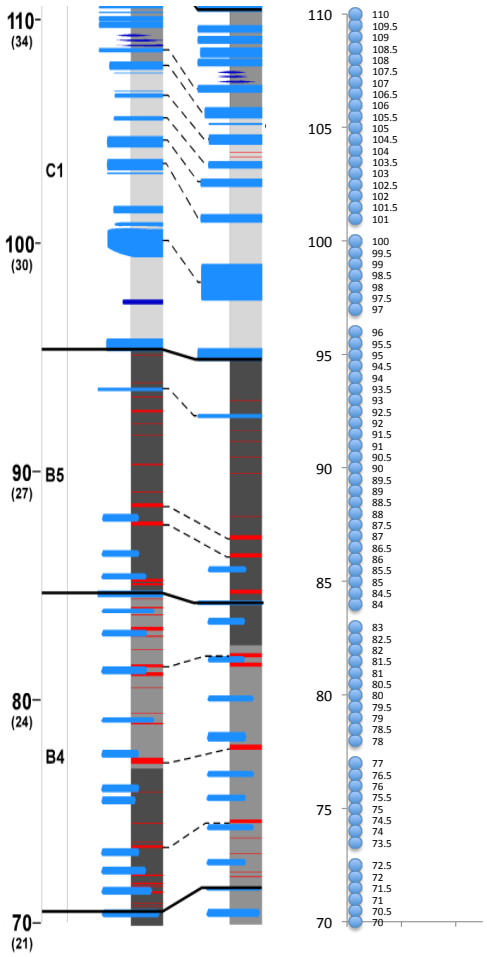

Figure C.3: Antonio Creek (prefix AC) part 3 from 70 ft to 110 ft. Samples are numbered by depth above Buda and have AC for prefix

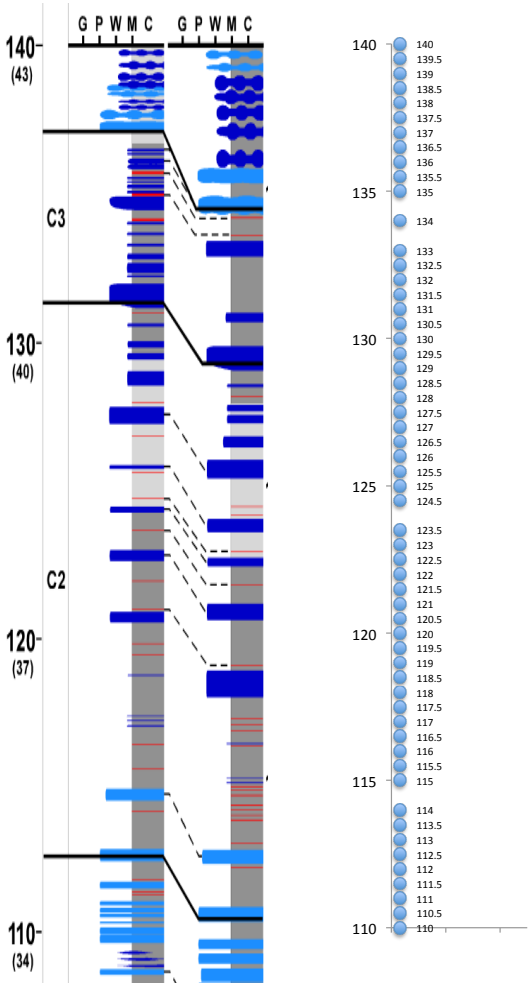

Figure C.4: Antonio Creek (prefix AC) part 4 from 110 ft to 140 ft. Samples are numbered by depth above Buda and have AC for prefix

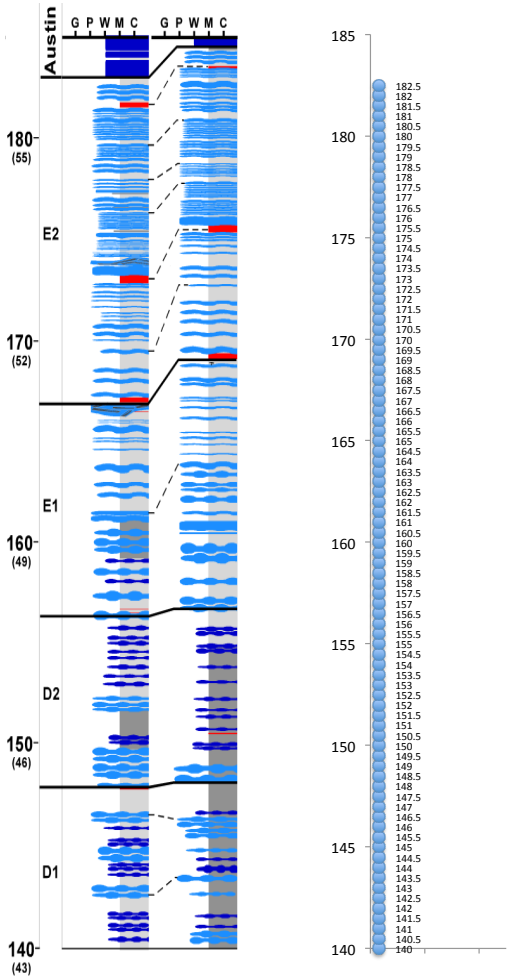

Figure C.5: Antonio Creek (prefix AC) part 5 from 140 ft to 185 ft. Samples are numbered by depth above Buda and have AC for prefix

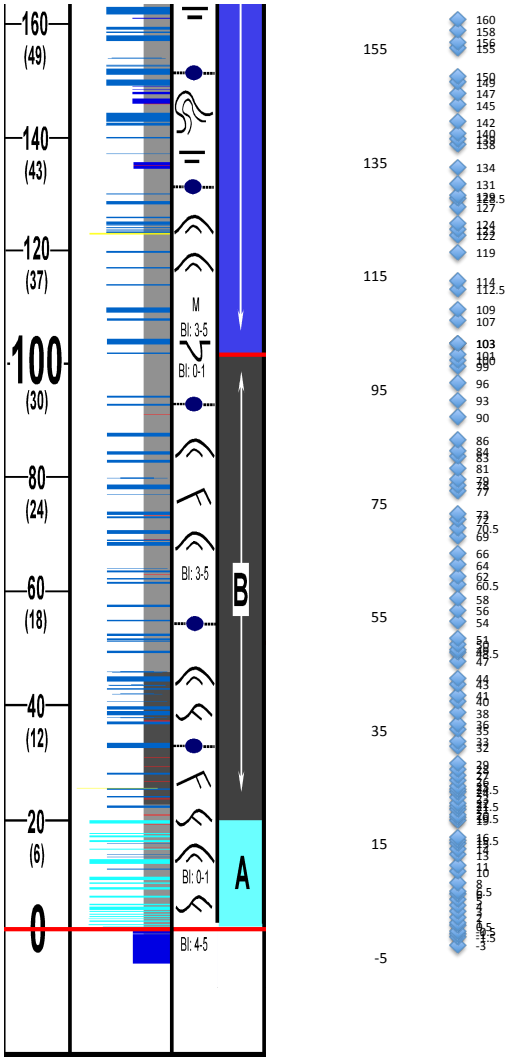

Figure C.6: Hot Springs (prefix HS) part 1 from 0 ft to 160 ft. Samples are numbered by depth above Buda and have HS for prefix

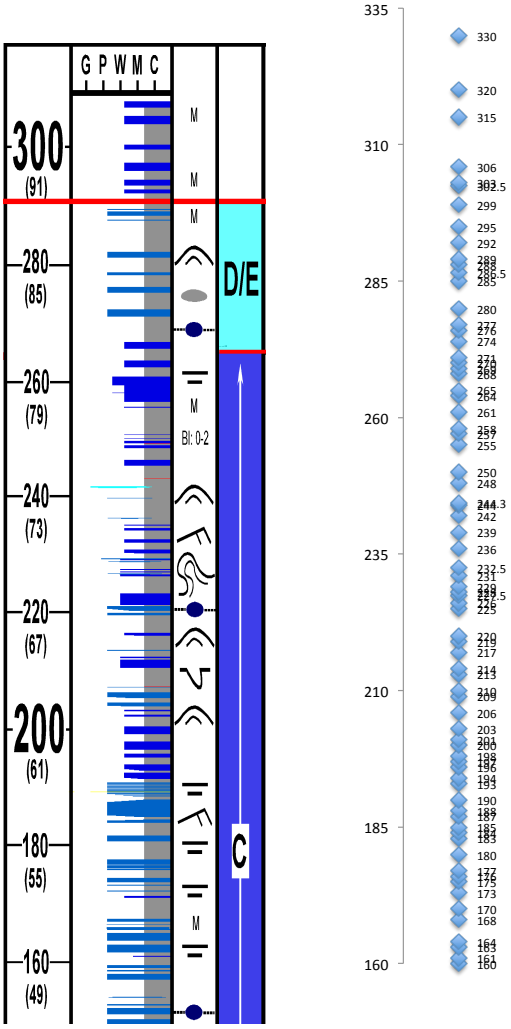

Figure C.7: Hot Springs (prefix HS) part 1 from 160 ft to 335 ft. Samples are numbered by depth above Buda and have HS for prefix

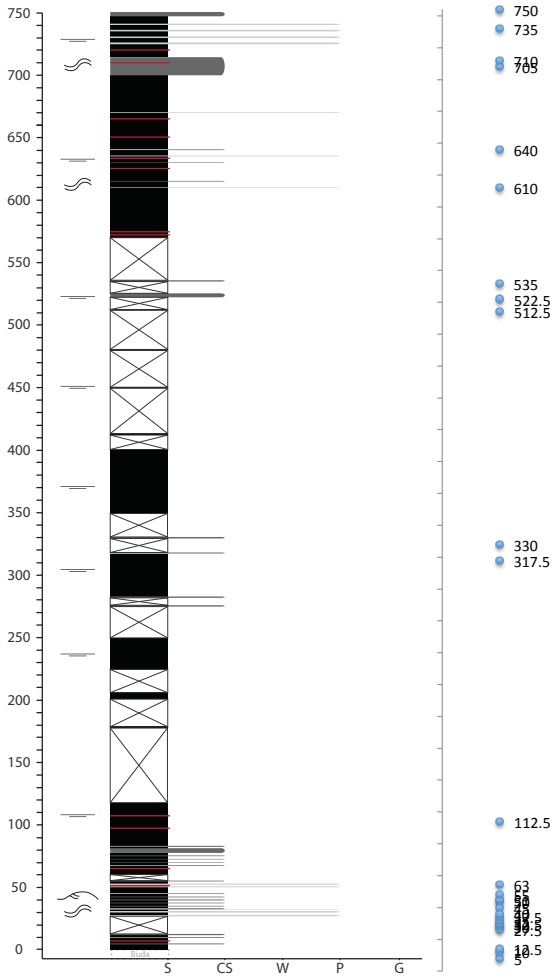

Figure C.8: Mule Canyon (prefix MC) from 0 ft to 750 ft. Samples are numbered by depth above Buda and have MC for prefix

APPENDIX D

DESCRIPTION OF SUPPLEMENTAL DATA

This appendix contains a list of supplemental data used for the studies described in this dissertation. They are spreadsheets (with file extension .xlsx) and should be viewable with Microsoft Office Excel or OpenOffice products. The abbreviations (e.g. AC, MC) are the same ones mentioned in Appendix C. These data files should be available with the dissertation at the Texas A&M dissertation repository.

The list of supplemental data files:

- AC-isotopes-SIGF.xlsx
- AC-SGR 2_5_2012 V3.xlsx
- AC-XRF-Niton-NaN.xlsx
- HS-isotopes-SIGF.xlsx
- HS-SGR-Culled.xlsx
- HS-XRF-Niton-nan.xlsx
- LC_AC_paleocurrent.xlsx
- MC-isotopes_bulk.xlsx
- MC-isotopes_org.xlsx
- MC-SGR-final.xlsx
- MC-TOC.xlsx
- MC-XRF.xlsx